Crack Growth in

Unidirectional Composites Using

Singular Finite Elements and

Interactive Computer Graphics

by

Gaurang Nalin Choksi

Dissertation submitted to the Faculty of the

Virginia Polytechnic Institute and State University

in partial fulfillment of the requirements for the degree of

Doctor of Philosophy

in

Engineering Mechanics

APPROVED:

Carl T. Herakovich, Chairman

O.H.Griffin

E.R.Johnson

J. N. Reddy

C.W. Smith

April, 1988

Blacksburg, Virginia

CRACK GROWTH IN UNIDIRECTIONAL COMPOSITES USING SINGULAR FINITE ELEMENTS AND INTERACTIVE COMPUTER GRAPHICS

by

Gaurang Nalin Choksi

Committee Chairman: Carl T. Herakovich
Engineering Science and Mechanics

(ABSTRACT)

Graphical simulation of crack growth using singular finite elements and interactive computer graphics is presented. The study consists of two main parts : (i) the formulation and application of an anisotropic singular element (ASE) for analyzing homogeneous anisotropic materials with cracks and, (ii) graphical simulation of crack growth in unidirectional composites.

Lekhnitskii's stress function method is used to formulate the traction-free crack boundary value problem with the stress function expressed in a Laurent series. The geometry of the element is arbitrary. The development of the stiffness matrix for general anisotropic materials is presented and it is shown how the singular element can be incorporated into a conventional displacement based finite element program. The anisotropic singular element (ASE) developed is implemented to analyze cracked anisotropic materials subjected to inplane loading. A 2-D, displacement based finite element code is used and center cracked on- and off-axis coupons under tensile loading are analyzed using the element developed.

A general, interactive menu driven program is developed to track crack growth in composite materials. PHIGS (Programmers Hierarchical Interactive Graphics System) is used as the application program interface to integrate the finite element program with interactive graphics. Simulation studies are performed for center cracked on- and off-axis laminae using the normal stress ratio theory as the crack propagation criterion. The direction of crack propagation and values of the crack initiation stresses predicted are in reasonable agreement with the experimental values for the cases analyzed.

Acknowledgements

This study was supported by Hercules, Inc. and the Center for Innovative Technology. The author would like to acknowledge Prof. C. T. Herakovich for his invaluable guidance and Profs. O.H. Griffin, E.R. Johnson, J.N. Reddy and C.W. Smith for serving as committee members and for their suggestions during the course of this study. A special thanks to and for providing the experimental data and to all my friends in the Composites Mechanics Group and CAD laboratory at Virginia Tech for their support. Finally, the author thanks his wife & family for their love and encouragement -- without them, none of this would have been possible.

Table of Contents

List of Illustrations

List of Tables

1.0 Introduction and Literature Review

1.1 Motivation

Composite material characterization is a rapidly developing and exciting field as it brings together a range of interdisciplinary principles. Optimization of material properties is a key factor behind the enormous interest and research in modern composite materials. Composites have provided a large number of research problems for theoreticians and experimentalists as well as opened up new possibilities for the design engineer. The ability to predict the properties and behavior of new materials successfully is of vital importance to the design process. Satisfactory exploitation of composites depends on the optimum use of the design flexibility that is inherently present for tailoring the properties of the material. At the present time mathematical models can predict some of the important properties and response characteristics of composites, but there remains a need for composite mechanics theories which completely treat toughness, fracture and failure response. Designers must be careful and accurate in their choice of design parameters or the potential for the economic use of composites will be lost in the use of safety factors that are needed to overcome the uncertainty.

Composites are highly resistant to corrosion and fatigue cracking. However, there is significant degradation if defects are present. Various types of defects can occur in composite laminates during both manufacture and service and knowledge of the failure mode(s) of a laminate is an important consideration for a rational approach to structural design. Experimental studies have shown the contrasting behavior for different laminate stacking sequences[1] . Figure 1 shows the failure modes for angle-ply graphite-epoxy laminates. Clustered $[(\pm\theta)_2]_s$ graphite-epoxy laminates failed in a pure matrix mode delamination and either fiber-matrix or intralaminar debonding. The alternating $[(\theta)_2/(-\theta)_2]_s$, laminates, however, exhibited a different behavior, with fiber breakage in half the plies and either fiber-matrix debonding or matrix cracking in the remaining plies. As shown by Herakovich[1] , the mode of failure has a significant effect on the strength of the laminate. The strength of 10° and 30° alternating laminates (with fiber breakage) was 30 and 50 percent greater, respectively, than the strength of the clustered laminates (no fiber breakage).

In the most basic problem of an unidirectional fibrous composite lamina, the propagation of a crack can occur in two basic modes : either between the fibers (matrix or fiber/matrix failure) or across the fibers (fiber breakage). Several criteria for predicting the direction of crack extension have been proposed by various researchers. The conditions for the case of a crack propagating by breaking fibers can be difficult to predict, and current research efforts are directed towards understanding the complete fracture process in composites.

Prediction of the direction of crack growth, crack path stability and failure loads for fracture of fibrous composite materials are important, related and unresolved questions. Development of an analytical model accounting for the detailed geometry of a cracked laminate is a formidable task which remains to be accomplished. Analytical solutions are available for the stress distribution in the vicinity of idealized cracks in homogeneous, anisotropic materials for idealized loading and geometric configurations. However, approximate solutions are required for more general materials (i.e. laminates), loading conditions and geometries. Finite element and boundary element methods are typically used as the numerical tools to calculate crack tip stress fields.

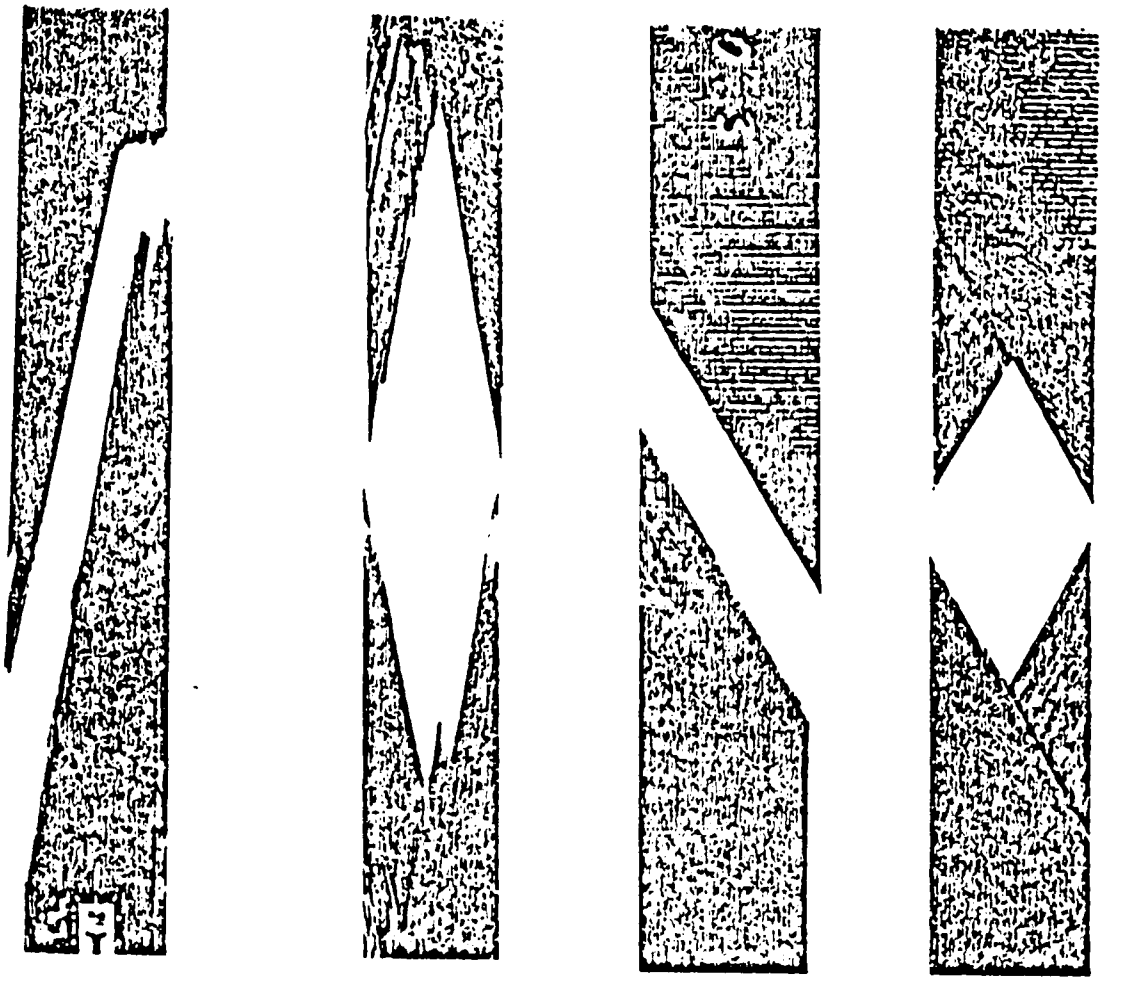

Figure 1. Failure Modes for Angle-Ply Graphite Epoxy Laminates

1.2 Scope of Study

It is the aim of this study to integrate computational anisotropic fracture mechanics with interactive computer graphics to predict the direction and stability of crack growth and gain a better understanding of the mechanics of failure in unidirectional composites. A singular finite element is developed to account for the presence of the crack. The research effort consists of two stages :

- Development of a two dimensional anisotropic singular finite element based on stress function expansions where the number of nodes and their position on the element, the number of terms considered in the stress function expansion and the element size can be varied, depending on the problem requirements. The formulation and validation of the element is discussed in Chapters 2 and 3.

- Integration of the singular element developed with interactive computer graphics and failure theories for composites to predict the direction and stability of crack growth in unidirectional composite materials. The element developed is placed around the crack tip and the use of just one element to model the crack avoids the use of complex remeshing algorithms. The method(s) of simulation adopted, criteria used for calculation of crack growth parameters and the graphics language interface are discussed in Chapter 4.

The material is assumed to be linear, elastic, homogeneous and anisotropic with the flaw treated as a sharp crack. It is known that fracture toughness and failure of these heterogeneous materials depends on microscopic parameters such as the stress transfer mechanism at the fiber/matrix interface and the molecular structure [2]. However, the microscopic behavior does not detract from the use of the macroscopic approach as the homogeneous assumption does provide an indication of the severity of the effect of the crack in the structure and a basis upon which to make engineering decisions in the design process. Indications from experiments are

that when the zone of the elastic crack tip singularity contains a sufficient number of fibers (high fiber volume fraction) for the class of materials considered in this study, the homogeneity assumption is justified and that the macroscopic failure response can be predicted using this approach [2].

1.3 Literature Review

The literature review is divided into the following three sections which include all areas of this research effort :

1. Singular Finite Elements
2. Crack Growth Criteria
3. Graphical Simulation of Crack Growth

1.3.1 Singular Finite Elements

Most available elasticity solutions for crack problems involve idealized crack geometries and infinite domains; hence numerical methods are generally used to analyze more practical or 'real world' problems in fracture mechanics. The use of the finite element method in fracture mechanics is becoming increasingly popular, and the degree of accuracy obtained by this method depends on the method of representing or accounting for the stress singularity associated with fracture mechanics. Early applications of the finite element method to fracture mechanics problems were presented by Swedlow[3] , Kobayashi[4] and Chan et al.[5] using a large number of conventional elements in regions of the large stress gradient, leading to high computer costs. Oglesby and Lomacky[6] have indicated that the maximum permissible element size using conventional elements, for an accuracy of 5%, is around 1/500 of the semi-crack length.

The need for developing elements which model the crack tip stress fields accurately without resorting to a large number of elements, and at the same time ensuring convergence, is the main motivation for developing "special elements". Accurate solutions to most fracture problems are obtained by placing these elements at the crack tip and surrounding them with conventional elements for the remaining portion of the region of interest. The various formulations used to generate singular elements incorporating the singular field behavior can be classified broadly into three major methods :

1. Elements employing singular geometric transformations
2. Elements employing shape functions with singular derivatives
3. Elements employing analytical asymptotic solutions :
    - Enriched isoparametric elements
    - Hybrid elements

Comprehensive reviews on the use of finite element and boundary element techniques in fracture mechanics have been given by Fawkes[7] , Gallagher[8] , Kobayashi[9] , Maschke and Kuna[10] , and Atluri[11] . Rather than duplicating these surveys, an attempt to introduce the fundamental ideas in the generation of the special elements is included here. Also, certain formulations which are not mentioned in the above surveys are included.

1.3.1.1 Elements employing singular geometric transformations

In general fracture problems the displacement field behaves as r^{λ} where r is the radial distance measured from the crack tip, and λ is a number that may be complex with the real part of $\lambda < 1$. This produces first displacement-derivatives (or strains in linear theory) which are singular. Such 'point singularities' arise at re-entrant corners, sharp cracks in 2-D domains, and at vertices (where 3 or more planes intersect) in 3-D domains. Also, 'line singularities' can exist for the function derivatives along a curve in a 3-D domain. The value of λ can be determined a priori from classical analytical solutions or numerically using an eigenvalue analysis.

In the case of sharp cracks in 2-D homogeneous isotropic or anisotropic linear elastic materials, the complete eigenfunction solution for the displacement (strain and stress) fields at the vicinity of the crack tip have been obtained. These solutions produce a singular solution in the strain/stress field of the form $r^{-\frac{1}{2}}F_{ij}(\theta)$ where r and θ are polar coordinates centered at the crack tip. Complete eigenfunction solutions are intractable for cracks lying at, terminating at, or intersecting bi-material interfaces and for the general problems of cracks in non-homogeneous 2-D linear elastic material domains.

Quadratic isoparametric elements can be used to generate the $r^{-\frac{1}{2}}$ crack tip stress singularity. Tracey[12] , Henshell and Shaw[13] and Barsoum[14] independently presented the popular 'quarter point element' (QPE) at about the same time. They demonstrated that the inverse square-root singularity can be obtained by placing the mid-side nodes at the quarter point of the sides intersecting the crack tip. The eight noded quadrilateral element (Q8) element can also be degenerated to a singular element in a similar way. Figure 2 shows a natural 6 noded triangle (T6) element converted to the quarter point point element.

Tracey and Freese[12] showed that the natural isoparametric triangular element is superior to the collapsed quadrilateral as it is essential that the sides of the collapsed element remain straight for modeling the singularity. Three dimensional prismatic and tetrahedral elements can be generated in a way similar to the two dimensional case. These elements are very popular and can be easily generated on commercial codes having a library of T6 or Q8 elements. Saouma[15] and Manu[16] conducted extensive parametric studies on the QPE to study the effects of the order of integration, aspect ratio and mesh geometry. Literature on the QPE has focused on isotropic materials; a large amount of published data is available regarding optimum mesh sizes, determination of stress intensity factors (SIF), and use of transition elements.

For sharp cracks in anisotropic materials, the magnitude of the crack tip stresses are not only a function of the applied load, specimen geometry, and crack length, but also of the material properties and the orientation of the crack relative to the principal material direction. For example, a symmetric loading may induce crack opening and sliding modes at the same time, depending on the above mentioned parameters. The QPE models the $r^{-\frac{1}{2}}$ singularity but does

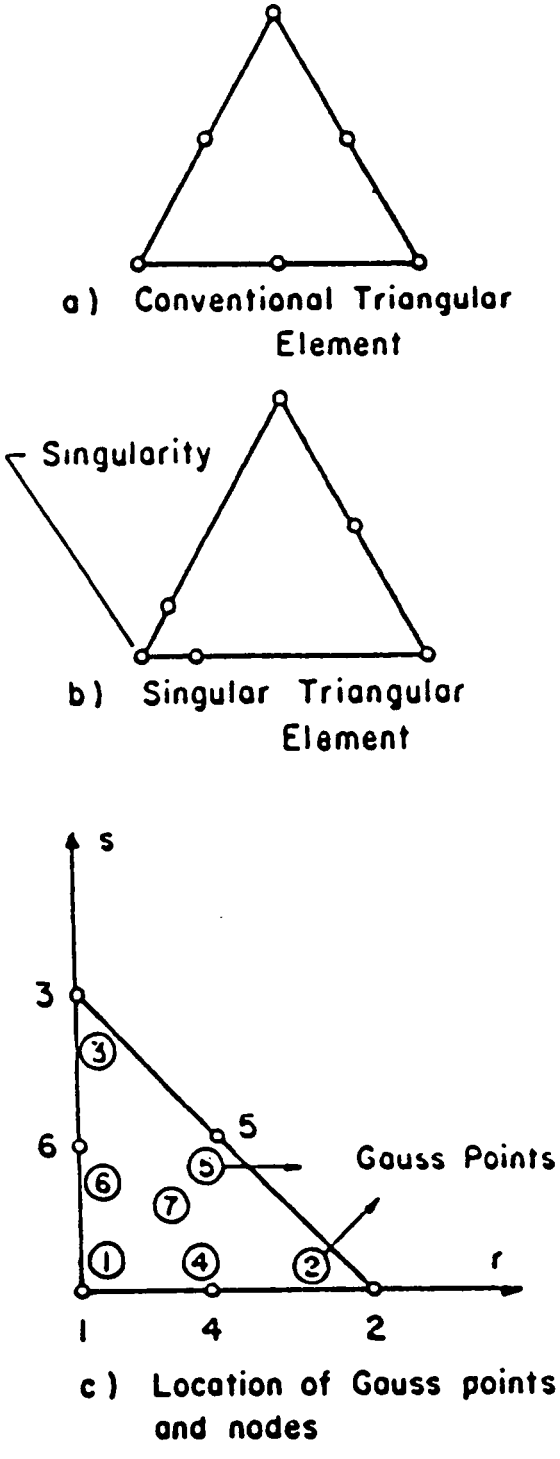

Figure 2. Geometry of the Quarter Point Element (QPE)

not account for the angular variation of the stresses which are associated with the anisotropy of the material. For highly anisotropic materials, this variation can be significant. Gregory et. al.[17] extended the use of the QPE to anisotropic materials. A paper by this author[18] describes the implementation of the T6 QPE for composites under Mode I and Mode II dominant loading conditions.

The formulation of the QPE for 2-D and 3-D analysis was further developed by Pu, et al.[19] who obtained the $r^{-\frac{1}{2}}$ singularity for a 12 noded cubic isoparametric quadrilateral by placing the two mid-side nodes at the location 1/9 and 4/9 the length of the sides from the common nodes of these two sides. Nayfeh and Nassar[20] later simulated the $r^{-\frac{1}{2}}$ singularity for isoparametric elements of arbitrary orders. They calculated the positions of the mid-side nodes for general quadrilaterals with (4n-1) nodes ('n' nodes along each side of the element). Therefore, the T6 and Q8 quarter point elements described earlier can be derived as special cases with n=3 and 4, respectively.

1.3.1.2 Elements employing shape functions with singular derivatives

Blackburn[21] proposed certain shape functions which produce singular derivatives of the form $r^{-\frac{1}{2}}$ to analyze cracked isotropic sheets. Stern[22] extended the above method to generate a conforming crack element with a singular field and generalized it to produce a family of consistent conforming elements with singular fields.

Akin[23] generated two dimensional conforming singularity elements from standard elements based on numerically integrated shape functions. Singularities of the general order r^{-p} can be modeled using this method. This is useful in numerical fracture mechanics when plasticity effects are included and the order of the singularity is a variable.

1.3.1.3 Elements employing analytical asymptotic solutions

The singular elements described above are used to model singularities of the type $r^{\lambda-1}$ $(0<\lambda<1)$ in the function derivatives, where λ is known a priori through eigenvalue, asymptotic or numerical analyses. As mentioned before, the eigenfunction solution can be obtained as a function of the radial distance and the angle from the crack tip in the form $r^{\lambda-1}F(\theta)$ for some class of problems. These solutions are generally obtained for infinite geometries under idealized loading and geometric conditions, but they can be used to generate special elements to analyze finite, irregular shaped bodies.

a) Enriched isoparametric elements :

Wilson[24] developed a circular crack tip element centered at the crack tip. The stresses were obtained using Williams'[25] stress function expansion and the displacement fields given by Gross, Roberts and Srawley[26] . Displacements along the edges common to the conventional elements were set equal at the nodes, but compatibility conditions on the edges were not met. Compatibility is satisfied only in the limit as the number of elements surrounding the crack tip increases.

Byskov[27] proposed a similar element which was triangular in shape. The same type of displacement incompatibility as in the Wilson element is encountered along the common edges between the nodes. Both elements gave satisfactory results for the cases analyzed.

Benzley[28] developed a generalized quadrilateral (Q4) element with a singular corner node. The formulation is general so as to include any singularity for which the near tip elasticity solution is available. The singularity is introduced by including the singular term in the displacement field approximation. Interelement compatibility is obtained using the bilinear function R where R is equal to 0 if the neighboring element is a conventional element and equals 1 if the neighboring element is also singular. This leads to continuity of displacements across the interelement boundaries. The main advantage of this method is that the stress intensity factors are treated as nodal variables and are calculated directly from the program. Moreover, accurate

results are obtained with relatively fewer elements around the crack tip. The determination of R, however, is difficult and parametric studies are required to obtain good estimates. Foschi and Barret[29] used a Q8 element based on Benzley's approach for analyzing a crack in an orthotropic plate. Heppler and Hansen[30] also used a similar approach for a Q12 element.

b) Hybrid elements :

Hybrid finite elements are based on variational formulations wherein relevant field variables in the element need not, a priori, satisfy the requirements of interelement displacement compatibility and/or interelement traction reciprocity. Lagrange multipliers are typically used to enforce the constraint conditions and these multipliers appear as additional variables in the formulation. This type of element was first developed by Tong and Pian[31] Depending on the method of formulation, the Lagrange multipliers can take on physical meaning. For fracture mechanics applications, the asymptotic solutions for the crack tip stress and displacement fields are incorporated in the element. The application of hybrid elements and the general method is discussed in detail by Tong and Pian[31] and Atluri[32] . This work was extended for rectilinear anisotropic materials by Tong[33] and for the analysis of interlaminar effects by Wang[34] .

As the literature survey indicates, the finite element method has proved to be a very effective approach for plane elastostatic problems with discontinuous boundaries. Many 'cracked' elements have been developed to date but many of them incorporate only the singular term of the actual series expansion for the crack tip stress field. Admittedly, this term is the dominant one, but good accuracy requires that the element be quite small and that neighboring conventional elements be placed in the region of the high stress gradient near the crack tip, losing the advantage gained by the singular formulation. Thus, much of the potential efficiency to be gained through the use of singular elements is lost. This study includes the development of a general singular element based on an elasticity solution (Chapter 2), where the number of terms, number of nodes and their positions and the size of the element can be varied depending on the requirements.

1.3.2 Crack Growth Criteria

The original Griffith criterion states that crack growth will occur when the surface energy required to extend the crack can be just delivered by the system. Irwin later accounted for the plasticity effects and proposed the term 'Stress Intensity Factor'. He showed that the critical strain energy release rate and critical stress intensity factor approaches were equivalent for the assumption of self similar crack growth.

The problem of crack growth and fracture response of composites has been addressed by several researchers. Various theories based on different physical quantities, such as energy, the stress tensor, and stress and strain components have been presented in the literature. Wu[35] and Sih[36] [37] independently investigated the fracture behavior of unidirectional glass/epoxy composites as early as 1972.

The majority of crack propagation theories for anisotropic materials assume homogeneous, linear material behavior and are developed, in many cases, as natural extensions of the classical fracture mechanics approaches for isotropic materials. The directional dependence of material stiffness and strength typically does not result in self-similar crack growth and hence the extension of the original flaw is not only a function of the applied far field loading, but also of the material properties and specimen geometry. Moreover, depending on the type of composite material analyzed, material homogeneity assumptions can become invalid. Zweben[38] describes the typical approaches taken to study fracture of composites and they can be broadly classified into two categories :

- macromechanical approach, treating the composite as a homogeneous material
- micromechanical approach, taking into account the heterogeneity of the material

Both methods are employed by current researchers and have shown success in predicting the fracture response for special cases when compared to experimental data.

The Tensor Polynomial theory, proposed by Tsai and Wu[35] treats the material as homogeneous and was originally derived for the prediction of the failure of unnotched laminates [39] [40] [41]. The Tensor Polynomial theory is a criterion based on the existence of a failure surface in stress space. It assumes that crack growth is governed by all the components of the stress tensor. The Strain Energy Density theory and its application to composites is given by Sih[42], along with a compilation of analytical solutions available for fracture of composites. It was originally derived to study mixed mode fracture in isotropic materials and in its application to composites, it does not account for the directional dependence of material strength. It is based on variations in the energy stored along the periphery of a core region surrounding the crack. Crack initiation is assumed to take place in a radial direction which corresponds to a minimum value of the strain energy density factor.

The Point Stress criterion of Whitney and Nuismer[43] attempts to explain the size effect of the crack on the determination of stresses at a finite distance, R, from the crack tip. More recently, Herakovich and co-workers have developed the Normal Stress Ratio (NSR) theory for notched composites[44–53].

1.3.2.1 Normal Stress Ratio Theory

Buczek and Herakovich[44,45,49] proposed the normal stress ratio theory as a crack growth direction criterion for composite materials. The normal stress ratio, R, is defined by

$$R(r_s,\phi) = \frac{\sigma_{\phi\phi}}{T_{\phi\phi}} \quad . \tag{1.1}$$

In this expression, $\sigma_{\phi\phi}$ corresponds to the normal stress acting on the radial plane defined by ϕ, at a specified distance, r_s, from the crack tip. $T_{\phi\phi}$ is the tensile strength on the ϕ plane. Figure 3 depicts the parameters of the NSR theory. The model assumes that the direction of crack extension corresponds to the radial direction having the maximum value of the normal

stress ratio. In the present study, the normal stress ratio theory will be used to predict the stability of crack growth. The normal stress ratio theory is an extension of the maximum normal stress theory, formulated to make it applicable to anisotropic materials by considering the directional dependency of strength. Like the maximum normal stress theory, it is based upon the assumption that Mode I crack growth controls crack extension.

Because no experimental method currently exists for measuring the tensile strength on an arbitrary plane, $T_{\phi\phi}$ must be defined mathematically, in a manner consistent with tests that can be performed. Such tests require that $T_{\phi\phi}$ satisfy the following conditions:

1. for an isotropic material, $T_{\phi\phi}$ must be independent of ϕ;
2. for crack growth parallel to the fibers in a composite material, $T_{\phi\phi}$ must equal the transverse tensile strength, Y_t ;
3. for crack growth perpendicular to the fibers in a composite material, $T_{\phi\phi}$ must equal the longitudinal strength, X_t .

The definition of $T_{\phi\phi}$ used to satisfy these conditions is

$$T_{\phi\phi} = X_t \sin^2\beta + Y_t \cos^2\beta \ , \tag{1.2}$$

where β is the angle from the ϕ plane to the fiber axis (Figure 3).

Souma et al.[54] have recently proposed a theory for predicting fracture toughness (K_{IC}) as a function of the fiber angle for homogeneous anisotropic materials. The method of transforming the fracture toughness is very similar to that of the normal stress ratio theory :

$$K_{IC} = K_{IC}^{0} \cos^2\beta + K_{IC}^{90} \sin^2\beta \tag{1.3}$$

where K_{IC}^{0} and K_{IC}^{90} are derived as shown in Figure 4.

A description of the popular mixed mode fracture criteria in linear elastic fracture mechanics (LEFM) is given by Yehia[55] .

Another approach to fracture of composites has been at a more microscopic level and theories that take into account the heterogeneity of the material have been proposed. However, most of them have only been applied to special cases of crack orientation and loading condi-

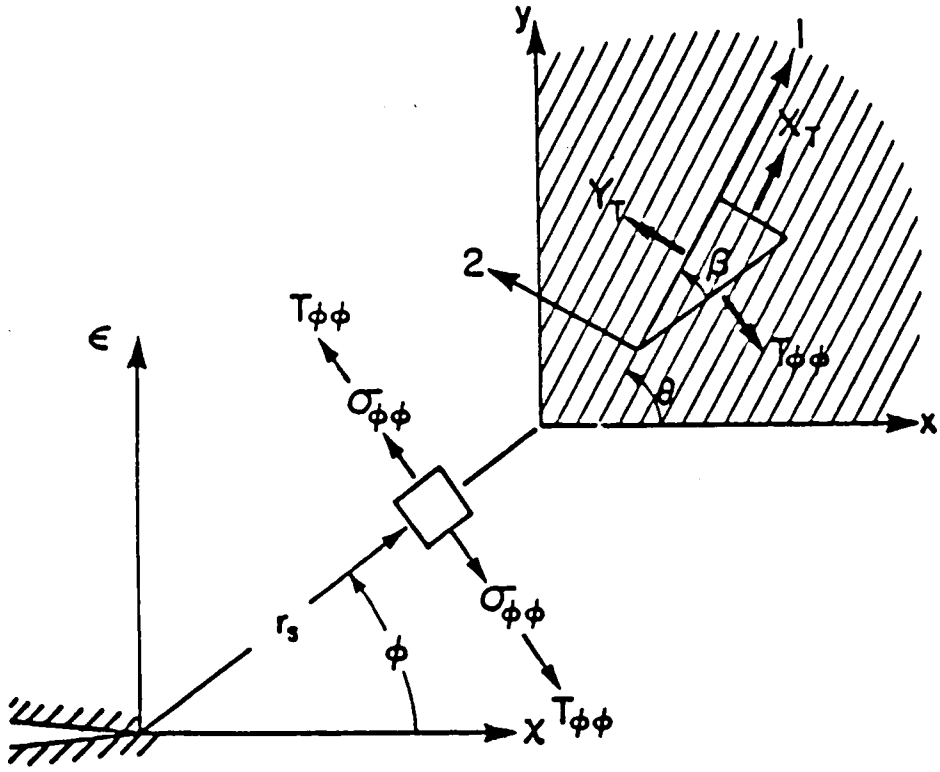

Figure 3. Parameters used in the NSR Theory

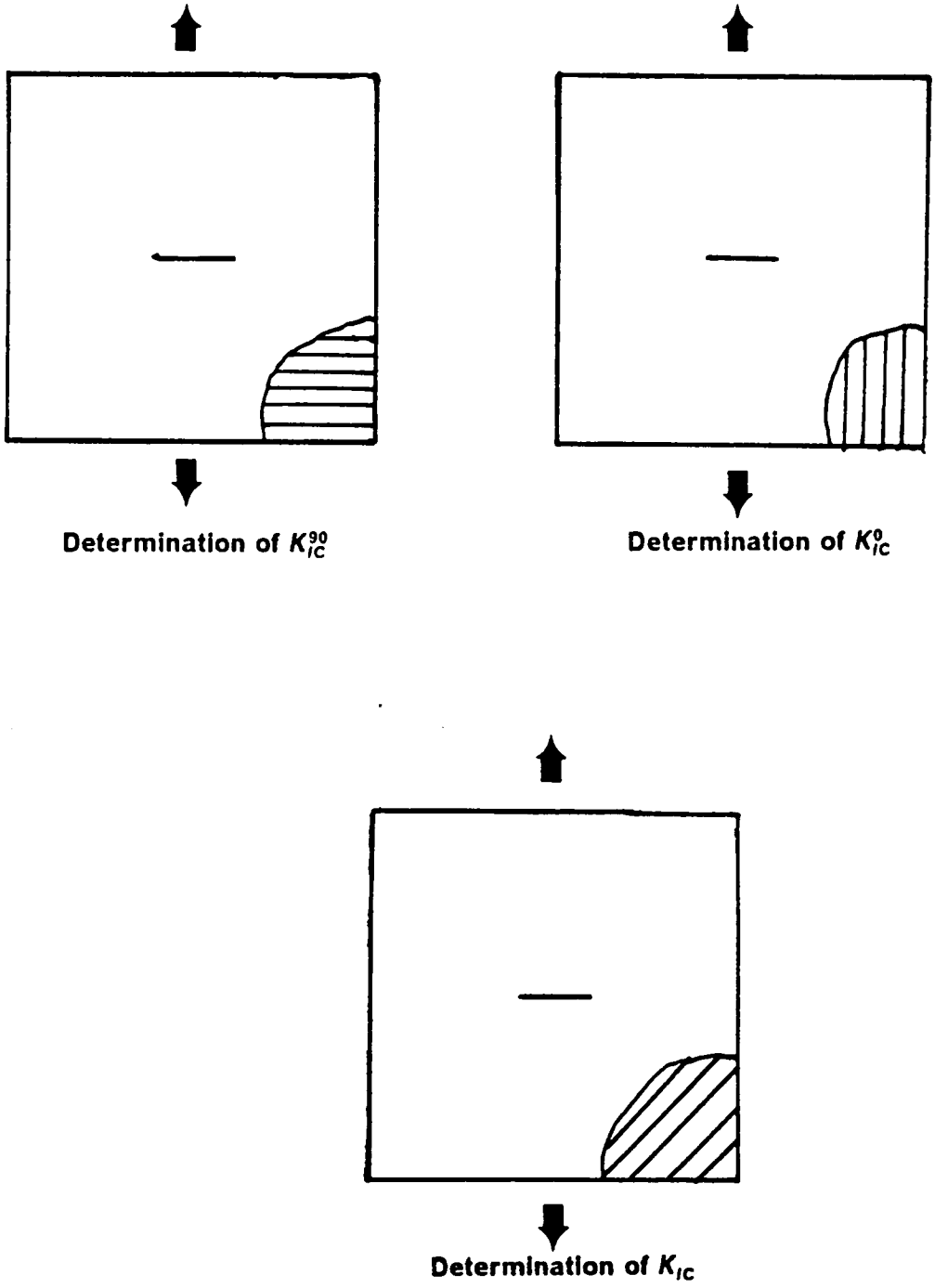

Figure 4. Calculation of K_{IC}

tions. The extension of the Strain Energy Density theory to a matrix model has been successful for cracks parallel to the fibers by Sih[56] . Poe and Sova[57] use a fracture toughness approach based on the determination of strains in the fiber near the crack tip, and have applied it to cracks perpendicular to fibers. The Hedgepeth[58] model determines a stress concentration factor using a shear-lag approach at the vicinity of the broken fibers.

From the outline of anisotropic fracture theories just given, it is obvious that a great deal of effort has been made to extend, with or without modification, mixed-mode isotropic theories to the analysis of anisotropic materials. All the above research efforts have made significant contributions to the prediction of fracture behavior of composites. The numerous theories proposed, based on different assumptions, have not yet proven to be completely compatible with experimental results.

1.3.3 Graphical Simulation of Crack Growth

The last two decades have witnessed rapid development in the areas of composite material analysis, finite element techniques, fracture mechanics and computer processing power. There is a need to integrate all these tools to provide the designer with information essential to the decision making process. Perhaps the most important and exciting development in computer analysis in the last decade is the advancement in the area of computer graphics. It has become a vital element in all CAD/CAM systems and analytical approaches which integrate computer graphics are an area to be exploited. For the engineer using computer based analytical approaches such as the finite element method or the boundary element method, graphical input and output of information provides control over the sophisticated analyses. Pre and post-processing of data can be extremely complex and time consuming and are subject to frequent human error. Interactive computer graphics systems eliminate a large portion of the man-machine interaction time to define the problem. Also, finite element programs typically

generate a large amount of numerical data, especially in three-dimensional problems, and the analyst can lose control over the postprocessing. Automatic graphical output and display provide a means of interpreting the results in an efficient way and numerical efforts popularly known as 'GIGO' (garbage in - garbage out) can be avoided. Two- and three- dimensional processors and high level language graphics standards which can serve as application program interfaces (API) are commercially available. It is the duty of the analyst to take advantage of these developments to achieve greater efficiency and reliability in the analysis procedure. With respect to this research effort, graphics provides a means to display,

- a menu driven simulation program
- 'zoomed' details of meshes
- deformed geometries and deflected shapes
- stress fields and contours (shaded and line drawings)
- crack growth paths
- updated plots of various parameters
- graphical output of other numerical information which can aid the design and decision making process.

The early approaches to crack modeling using finite elements and graphics assumed that the crack trajectory was known a priori and cracks were modeled with double nodes. These double nodes would be provided along the crack path, along the element edges, and as the crack propagated the nodes along the path would be separated. This lacked physical significance, as the crack was constrained to follow predefined elemental boundaries. Criteria for initiation of crack growth, direction and instability were based on simple tensile strength approaches and did not include any fracture mechanics principles. These techniques date back to the formative years of the finite element method when constant strain triangular elements, key punch input and simple algorithms were state-of-the-art.

Pioneering work which included procedures incorporating fracture mechanics principles and modern interactive computer graphics in crack propagation was done by Souma[59] , Ingraffea[60] and Yehia[55] . Their work was limited to isotropic materials. The methods adopted involved complex remeshing algorithms as conventional or quarter point elements were typi-

cally used to calculate the crack tip displacement and stress fields. Also, quarter point elements do not satisfy the field equations of elasticity around the crack, and determination of crack growth criteria parameters can depend on the size and shape of the element. There have been no attempts to employ special elements in modeling crack growth. To the author's knowledge, no attempt has been made in the past to analytically monitor crack growth in fibrous composites.

2.0 Singular Element Formulation

2.1 Element Stress and Displacement Fields

Figure 5 shows a through cracked composite lamina which can be assumed to be in a state of plane stress when modeled as a homogeneous anisotropic material subjected to in-plane loading. A stress function expansion in the vicinity of the crack tip is developed to formulate the stiffness matrix for the singular element. The stress function method of Lekhnitskii [61] is followed in the derivation.

The equations of equilibrium in the absence of body forces are :

$$\sigma_{ji,j} = 0 \tag{2.1}$$

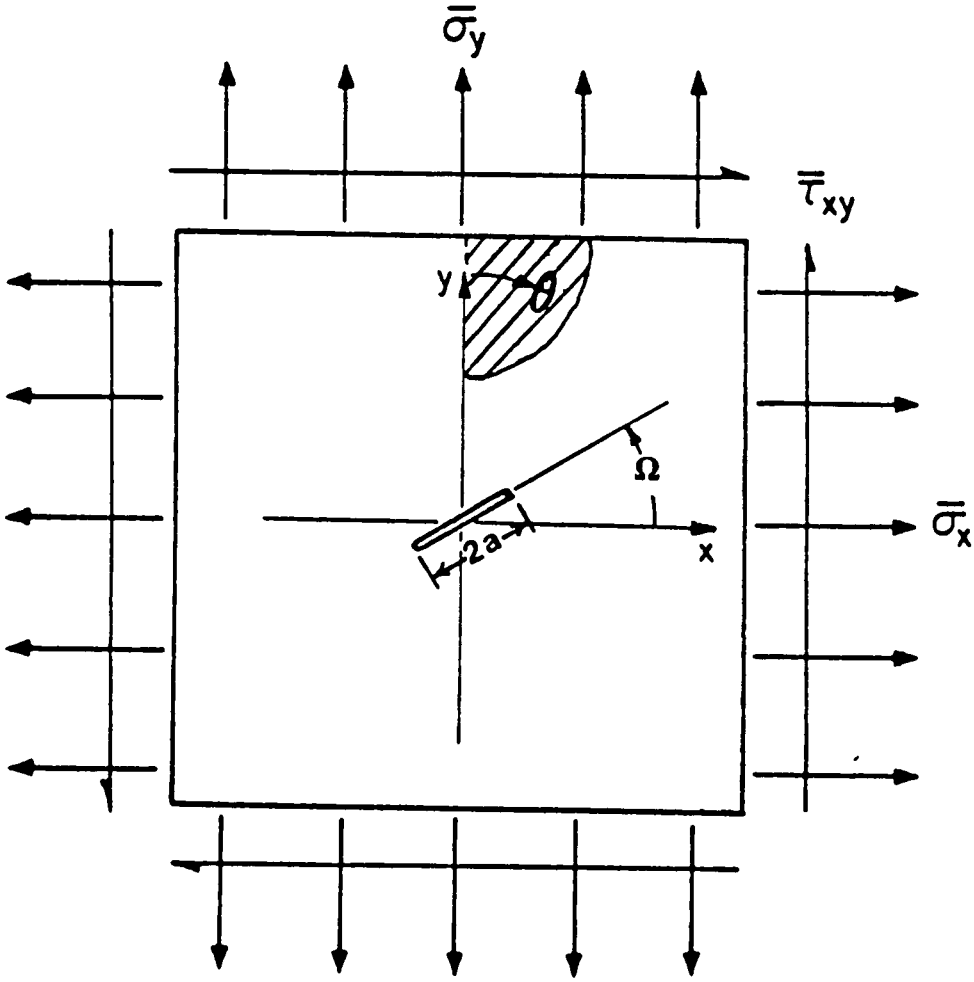

Figure 5. Unidirectional Lamina and Geometry of Problem

The strain-stress relations for the composite modelled as a homogeneous anisotropic material are :

$$\begin{Bmatrix} \varepsilon_x \\ \varepsilon_y \\ \gamma_{xy} \end{Bmatrix} = \begin{bmatrix} a_{11} & a_{12} & a_{16} \\ a_{12} & a_{22} & a_{26} \\ a_{16} & a_{26} & a_{66} \end{bmatrix} \begin{Bmatrix} \sigma_x \\ \sigma_y \\ \tau_{xy} \end{Bmatrix} \tag{2.2}$$

where a_{ij} are compliance coefficients which can be expressed (Appendix A) in terms of the elastic constants E_1, E_2, ν_{12} and G_{12}, defined in the material principal coordinate system, and the fiber orientation angle θ as shown in Figure 5.

A stress function, F, is defined such that :

$$\sigma_x = \frac{\partial^2 F}{\partial y^2}, \qquad \sigma_y = \frac{\partial^2 F}{\partial x^2}, \qquad \tau_{xy} = -\frac{\partial^2 F}{\partial x \partial y} \tag{2.3}$$

Substituting the stress-strain relations (2.2) into the compatibility equation :

$$\frac{\partial^2 \varepsilon_x}{\partial y^2} + \frac{\partial^2 \varepsilon_y}{\partial x^2} - \frac{\partial^2 \gamma_{xy}}{\partial x \partial y} = 0 \tag{2.4}$$

results in :

$$\frac{\partial^2}{\partial y^2}(a_{11}\sigma_x + a_{12}\sigma_y + a_{16}\tau_{xy}) + \frac{\partial^2}{\partial x^2}(a_{12}\sigma_x + a_{22}\sigma_y + a_{26}\tau_{xy})$$

$$- \frac{\partial^2}{\partial x \partial y}(a_{16}\sigma_x + a_{26}\sigma_y + a_{66}\tau_{xy}) = 0 \tag{2.5}$$

Substituting for the stresses in terms of the stress function F (eqn. (2.3)) the governing equation is obtained as :

$$a_{22}\frac{\partial^4 F}{\partial x^4} - 2a_{26}\frac{\partial^4 F}{\partial x^3 \partial y} + (2a_{12} + a_{66})\frac{\partial^4 F}{\partial x^2 \partial y^2} - 2a_{16}\frac{\partial^4 F}{\partial x \partial y^3} + a_{11}\frac{\partial^4 F}{\partial y^4} = 0 \tag{2.6}$$

This equation can be written in terms of differential operators as :

$$D_1 D_2 D_3 D_4 F = 0 \tag{2.7}$$

$$\text{where} \quad D_i = \left(\frac{\partial}{\partial y} - \mu_i \frac{\partial}{\partial x}\right), \quad i = 1,2,3,4$$

and μ_i are the roots of the characteristic eqn. :

$$a_{11}\mu^4 - 2a_{16}\mu^3 + (2a_{12} + a_{66})\mu^2 - 2a_{26}\mu + a_{22} = 0 \tag{2.8}$$

The four roots are never real; they are complex or purely imaginary[61] . The roots are denoted as :

$$\mu_1 = \alpha + i\beta, \quad \mu_2 = \gamma + i\delta$$

$$\mu_3 = \bar{\mu}_1 = \alpha - i\beta, \quad \mu_4 = \bar{\mu}_2 = \gamma - i\delta \tag{2.9}$$

Considering the case of unequal roots, $\mu_1 \neq \mu_2$, the stress function , F, obtained as a solution to (2.6) can be written as :

$$F = F_1(x + \mu_1 y) + F_2(x + \mu_2 y) + F_3(x + \bar{\mu}_1 y) + F_4(x + \bar{\mu}_2 y) \tag{2.10}$$

Introducing the notation : $Z_1 = x + \mu_1 y$ and $Z_2 = x + \mu_2 y$ and recognizing that F must be real, we obtain F from equation (2.10) as :

$$F = 2\,Real\,[F_1(Z_1) + F_2(Z_2)] \tag{2.11}$$

The stresses (2.3) can now be written in terms of the stress function as :

$$\sigma_x = 2\,Real\,[\ \mu_1^2 F_1''(Z_1) + \mu_2^2 F_2''(Z_2)\ ]$$

$$\sigma_y = 2\,Real\,[\ F_1''(Z_1) + F_2''(Z_2)\ ] \tag{2.12}$$

$$\tau_{xy} = -2\,Real\,[\ \mu_1 F_1''(Z_1) + \mu_2 F_2''(Z_2)\ ]$$

where the primes denote differentiation. After integration of the strain-displacement equations the displacements are obtained as :

$$u = 2\,Real\,[p_1F_1'(Z_1) + p_2F_2'(Z_2)] + rigid\ body\ terms$$

$$v = 2\,Real\,[q_1F_1'(Z_1) + q_2F_2'(Z_2)] + \ rigid\ body\ terms \qquad (2.13)$$

where :

$$p_k = a_{11}\mu_k^2 + a_{12} - a_{16}\mu_k \ \wedge \ q_k = a_{12}\mu_k + \frac{a_{22}}{\mu_k} - a_{26} \ , \quad (k = 1\,,\,2)$$

p_k and q_k can be written in complex form (as μ_k is complex) for k = 1,2 as :

$$p_1 = \hat{p}_1 + i\hat{p}_2 \ , \quad p_2 = \tilde{p}_1 + i\tilde{p}_2 \ , \ q_1 = \hat{q}_1 + i\hat{q}_2 \ , \quad q_2 = \tilde{q}_1 + i\tilde{q}_2$$

where :

$$\hat{p}_1 = a_{11}(\alpha^2 - \beta^2) + a_{12} - a_{16}\alpha \ , \quad \hat{p}_2 = 2a_{11}\alpha\beta - a_{16}\beta$$

$$\tilde{p}_1 = a_{11}(\gamma^2 - \delta^2) + a_{12} - a_{16}\gamma \ , \quad \tilde{p}_2 = 2a_{11}\gamma\delta - a_{16}\delta$$

$$\hat{q}_1 = a_{12}\alpha + a_{22}\frac{\alpha}{\alpha^2 + \beta^2} - a_{26} \ , \quad \hat{q}_2 = a_{12}\beta - a_{22}\frac{\beta}{\alpha^2 + \beta^2}$$

$$\tilde{q}_1 = a_{12}\gamma + a_{22}\frac{\gamma}{\gamma^2 + \delta^2} - a_{26} \ , \quad \tilde{q}_2 = a_{12}\delta - a_{22}\frac{\delta}{\gamma^2 + \delta^2}$$

The stresses (2.12) can be written in the form [62] :

$$\sigma_x + \sigma_y = 2\,Re\,[\ (1 + \mu_1^2)F_1''(Z_1) + (1 + \mu_2^2)F_2''(Z_2)\ ]$$

$$\sigma_y - \sigma_x + 2i\tau_{xy} = 2\,Re[\,(1 - \mu_1^2)\,F_1''(Z_1) \ + \ (1 - \mu_2^2)\,F_2''(Z_2)\ ] \qquad (2.14)$$

$$- 4iRe[\mu_1F_1''(Z_1) + \mu_2F_2''(Z_2)]$$

Transformation of the stresses into polar coordinates (Figure 6) results in :

$$\sigma_\phi + i\tau_r\phi = Re[(1+\mu_1^2)F_1''(Z_1) + (1+\mu_2^2)F_2''(Z_2)]$$

$$+ e^{2i\phi}\ Re[(1-\mu_1^2)F_1''(Z_1) + (1-\mu_2^2)F_2''(Z_2)]$$

$$- \ 2i\ Re[\mu_1 F_1''(Z_1) + \mu_2 F_2''(Z_2)] \qquad (2.15)$$

where :

$Z_1 = x + \mu_1 y = r_1 e^{i\theta_1}$, $Z_2 = x + \mu_2 y = r_2 e^{i\theta_2}$

$r_1 = r\sqrt{\cos\phi + \alpha \sin\phi^2 + \beta^2 \sin^2\phi}$, $r_2 = r\sqrt{\cos\phi + \gamma \sin\phi^2 + \delta^2 \sin^2\phi}$

$\theta_1 = arctan\dfrac{\beta \sin\phi}{\cos\phi + \alpha \sin\phi}$, $\theta_2 = arctan\dfrac{\delta \sin\phi}{\cos\phi + \gamma \sin\phi}$

and r and ϕ are the polar coordinates shown in Figure 6.

Expanding the stress functions in Laurent series of the forms :

$$F_1(Z_1) = \sum_{-\infty}^{\infty} A_j \frac{Z_1^{\lambda_j+1}}{\lambda_j+1} \ , \ F_2(Z_2) = \sum_{-\infty}^{\infty} B_j Z_2^{\lambda_j+1} \ ; \ (\ j = 0, \pm 1, \pm 2, ..) \qquad (2.16)$$

where A_j, B_j, λ_j are unknowns obtained from the boundary conditions. A_j and B_j are, in general, complex constants and can be written as $A_j = a_{1j} + ia_{2j}$ and $B_j = b_{1j} + ib_{2j}$.

For the stress free crack shown in Figure 6, the boundary conditions are :

$$[\sigma_\phi + i\tau_{r\phi}]_{\phi=\pm\pi} = 0 \qquad (2.17)$$

Substituting into (2.15) for the stresses in terms of the stress function F, (eqn. (2.16)), and solving the resulting eigenvalue problem associated with the above boundary conditions yields

$$A_j + B_j(\lambda_j + 1) + \{[\bar{A}_j + \bar{B}_j(\lambda_j + 1)]e^{-2(\lambda_j - 1)i\phi}\}_{\phi=\pm\pi} = 0$$

and

$$\mu_1 A_j + \mu_2 B_j(\lambda_j + 1) + \{[\bar{\mu}_1\bar{A}_j + \bar{\mu}_2\bar{B}_j(\lambda_j + 1)]e^{-2(\lambda_j - 1)i\phi}\}_{\phi=\pm\pi} = 0 \qquad (2.18)$$

where $j = \pm 1, \pm 2, \pm 3, ...$

For a non-trivial solution at $\phi = \pm \pi$, the eigenvalues are :

$$\lambda_j = \frac{j}{2} \quad , \quad (j = +1, +2, \ etc.) \qquad (2.19)$$

where j begins from 1 for the displacements to be finite.

Other forms for the complex stress functions F_1 and F_2 can be assumed. They will produce the same final result although the eigenvalues may be different. Wang [34] used the form :

$$F_k = \sum \frac{C_k Z_k^{n+2}}{(n+1)(n+2)} \quad , \quad k = 1,2. \qquad (2.20)$$

for analyzing the free edge effect in composite laminates.

Two cases arise depending on the material properties:

(i) The real parts of the roots of the characteristic equation (2.8) are equal ($\alpha = \gamma$),

For the material systems studied, this case is obtained when the fibers are at 0° or 90° relative to the crack.

(ii) The real parts of (2.8) are different ($\alpha \neq \gamma$) .

Typically, for the material systems studied, this case is obtained when the fibers are at angles other then 0° or 90° relative to the crack.

Substituting for the stresses (2.15) in equation (2.18), the constants of the stress function can be obtained as :

Case (i) : $\alpha = \gamma$

$$a_{1j} = \frac{-\delta(2j+1)b_{1j}}{2\beta}$$

$$a_{2j} = \frac{-(2j+1)b_{2j}}{2} \tag{2.21}$$

Case (ii) : $\alpha \neq \gamma$

$$a_{2j} = \frac{-\left[\beta a_{1j} + b_{1j}\gamma\frac{(2j+1)}{2}\right]}{\alpha-\gamma}$$

$$b_{2j} = \frac{\left[\beta a_{1j} + b_{1j}\gamma\frac{(2j+1)}{2}\right]}{\frac{(2j+1)}{2}(\alpha-\gamma)} \tag{2.22}$$

As the constants are dependent, the number of unknowns in the stress function expansions reduces by half. The stress function can be obtained in series form from which the stresses (2.12) and displacements (2.13) can be written in series form for the above two cases.

Note that the following definitions have been used in equations (2.23-2.26) :

$$\lambda_j = \frac{2j-1}{2} \quad , \quad \zeta = \lambda_j + 1 \quad , \quad \psi = \lambda_j \quad , \quad \omega = \lambda_j - 1 \quad , \quad \chi = \alpha - \gamma$$

Case (i) ($\alpha = \gamma$)

Stress Components :

$$\sigma_x = 2\sum_{j=1}^{\infty} \zeta\psi\left[b_{1j}\left\{r_1^{\omega}\left(-(\alpha^2-\beta^2)\frac{\delta}{\beta}\cos\omega\theta_1 + 2\alpha\delta\sin\omega\theta_1\right)\right.\right.$$

$$+ r_2^{\omega} \left((\gamma^2 - \delta^2) \cos \omega\theta_1 - 2\gamma\delta \sin \omega\theta_1\right) \Big\}$$

$$+ b_{2j} \Big\{ r_1^{\omega} \left(2\alpha\beta \cos \omega\theta_1 + (\alpha^2 - \beta^2) \sin \omega\theta_1 \right)$$

$$+ r_2^{\omega} \left(- \gamma\delta \cos \omega\theta_1 - (\gamma^2 - \delta^2) \sin \omega\theta_1\right) \Big\} \Big] \qquad (2.23)$$

$$\sigma_y = 2\sum_{j=1}^{\infty} \zeta\psi \left[b_{1j} \left\{ - r_1^{\omega} \frac{\delta}{\beta} \cos \omega\theta_1 + r_2^{\omega} \cos \omega\theta_2 \right\} + b_{2j} \left\{ r_1^{\omega} \sin \omega\theta_1 - r_2^{\omega} \sin \omega\theta_2 \right\} \right]$$

$$\tau_{xy} = -2\sum_{j=1}^{\infty} \zeta\psi \left[b_{1j} \left\{ r_1^{\omega} \left(- \alpha \frac{\delta}{\beta} \cos \omega\theta_1 + \delta \sin \omega\theta_1 \right) + r_2^{\omega} \left(\gamma \cos \omega\theta_2 - \delta \sin \omega\theta_2 \right) \right\} \right.$$

$$\left. + b_{2j} \left\{ r_1^{\omega} \left(\beta \cos \omega\theta_1 + \alpha \sin \omega\theta_1 \right) - r_2^{\omega} \left(\delta \cos \omega\theta_2 + \gamma \sin \omega\theta_2 \right) \right\} \right]$$

Displacements :

$$u = 2\sum_{j=1}^{\infty} \zeta \left[b_{1j} \left\{ r_1^{\psi} \left(\frac{\delta}{\beta} - \hat{p}_1 \cos \psi\theta_1 + \hat{p}_2 \sin \psi\theta_1 \right) \right.\right.$$

$$\left. + r_2^{\psi} \left(\tilde{p}_1 \cos \psi\theta_2 - \tilde{p}_2 \sin \psi\theta_1 \right) \right\} + b_{2j} \left\{ r_1^{\psi} \left(\hat{p}_2 \cos \psi\theta_1 + \hat{p}_1 \sin \psi\theta_1 \right) \right. \qquad (2.24)$$

$$\left.\left. - r_2^{\psi} (\tilde{p}_2 \cos \psi\theta_2 + \tilde{p}_1 \sin \psi\theta_2) \right\} \right]$$

The v component of the displacement is obtained by replacing $\hat{p}_k$ by $\hat{q}_k$ and $\tilde{p}_k$ by $\tilde{q}_k$, (k = 1,2) in the above equation (2.24).

Case (ii) ($\alpha \neq \gamma$)

Stress Components :

$$\sigma_x = 2\sum_{j=1}^{\infty} \psi\ a_{1j}\left\{r_1^{\omega}\left((\alpha^2-\beta^2)+2\beta^2\frac{\alpha}{\chi}\ \cos\omega\theta_1+\beta\frac{(\alpha^2-\beta^2)}{\chi}-2\alpha\beta\sin\omega\theta_1\right)\right.$$

$$\left.-r_2^{\omega}\left(2\alpha\beta\frac{\delta}{\chi}\cos\omega\theta_2+\ (\gamma^2-\delta^2)\frac{\beta}{\chi}\sin\omega\theta_2\right)\right\}$$

$$+\zeta\psi\ \ b_{1j}\left\{r_1^{\omega}\left(2\alpha\beta\frac{\delta}{\chi}\cos\omega\theta_1+\delta\frac{(\alpha^2-\beta^2)}{\chi}\sin\omega\theta_1\right)\right.$$

$$\left.+r_2^{\omega}\left((\gamma^2-\delta^2)-2\delta^2\frac{\gamma}{\chi}\cos\omega\theta_2-1\right)\right\}$$

$$\sigma_y = 2\sum_{j=1}^{\infty} \psi\ \ a_{1j}\left\{r_1^{\omega}\left(\cos\omega\theta_1+\frac{\beta}{\chi}\sin\omega\theta_1\right)-r_2^{\omega}\frac{\beta}{\chi}\sin\omega\theta_2\right\}$$

$$+\zeta\psi\ \ b_{1j}\left\{r_1^{\omega}\ \ \frac{\delta}{\chi}\sin\omega\theta_1+r_2^{\omega}\left(\cos\omega\theta_2-\frac{\delta}{\chi}\sin\omega\theta_2\right)\right\} \qquad (2.25)$$

$$\tau_{xy} = -2\sum_{j=1}^{\infty} \psi\ a_{1j}\left\{r_1^{\omega}\left(\alpha+\frac{\beta^2}{\chi}\ \ \cos\omega\theta_1-\beta+\alpha\frac{\beta}{\chi}\sin\omega\theta_1\right)\right.$$

$$- r_2^{\omega}\left(\beta\frac{\delta}{\chi}\cos\omega\theta_2 - \beta\frac{\gamma}{\chi}\sin\omega\theta_2\right)\Bigg\}$$

$$+\zeta\psi\ \ b_{1j}\Bigg\{r_1^{\omega}\left(\beta\frac{\delta}{\chi}\cos\omega\theta_1 + \alpha\frac{\delta}{\chi}\sin\omega\theta_1\right)$$

$$+ r_2^{\omega}\left(\gamma - \frac{\delta^2}{\chi}\ \ \cos\omega\theta_2 - \ \delta + \gamma\frac{\delta}{\chi}\ \ \sin\omega\theta_2\right)\Bigg\}$$

Displacements :

$$u = 2\sum_{j=1}^{\infty} a_{1j}\Bigg\{r_1^{\psi}\left(\hat{p}_1\cos\psi\theta_1 + \hat{p}_2\frac{\beta}{\chi}\cos\psi\theta_1 - \hat{p}_2\sin\psi\theta_1 + \hat{p}_1\frac{\beta}{\chi}\sin\psi\theta_1\right)$$

$$- r_2^{\psi}\left(\tilde{p}_2\frac{\beta}{\chi}\cos\psi\theta_2 + \tilde{p}_1\frac{\beta}{\chi}\sin\psi\theta_2\right)\Bigg\}$$

$$+\ \ b_{1j}\ \zeta\Bigg\{r_1^{\psi}\left(\hat{p}_2\frac{\delta}{\chi}\cos\psi\theta_1 + \hat{p}_1\frac{\delta}{\chi}\sin\psi\theta_1\right) \qquad (2.26)$$

$$+ r_2^{\psi}\left(\tilde{p}_1\cos\psi\theta_2 - \tilde{p}_2\frac{\delta}{\chi} - \tilde{p}_2\sin\psi\theta_2 - \tilde{p}_1\frac{\delta}{\chi}\sin\psi\theta_2\right)\Bigg\}$$

The v component of the displacement is obtained by replacing $\hat{p}_k$ by $\hat{q}_k$ and $\tilde{p}_k$ by $\tilde{q}_k$, (k = 1,2) in the above equation (2.26).

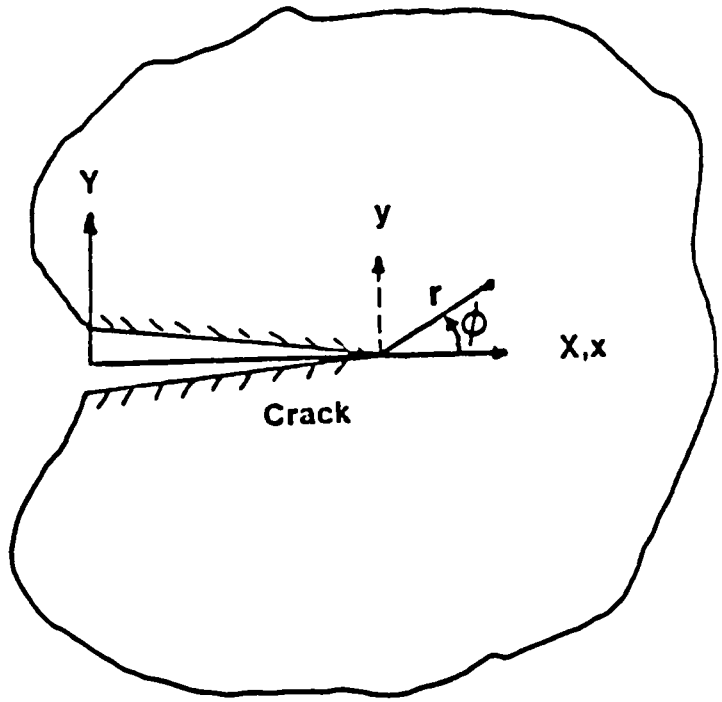

Figure 6. Crack Tip Coordinate System

2.2 Element Stiffness Matrix

The strain energy of an element V^e can be written :

$$V^e = h^e \iint \{ \frac{1}{2} a_{11}\sigma_x^2 + a_{12}\sigma_x\sigma_y + a_{16}\sigma_x\tau_{xy} + \frac{1}{2} a_{22}\sigma_y^2 + a_{26}\sigma_y\tau_{xy} + \frac{1}{2} a_{66}\tau_{xy}^2 \} \, d\Omega \qquad (2.27)$$

where Ω is the element domain and h^e the element thickness. Each term in the stress expansions (2.23 & 2.25) has four constants a_{1j}, a_{2j}, b_{1j} and b_{2j}. Taking S terms in the stress expansions (2.23 & 2.25), 2S constants are obtained as the constants are related (2.21,2.22). The 2S constants denote in matrix form as :

$$\overline{C}^T = [c_1 \; c_2 \; ..... \; c_{2S}] \qquad (2.28)$$

where c_1, c_2, c_3, c_4, *etc.* are :

from (2.21) : b_{1j}, b_{2j}, $j = 1,2....$ (for $\alpha = \gamma$)

and from (2.22) : a_{2j}, b_{2j}, $j = 1,2....$ (for $\alpha \neq \gamma$)

Differentiating V^e with respectto each term in $\overline{C}$, the element 'sub-stiffness' matrix , $[k^e]$, is obtained by minimizing the strain energy of the element with respect to the unknown constants

$$[k^e]\overline{C} = \frac{\partial V^e}{\partial \overline{C}} \qquad (2.29)$$

Substituting for the stresses (2.23 & 2.25), the element 'sub-stiffness' matrix can be written:

$$k_{ij}^e = h^e \iint \{a_{11}\overline{\sigma}_{xi}\overline{\sigma}_{xj} + a_{12}(\overline{\sigma}_{xi}\overline{\sigma}_{yj} + \overline{\sigma}_{yi}\overline{\sigma}_{xj}) ..... \} d\Omega \qquad (2.30)$$

where $\overline{\sigma}_{\xi}$ is the coefficient of the term c_i in the expansion for σ_x , $\overline{\sigma}_{yi}$ is the coefficient of the term c_i in the expansion for σ_y , etc. in equations (2.23) and (2.25).

The evaluation of the above double integral (2.27) can be performed numerically. As shown in Figure 7, a circular domain can be chosen for the element. The stresses are then expressed in terms of polar coordinates r and ϕ. If a circular element is used as the singular element, it can then be surrounded by quadratic quadrilateral or triangular elements which match the geometry of the singular element exactly.

However, the formulation is general and the shape can be changed to an n-sided polygon as desired, depending on the details of the mesh surrounding the singular element and on the requirements and capabilities of automatic mesh generators, if used. The number of terms, S, in the stress expansion (2.23 & 2.25), the number of nodes, N, of the element and the element size can be varied depending on mesh parameters.

For a singular element with N nodes, the cartesian components of the displacements u and v can be written in matrix form as :

$$\underline{\delta}^T = [u_1 \; v_1 \; u_2 \; v_2 \quad \ldots\ldots \quad u_N \; v_N] \tag{2.31}$$

Substituting the nodal coordinates of the singular element into the displacement equations (2.24 & 2.26) a matrix equation of the form

$$[L]\{\bar{C}\} = \underline{\delta} \tag{2.32}$$

is obtained. $[L]$ is the matrix of the coefficients of the constants of expansion c_i in the displacement equations and is of the order 2N x 2S. Using a least squares fit to minimize the displacement discontinuity between the singular element and the adjoining conventional elements[63] , equation (2.32) yields :

$$\{\bar{C}\} = (L^T L)^{-1} L^T \underline{\delta} \tag{2.33}$$

Therefore, the total stiffness matrix of the singular element is :

$$\bar{K}^e = \{\bar{C}\}^T k^e \{\bar{C}\}$$

$$\bar{K}^e = ((L^T L)^{-1} L^T)^T \; [k^e] \; (L^T L)^{-1} L^T \tag{2.34}$$

$\bar{K}^e$ is a 2N x 2N symmetric matrix of known quantities, and the least squares 'smoothing' makes the nodal displacements the nodal degrees of freedom in the singular element. Once $\bar{K}^e$ is calculated, it can be superposed onto any conventional displacement based finite element program to form the global stiffness matrix of the problem. The resulting displacements are used to calculate the coefficients of the stress expansions using equation (2.33). The stresses at any point around the crack tip can be obtained by substituting for the calculated coefficients of the stress expansions (2.28) in the equations for the stresses (2.23 & 2.25).

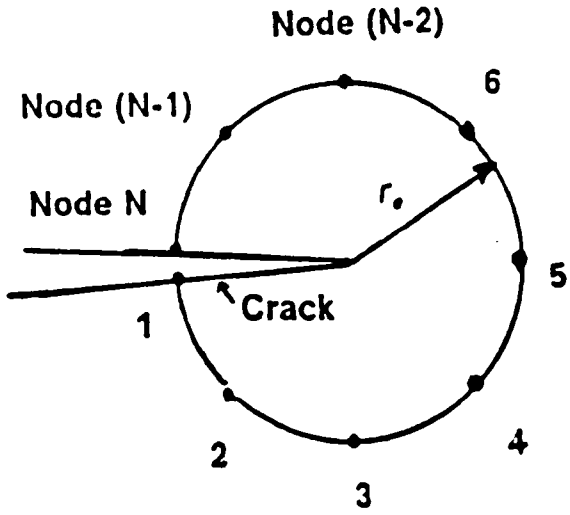

Figure 7. Singular Element Geometry and Node Numbering System

3.0 Validation of the Singular Element

3.1 Introduction

Chapter 2 describes the formulation of an anisotropic singular finite element (ASE) based on stress function expansions. This chapter presents results obtained using the element to study cracked, homogeneous anisotropic materials subjected to far field tensile loading.

The singular element was used to obtain stress intensity factors and stress distributions around the crack tip of a cracked anisotropic material representative of unidirectional graphite epoxy. Fiber angles of $\theta = 0°$, $60°$ and $90°$ (measured from the Y axis, Figure 8) with a crack parallel to the X axis, and a fiber angle of $\theta = 0°$ with the crack oriented at an angle of $-30°$ to the positive X axis were analyzed for tensile loading in the Y direction in order to demonstrate the generality and validity of the formulation.

The individual terms of the stiffness matrix of the singular element derived in Chapter 2 were incorporated into the global stiffness matrix of the region modeled, at the corresponding degrees of freedom, in an existing, conventional, displacement based finite element program which includes the capability for analyzing anisotropic materials. Meshes employing quadratic

triangular and/or quadrilateral elements (Figure 8) can be used in the analysis. The parameters which can be varied are :

- The number of nodes, N, of the singular element and their locations (Figure 7)
- The number of terms, S, in the stress and displacement expansions (eqns. 2.23-2.26)
- The singular element radius, r_e (Figure 7)

The element parameters N and r_e can be suitably chosen to meet the requirements of the surrounding finite element mesh.

Implementation of the singular element into a global mesh is flexible. The crack tip need not be at the center of the singular element. It is only required that the geometry of the element and the crack be specified and that the integration scheme adopted for the 'sub-stiffness' matrix be general enough to account for the shape of the element (It is noted that the formulation in Chapter 2 is based upon a coordinate system centered at the crack tip). The interelement continuity requirement between the singular element and the adjacent elements is satisfied only in a least squares sense, but the results show that the least squares procedure appears to be adequate for coupling the singular element to conventional elements.

3.2 Results and Discussion

3.2.1 Case (i)

For a plate with a central horizontal crack (along the X axis) and for fiber angles of $\theta = 0°$ and 90°, only a quarter of the plate need be analyzed due to the symmetry of the problem (Figure 8). As stated in Chapter 2 , these cases yield equal real parts of the characteristic equation (eqn. 2.8), ($\alpha = \gamma$) for the material system and crack geometry studied. In fact, for these cases, α and γ are both zero and the roots are purely imaginary. Figure 8 shows the

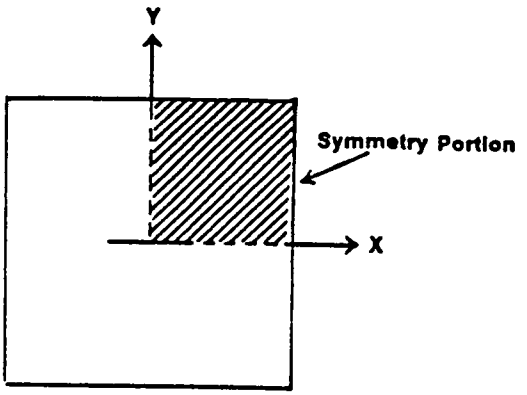

Full Plate

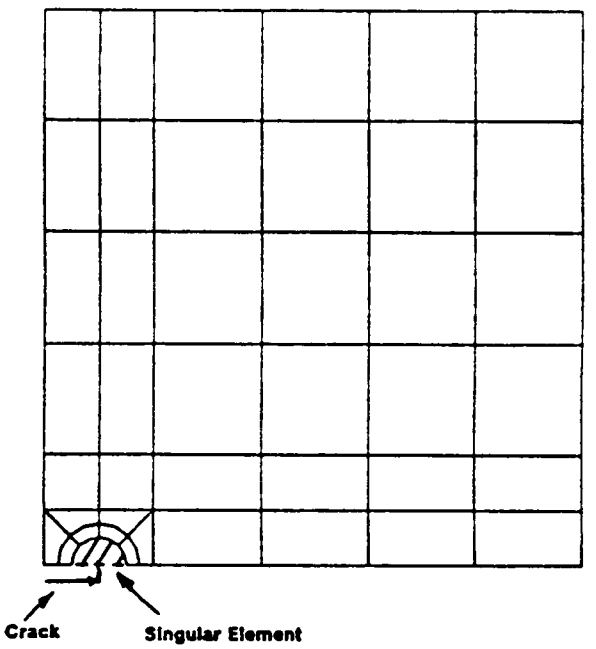

Figure 8. Quarter Symmetry Mesh Employed for Case (i)

mesh of the quarter plate used for the analysis. Studies were performed using the singular element to analyze the effect of changing the variable parameters N,S, and r_e.

Stress Intensity Factors :

Stress intensity factors (SIF) can be calculated directly using the stress function expansions. A derivation based on the formulation of Chapter 2 follows. By definition, the mode I stress intensity factor K_I is :

$$K_I = \lim_{r \to 0} \sqrt{2\pi r}\, \sigma_y|_{\phi=0} \tag{3.1}$$

Substituting for the first term of the stress expansion, for $\sigma_y|_{\phi=0}$, (eqn. 2.23) yields :

$$\sigma_y|_{\phi=0} = 2\zeta\psi \;\; b_{1j} \; (-r_1^{\omega} \frac{\delta}{\beta} + r_2^{\omega})$$

and

$$\omega = -\frac{1}{2}, \quad \zeta = \frac{3}{2}, \quad \psi = \frac{1}{2}, \quad r_1^{\omega} = r_2^{\omega} = \frac{1}{\sqrt{r}}, \quad \theta_1 = \theta_2 = 0 \tag{3.2}$$

giving,

$$\sigma_y|_{\phi=0} \;\; = \;\; \frac{3}{2} \; b_{1j} \; \frac{1}{\sqrt{r}} (-\frac{\delta}{\beta} + 1) \tag{3.3}$$

Substituting (3.3) into (3.1) :

$$K_I = \sqrt{2\pi} \; \frac{3}{2} \, b_{1j} (-\frac{\delta}{\beta} + 1) \tag{3.4}$$

where β and δ are the imaginary parts of the roots of the characteristic equation (eqn. 2.8) and the term b_{1j} is the value of the constant in the stress function obtained by substituting the displacements $\underline{\delta}$ from the finite element solution into equation (2.33).

The SIF can be represented in terms of the 'finite width correction factor', Y, as

$$K_I = Y\,\bar{\sigma}\sqrt{a} \quad \Rightarrow \quad Y = \frac{K_I}{\bar{\sigma}\sqrt{a}} \tag{3.5}$$

Using (3.4) :

$$Y = \frac{\sqrt{2\pi}\,\frac{3}{2}\,b_{1j}\left(-\frac{\delta}{\beta}+1\right)}{\bar{\sigma}\sqrt{a}} \tag{3.6}$$

where $\bar{\sigma}$ is the applied uniform far-field loading and 'a' is the semi crack length. Appendix C presents a complete derivation of the stress intensity factors for the various cases.

Finite width correction factors for a representative unidirectional graphite epoxy material were calculated using the above formula and the results were compared with those obtained by other authors[29,64,65] . A 9" long x 3" wide plate with a central crack of 1.2" was analyzed under inplane tensile loading. The material properties used are given in Table 6 (Appendix B). Only a quarter of the plate was modeled due to symmetry and the ASE had a radius of 0.3" (half the semi-crack length) and nine nodes.

This same problem has been solved by others. Snyder and Cruse [64] used a boundary integral equation method. A special finite element employing the elasticity solution based on Wilson's[24] approach was used by Chou, et al. [65] for both 8 and 10 noded elements. Heppler and Hansen [30] used a singular element with a formulation analogous to Benzley[28] . Figures 9 and 10 show the variation in the correction factor, Y, obtained using the ASE as a function of the number of terms, S, in the stress expansions compared with results from literature[30,64,65] . In the figures, two values are shown for Ref. [30]. They correspond to the highest and lowest values obtained from five different mesh configurations.

For the fiber at $\theta = 90°$ (Figure 9), a converging trend is observed as the number of terms is increased from one to three, and Y remains essentially constant for three to six terms. All the results shown fall within the bounds provided by the other methods. Addition of more than six terms in the stress expansion results in a downward trend in the value of Y. It is noted that

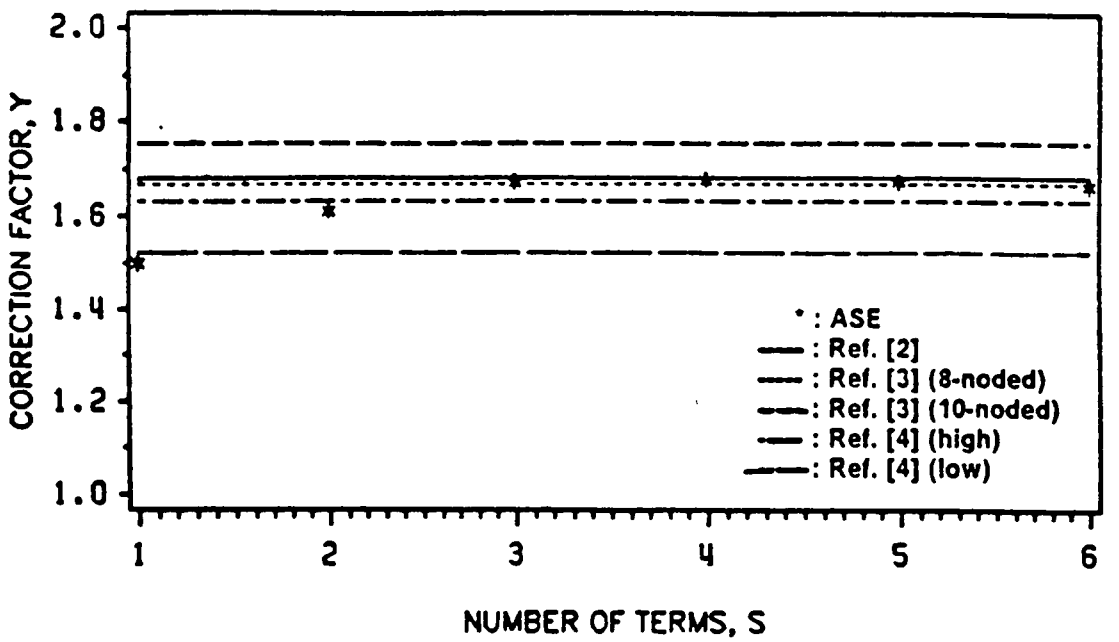

Figure 9. Correction Factor, Y versus Number of Terms, S (θ = 90°)

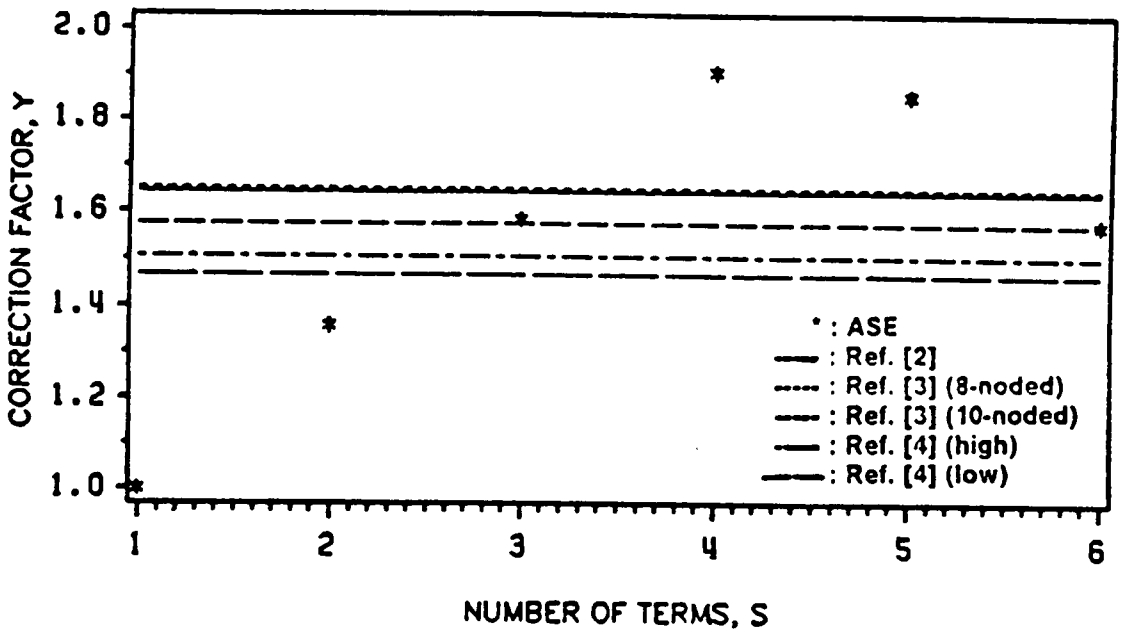

Figure 10. Correction Factor, Y versus Number of Terms, S (θ = 0°)

the stress expansions contain the term $r_{\bullet}^{\lambda}$, where $\lambda = \frac{2j-1}{2}$ (j = 1,2,3..S) and an increase in the number of terms results in a stiffening effect, thereby reducing the value of Y.

The case of $\theta = 0°$ (Figure 10) shows an oscillatory behavior of the ASE results as the number of terms is increased. A similar oscillation for this case of $\theta = 0°$ was also observed in Ref. [30] where a non-converging pattern was obtained for the different mesh parameters used. For this case, the principal material direction is along the direction of loading and experiences the majority of the load resulting in high stress gradients around the crack tip. The values of the finite width correction factor, Y, obtained using the singular element are compared with the values presented in Refs. [30,64,65] (Table 1).

The values obtained using the ASE are averages for S = 1 to 6 terms. It is noted that the value considered representative of Ref. [30] in Table 1 is the one which had the minimum percentage difference when compared to Refs. [64,65]. The values for $\theta = 0°$ and 90° taken from Ref. [30] correspond to two different meshes and, depending on the mesh parameters used, the percentage difference obtained (when compared to Refs. [64,65]) ranged from -0.3 percent to -13.6 percent.

It is evident from Table 1, Figure 9 and Figure 10 that the results obtained using the anisotropic singular element (ASE) are in excellent agreement for the 90° case and reasonable agreement for the 0° case with the other approaches. The correction factor, Y, predicted by the ASE falls between the values obtained by other methods (Refs. [64,65] and Ref. [30]) for the 90° fiber orientation. Unfortunately, the results are more sensitive to the number of terms for the 0° fiber orientation. The next section presents results of changing the various ASE parameters.

Stress Distributions :

Stress distributions around the crack tip obtained using the singular element are compared to those predicted using quarter point elements in Figs. 11-16. The quarter point element (QPE) is used as a basis for comparison, as it has been found to give reasonably accurate results when compared to an infinite plate elasticity solution and because the other references cited

Table 1. Finite Width Correction Factors, Y

FINITE WIDTH CORRECTION FACTORS, Y					
Fiber Angle θ	Anisotropic Singular Element (ASE)[a]	Ref [64] (difference from ASE)	Ref [65][b] (difference from ASE)	Ref [65][c] (difference from ASE)	Ref [30] (difference from ASE)
90°	1.633	1.683 (+2.9%)	1.669 (+2.1%)	1.755 (+6.9%)	1.523 (-7.2%)
0°	1.57	1.645 (+4.5%)	1.652 (+4.9%)	1.578 (+0.5%)	1.507 (-4.1%)

a : average of S = 1 to 6
b : 8 - noded element
c : 10 - noded element

did not present stress results. The comparison of ASE and QPE results demonstrates how well a coarse mesh with the singular element compares to a QPE solution with a high density mesh.

The elastic properties of the material system used for this portion of the study are presented in Table 5 (Appendix B). The three inplane components of stress, σ_x, σ_y, τ_{xy} were calculated at a distance r/a = 0.002 and plotted as a function of the angle ϕ about the crack tip, measured from the horizontal axis. The r/a ratio of 0.002 was chosen as the point of comparison because it corresponds to a Gauss point of the QPE. The mesh employing the singular element had 42 elements with 157 nodes (288 d.o.f) while the mesh employing the quarter point elements had 125 elements with 268 nodes (512 d.o.f). The length of the quarter point element radial side was 0.025 inches which is one-tenth the radius of the singular element. This small radius for meshes employing quarter point elements leads to a very fine mesh in the vicinity of the crack tip and a correspondingly higher number of degrees of freedom and increased requirements for computer resources.

There is a significant reduction in total computing time when the special element is used because :

- mesh generation is faster and simpler
- the number of degrees of freedom is reduced significantly
- the bandwidth of the global stiffness matrix is reduced significantly

Finally and possibly most importantly, the ASE gives analytic and continuous variations of stresses as opposed to the QPE which gives stresses at discrete points which must be followed by additional calculations if stresses are required at other points within the element.

Figures 11-13 show the angular variations of the three components of stress, σ_x, σ_y and τ_{xy}, respectively, with a varying number of terms, S, in the stress expansion for a fiber angle of $\theta = 90°$ and the crack parallel to the fiber direction. It is evident from these figures that the ASE results do not always converge monotonically with increasing number of terms, S but they do converge generally.

The results predicted by the anisotropic singular element are generally in good agreement with those obtained using quarter point elements. The mesh used for the analysis using quarter point elements (QPE) is shown in Figure 17. For all the stress components, the general trends from the ASE and QPE are quite similar. For some stress components and some ϕ locations, the ASE results converged towards the QPE results. However, for other components and locations, the ASE results converge away from the QPE results. It is noted that the comparison with the QPE is not absolute but only provides a means to predict and compare trends and relative magnitudes. Also, only a representative mesh using the QPE is used. Depending on the ASE parameters chosen, the three components of stress behave differently. All three components do not converge (or diverge) from the QPE results in a similar fashion. Figure 11 predicts that the σ_x component converges towards the QPE result as the number of terms increase, while the σ_y component shows better correlation with the QPE for lesser number of terms in the expansion. The τ_{xy} stresses predicted by the ASE gives good correlation with the QPE for ϕ (measured counter clockwise from the crack tip) up to 90° for a higher number of terms and then improves for a lesser number of terms as ϕ is increased. The oscillatory behavior of the stress

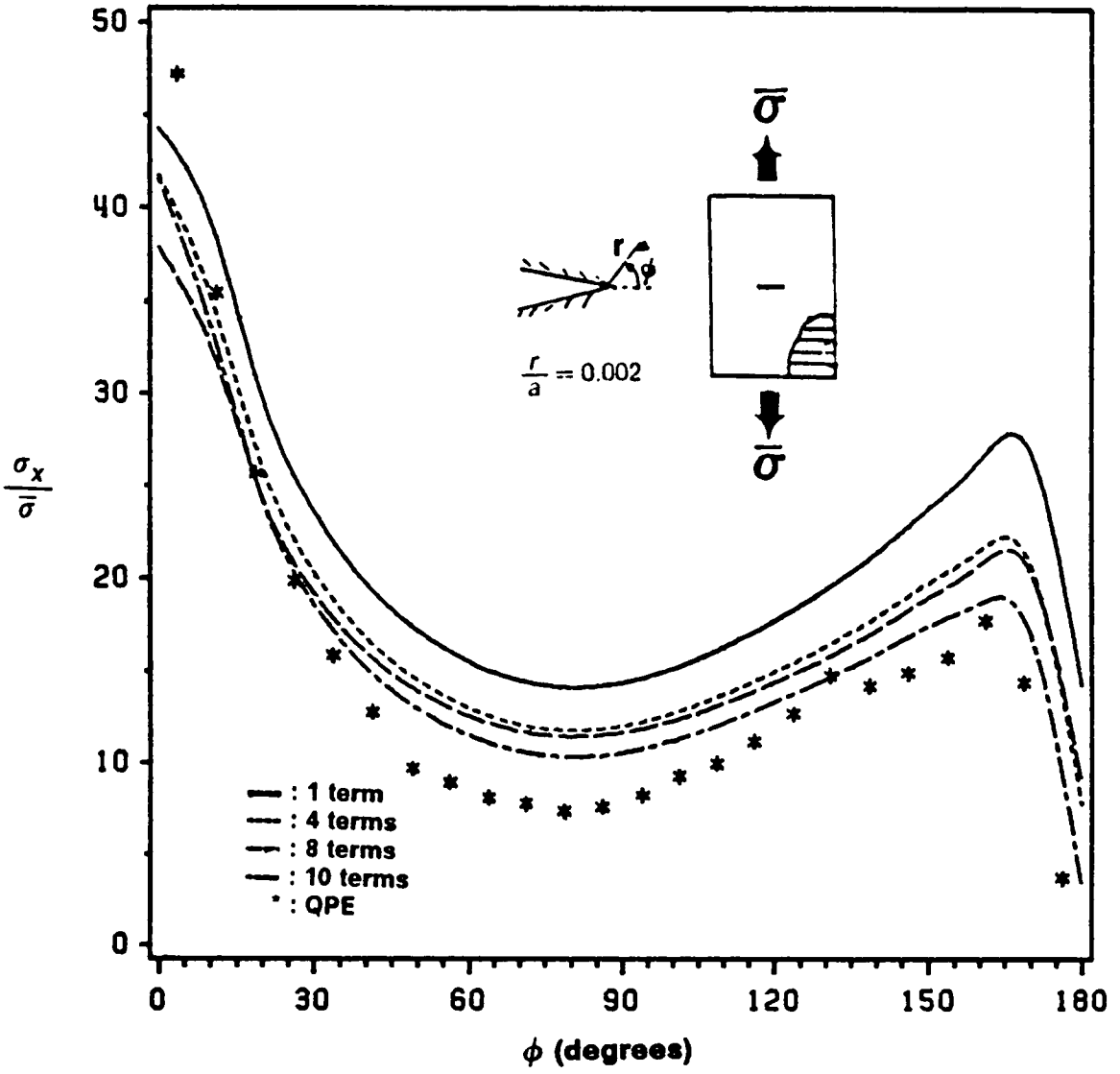

Figure 11. Angular Variation In σ_x with Number of Terms,S

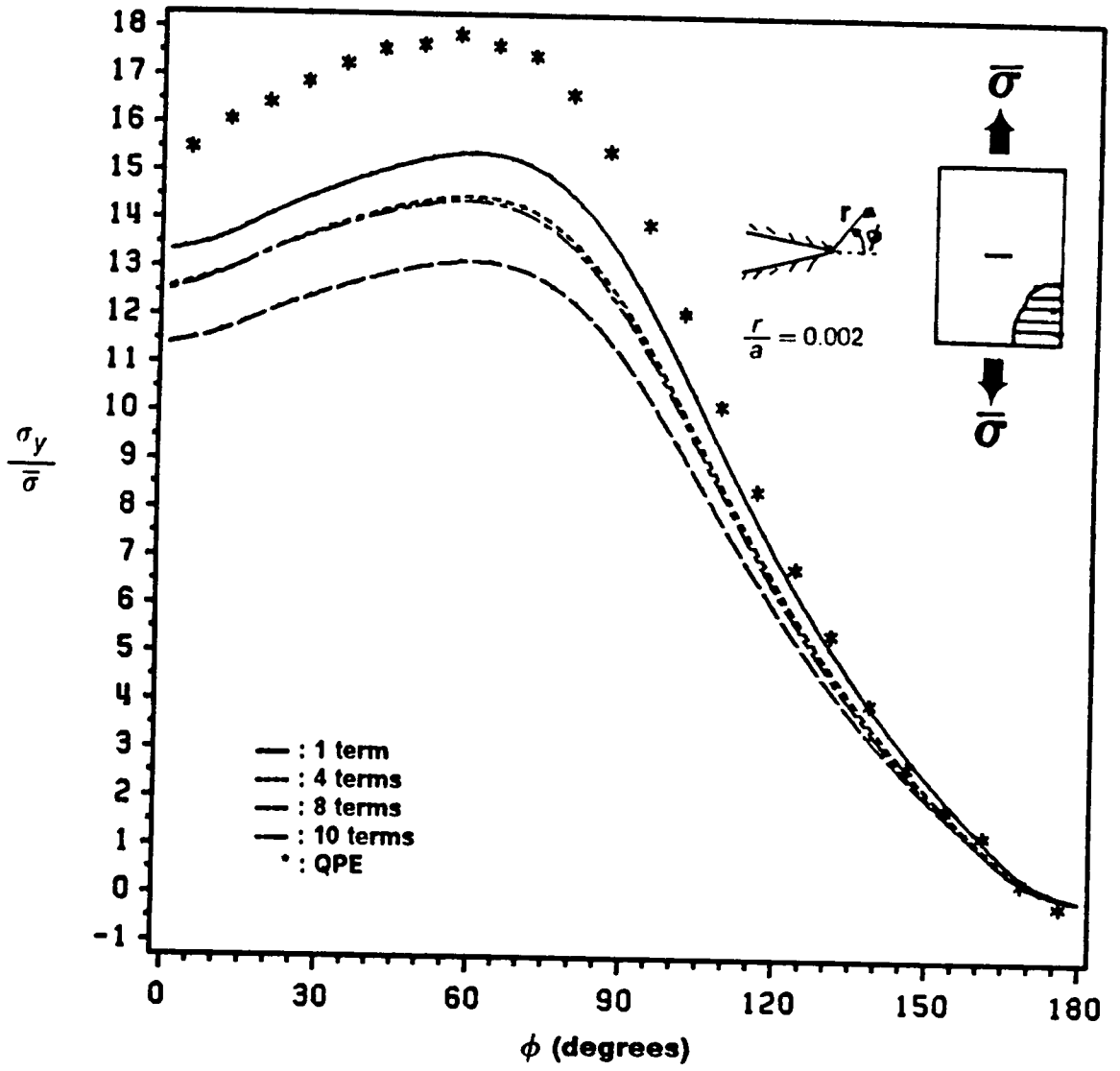

Figure 12. Angular Variation in σ_y with Number of Terms,S

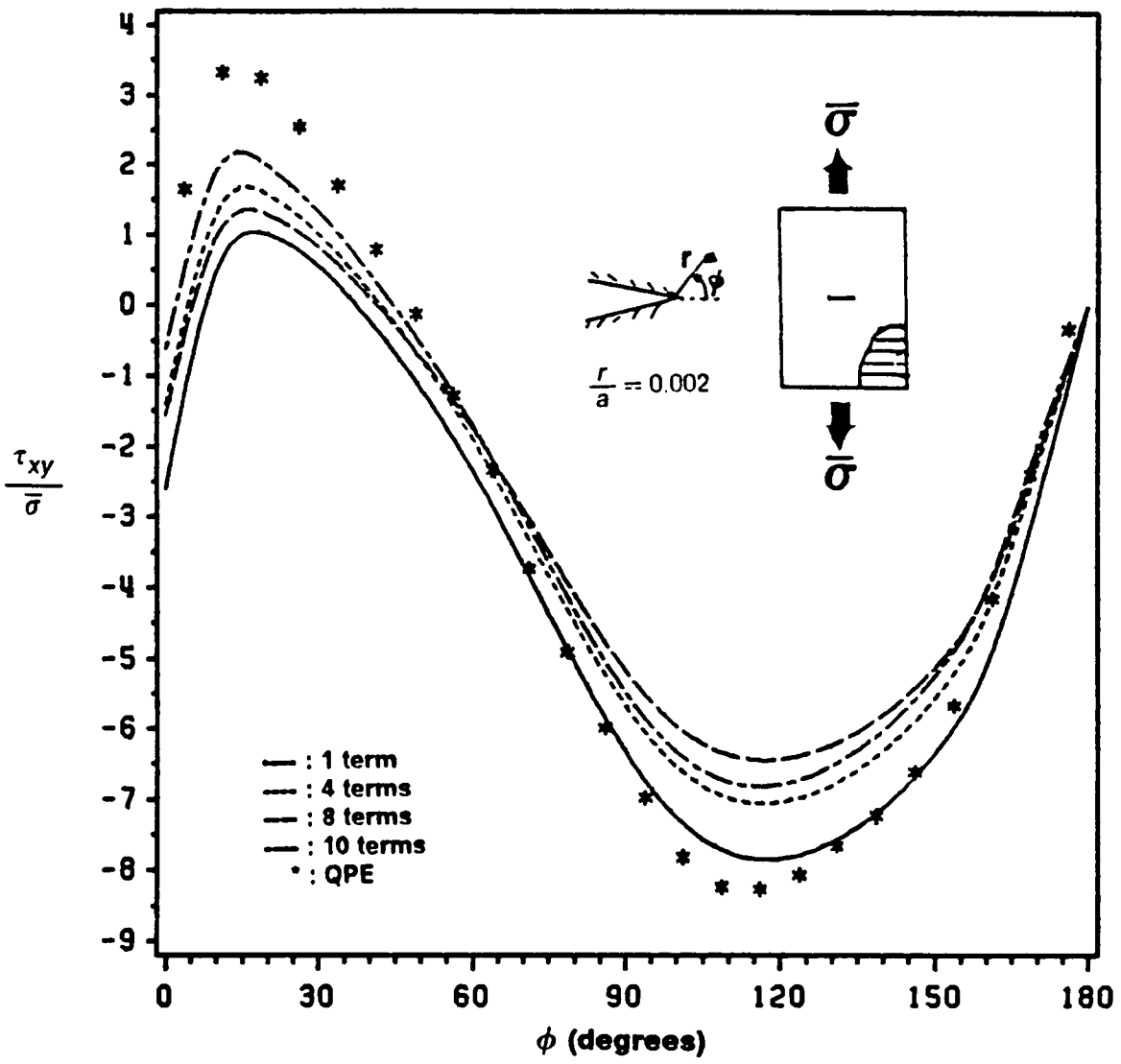

Figure 13. Angular Variation in τ_{xy} with Number of Terms,S

distributions predicted by the ASE may be attributed to the nature of the non-conforming element based on series solutions.

To make the parametric study more complete, the effects of ASE radius size, r_o, and the number of nodes of the singular element, N, on the predicted angular variations of the stress components were also studied. Figures 14-16 show stress component variations for the two radii $r_o = 0.125''$ and $r_o = 0.25''$ and different number of nodes for the singular element (N=9,11). The behavior of the various stress components for the different ASE parameters in Figs. 14-16 follows a similar trend as when different terms, S, are used in the stress expansion (Figs. 11-13). A large number of nodes (N=11) and a small radius ($r_o = 0.125''$) gives good correlation when compared to the QPE in the σ_x component, but deviates from the QPE for the σ_y component.

The ASE results are believed to be more accurate both because of the analytic formulation and the relative independence from mesh parameters. Also, the mathematical modelling of the $r^{-\frac{1}{2}}$ singularity in the QPE does not account for the angular variation in the stress field and the traction free boundary conditions on the crack surface.

3.2.2 Case (ii)

A. Crack along the X-axis :

Stress variations for a fiber angle of $\theta = 60°$ and with the crack along the X-axis were obtained using the ASE. Unequal real parts ($\alpha \neq \gamma$) are obtained for the roots of the characteristic equation for this case.

Inversion symmetry [68] was exploited for the off-axis cases so that only one half of the plate then need be modeled (as opposed to a full plate if inversion symmetry were not used). A finite element model is a set of N equations with N unknowns. Inversion symmetry conditions introduce M new equations, reducing the number of equations and unknowns to (N – M). Inversion symmetry is a symmetry condition present in anisotropic shells and plates whose geometry,

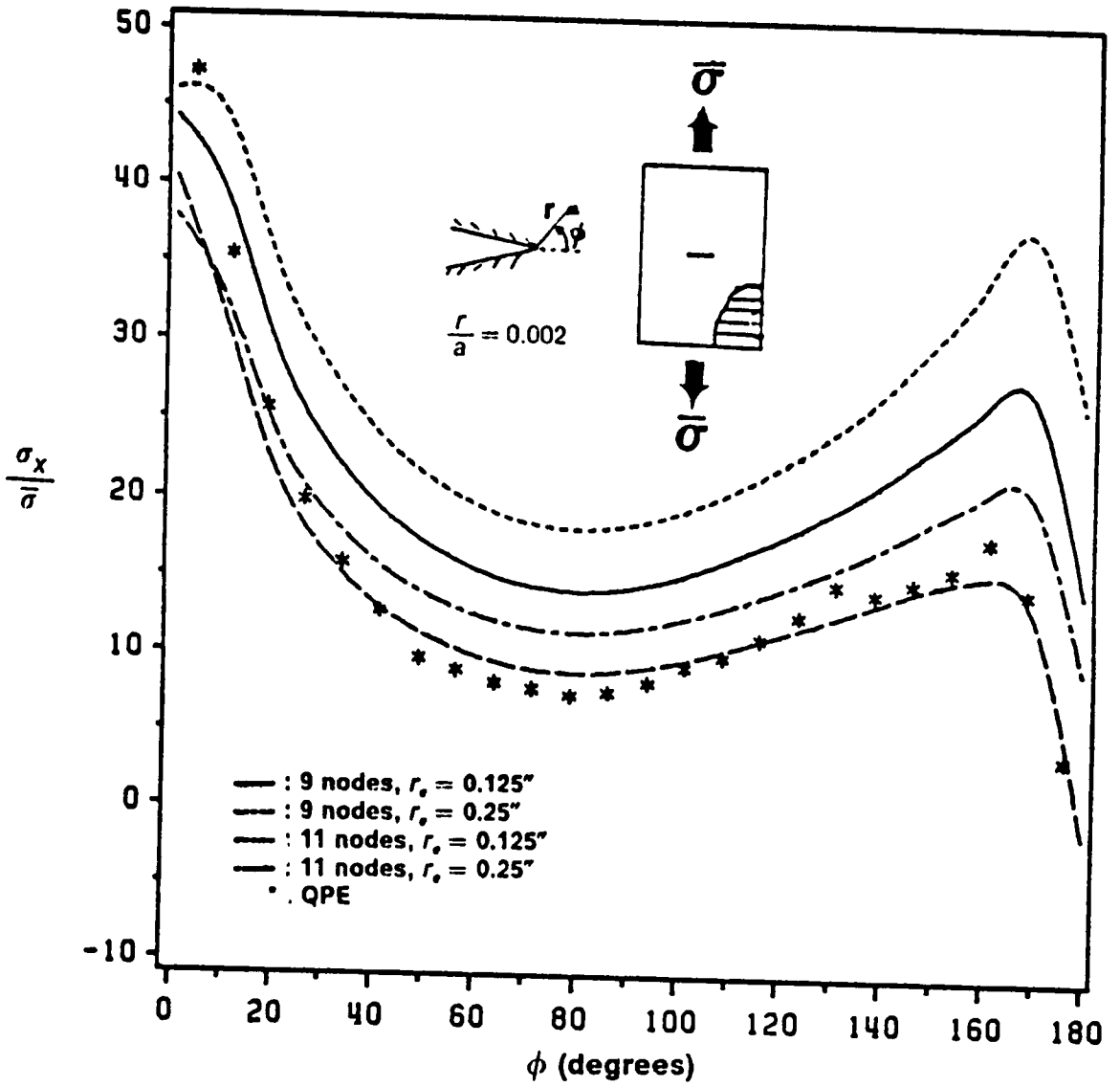

Figure 14. Angular Variation in σ_x

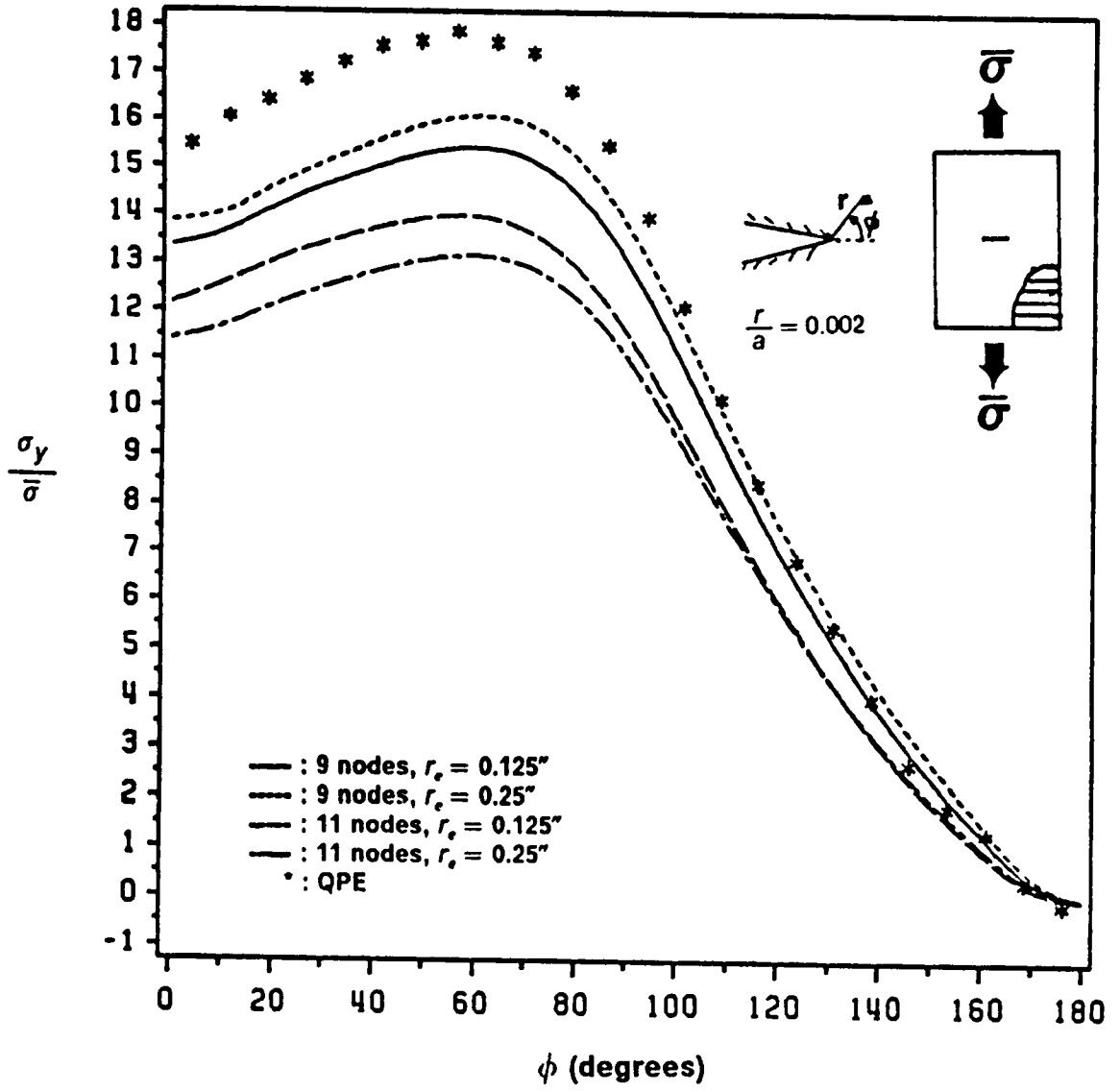

Figure 15. Angular Variation in σ_y

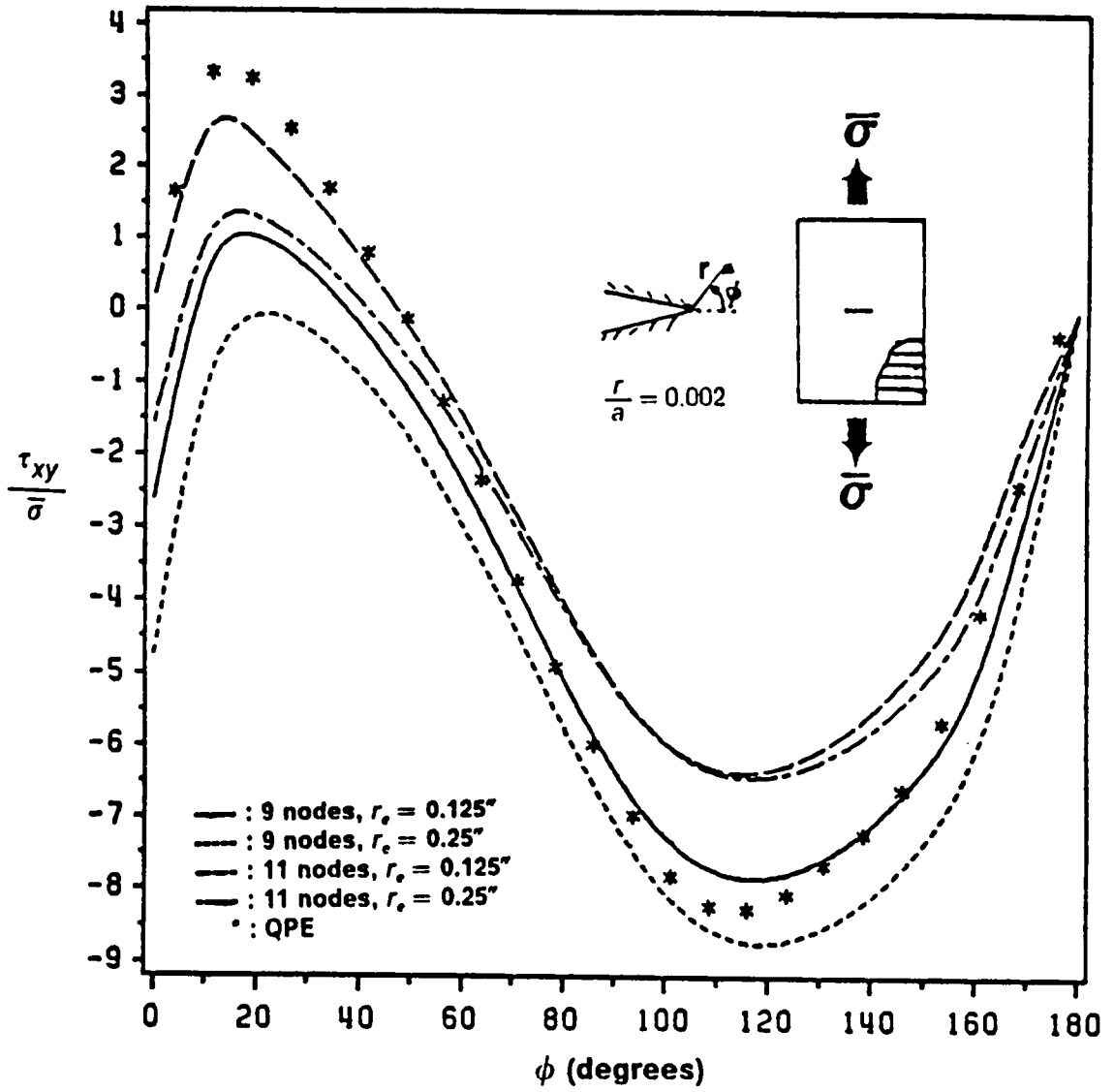

Figure 16. Angular Variation in τ_{xy}

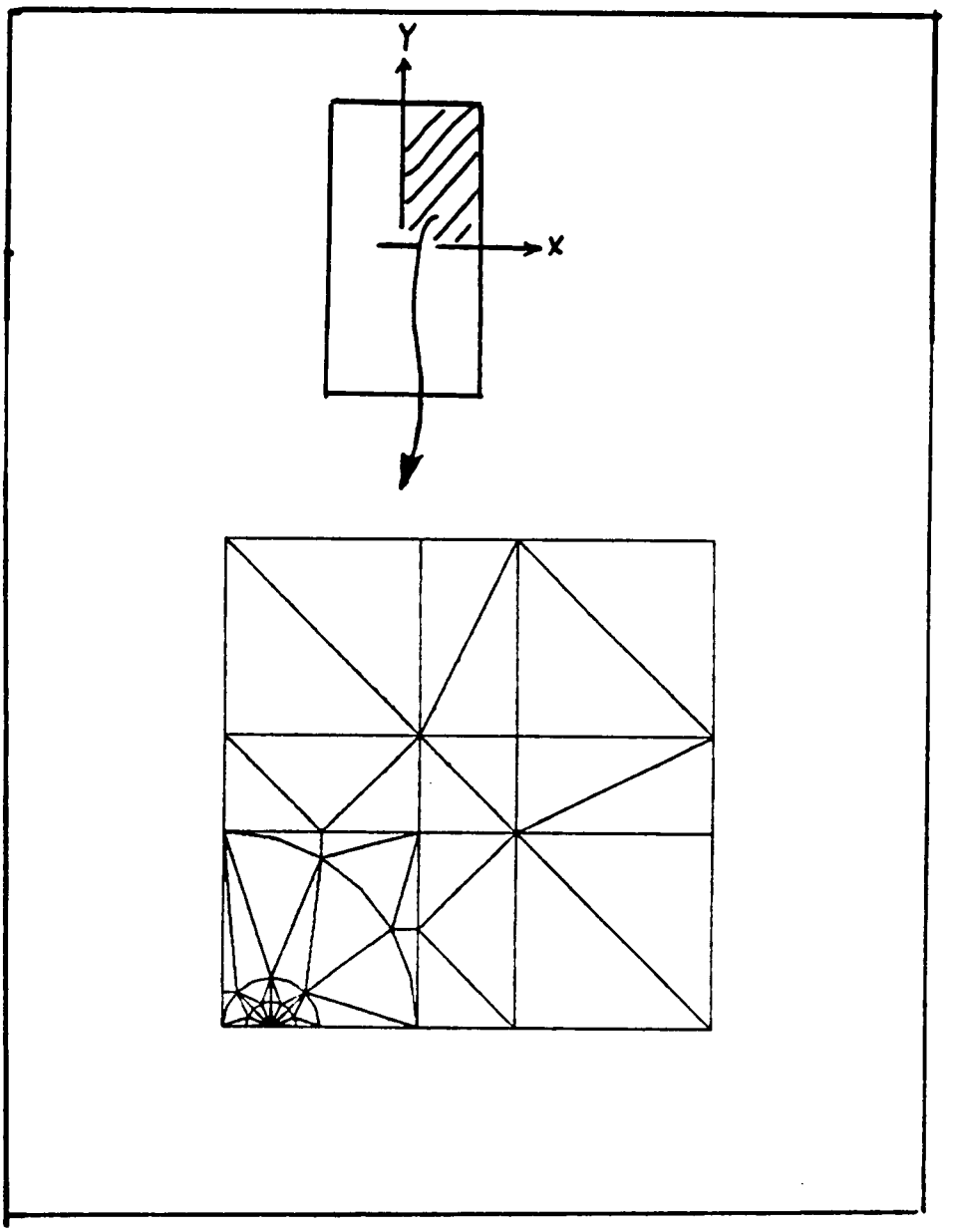

Figure 17. QPE Mesh Using Quarter Symmetry for Case (i)

elastic coefficients, boundary conditions and loading are 180° rotationally symmetric about some axis. The details of implementation of this method to finite element programs is given by Noor and Mathers [68].

An off-axis plate with a central crack under uniaxial loading exhibits inversion symmetry. The center of symmetry coincides with the center of the crack. Any line passing through the center of symmetry and dividing the plate into two half sections may be used to reduce the region of study for the finite element model. A 6" long x 2" wide plate with a 0.2" central crack was analyzed. The axial center line was chosen as the line of symmetry in this study. Figure 18 shows the mesh employed with inversion symmetry taken into account. The half-plate mesh (dimensions : 6" long x 1.0" wide and semi-crack length of 0.1") using the ASE consists of 62 elements and 219 nodes (438 d.o.f.) while the mesh employing quarter point elements (also incorporating inversion symmetry) employ 208 elements with 480 nodes (958 d.o.f.). Figure 22 shows the mesh used when the QPE is employed with inversion symmetry taken into account. There is a significant savings in CPU time when the singular element is used due to a large reduction in bandwidth. The quarter point element program required approximately ten times the CPU time required by the program incorporating the ASE.

Stress fields for a 60° coupon with a central crack under tensile loading obtained using the ASE are compared with results using the QPE in Figs. 19a,20a,21a. The stress components are plotted as function of the angle from the crack tip (ϕ , measured counter clockwise). There is good correlation between the QPE results and the results predicted by the ASE. The radius of the ASE for the case presented was $r_e = 0.05$" (half the semi-crack length) with the number of nodes, N equal to 17. It is seen from the figures (Figs. 19a-21a) that the trends and the magnitudes of the various stress components predicted by the ASE and QPE are in good agreement.

B. Crack inclined to the X-axis :

A crack inclined at $-30°$ to the X-axis with the fibers at $\theta = 90°$ (along the X-axis) also yields unequal real parts of the roots of the characteristic equation. The crack analyzed for this case was at an angle of $-30°$ to the positive X-axis and with the fibers at $\theta = 0°$. A superposition method was adopted so that the same mesh with the crack along the X-axis could be used for the $-30°$ crack case. Figure 24 shows this procedure. This case also exhibits inversion symmetry and only one half of the plate need be modelled. The same finite element mesh as in the previous case (Sec. 2.2.1) was used in the analysis and the program accounts for the crack rotation by transforming the loadings (Figure 24). The results obtained using this method are compared to those obtained using the quarter point element and are shown in Figs. 19b,20b,21b. The mesh employing quarter point elements is shown in Figure 23. There is excellent correlation between the stress components predicted by the ASE and the QPE.

The good comparison also gives confidence to the superposition method adopted for angle cracks as the QPE results did not employ this procedure of separation for far-field stresses used in the ASE program.

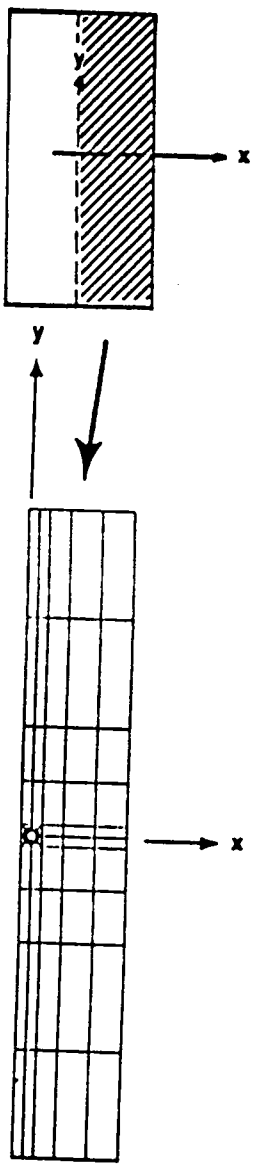

Figure 18. Inversion Symmetry Mesh used for Case (ii)

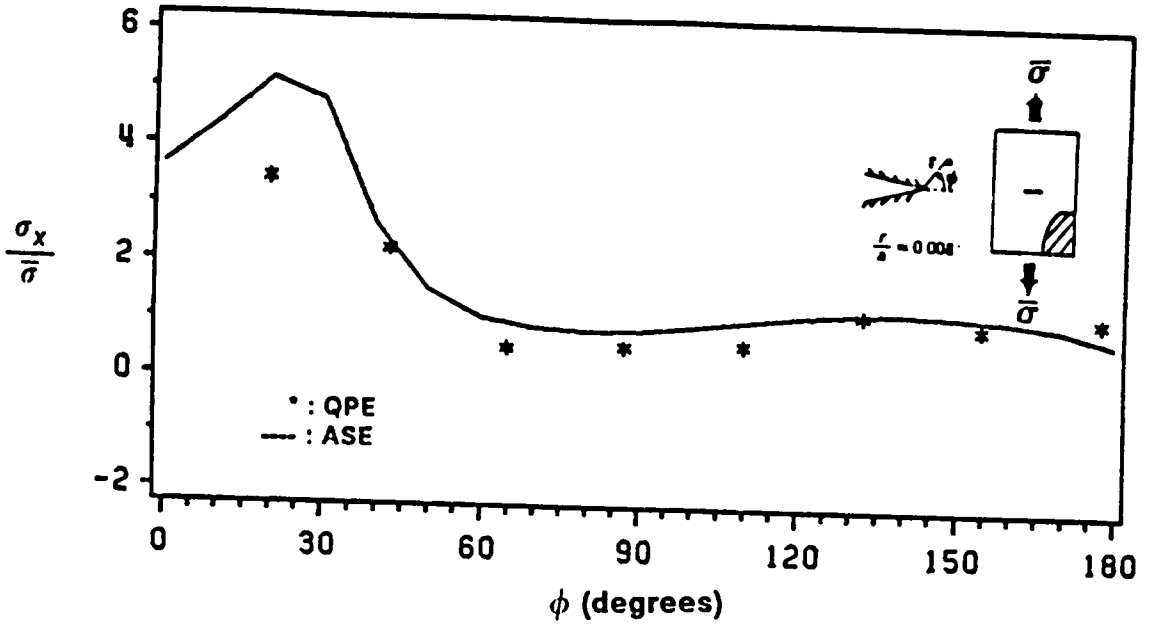

a Angular Variation in σ_x for $\theta = 60°$, $\Omega = 0°$

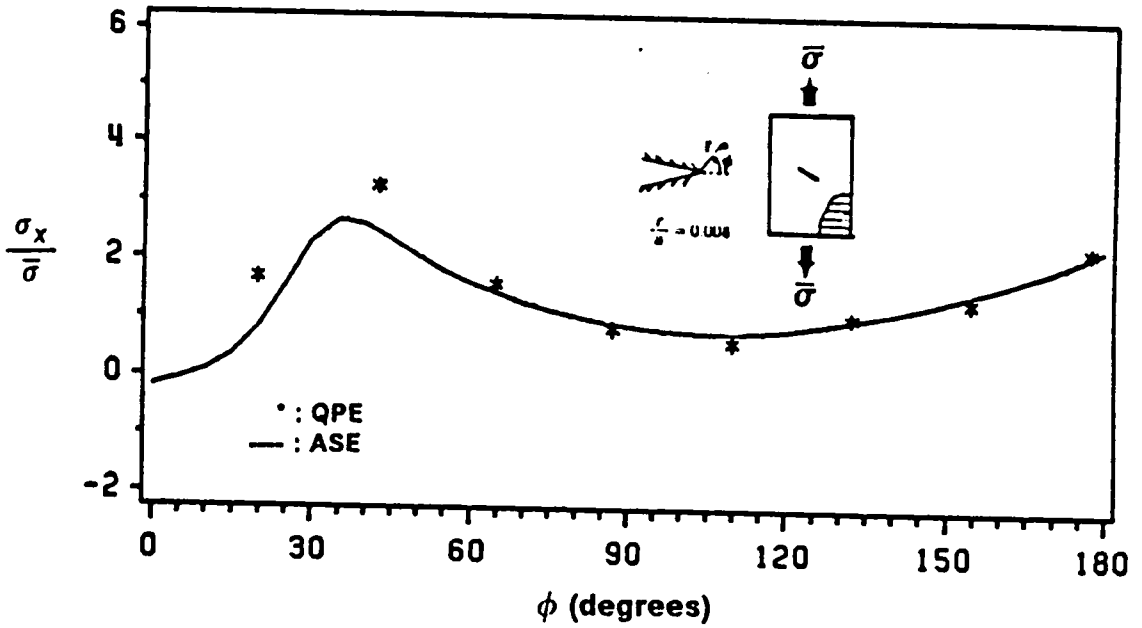

b Angular Variation in σ_x for $\theta = 90°$, $\Omega = -30°$

Figure 19. Angular Variation in σ_x for Case (ii)

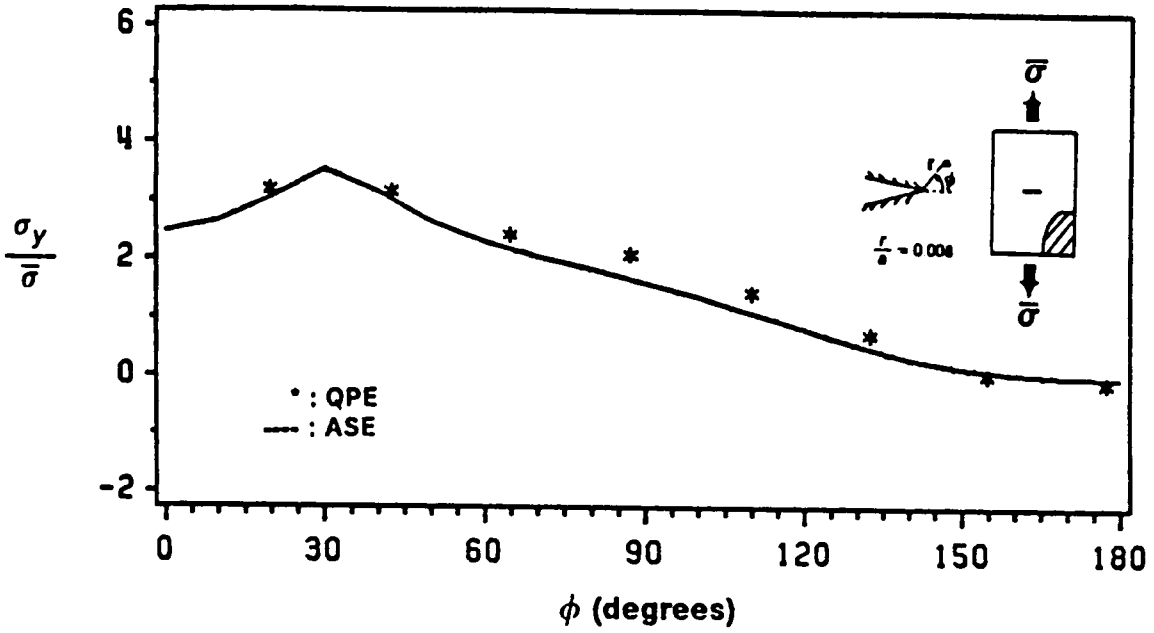

a Angular Variation in σ_y for $\theta = 60°$, $\Omega = 0°$

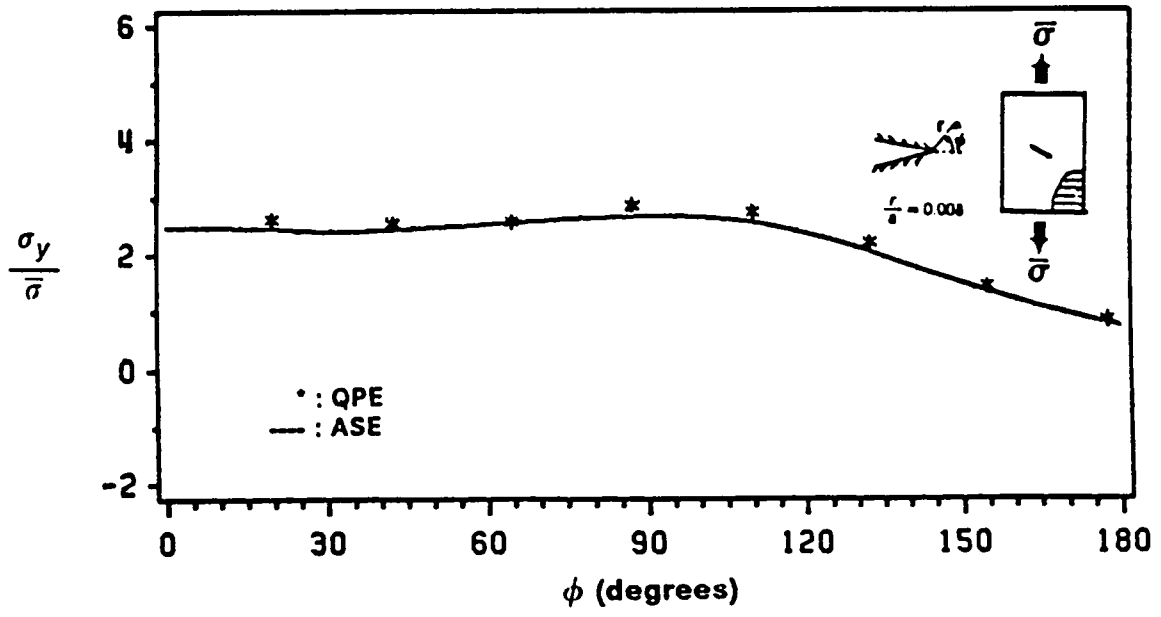

b Angular Variation in σ_y for $\theta = 90°$, $\Omega = -30°$

Figure 20. Angular Variation in σ_y for Case (ii)

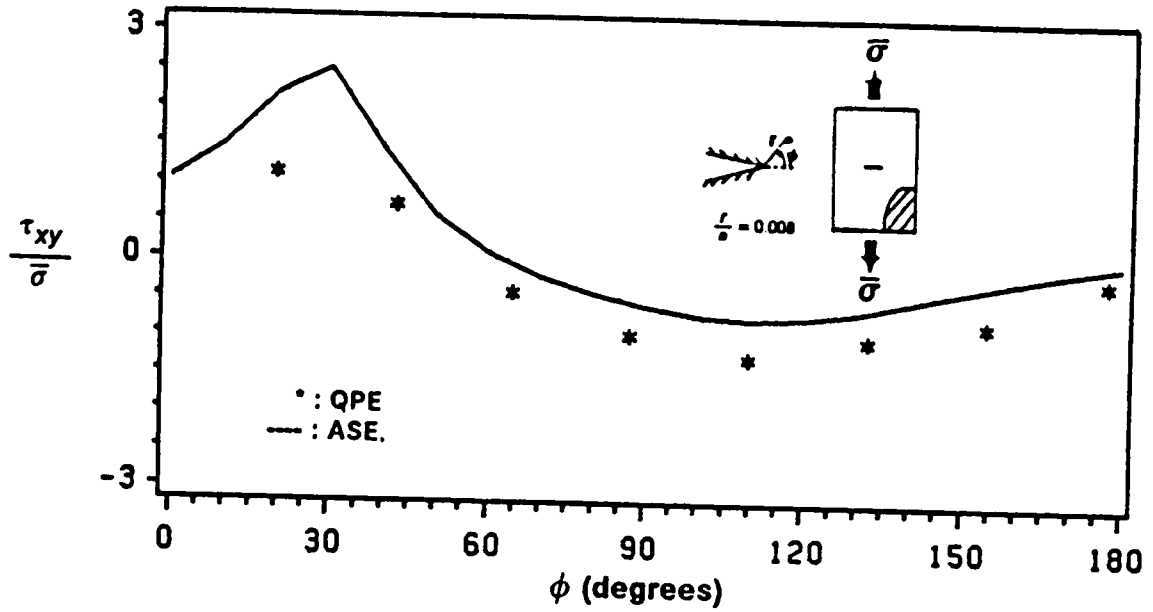

a Angular Variation in τ_{xy} for $\theta = 60°$, $\Omega = 0°$

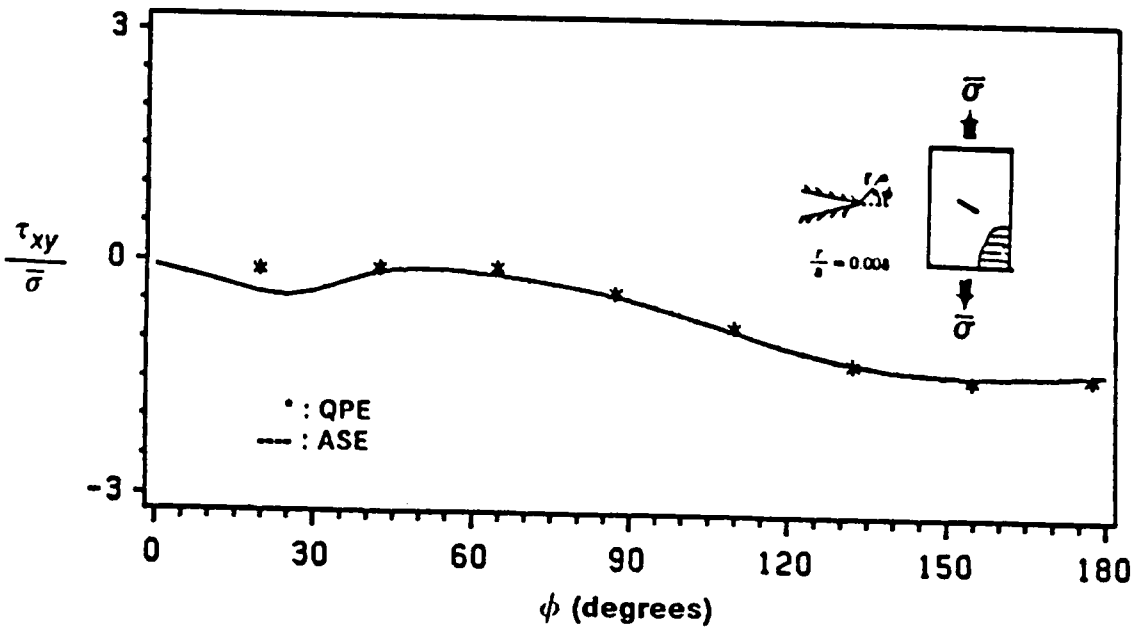

b Angular Variation in τ_{xy} for $\theta = 90°$, $\Omega = -30°$

Figure 21. Angular Variation in τ_{xy} for Case (ii)

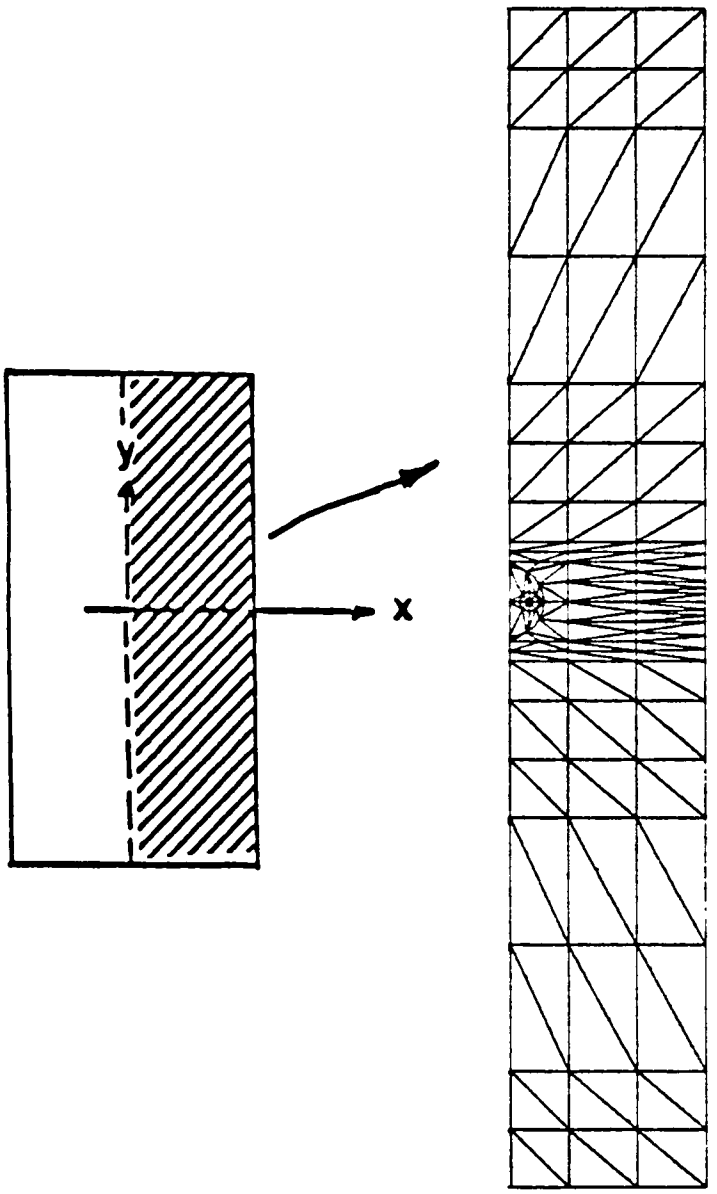

Figure 22. QPE Mesh Using Inversion Symmetry, Crack = 0°

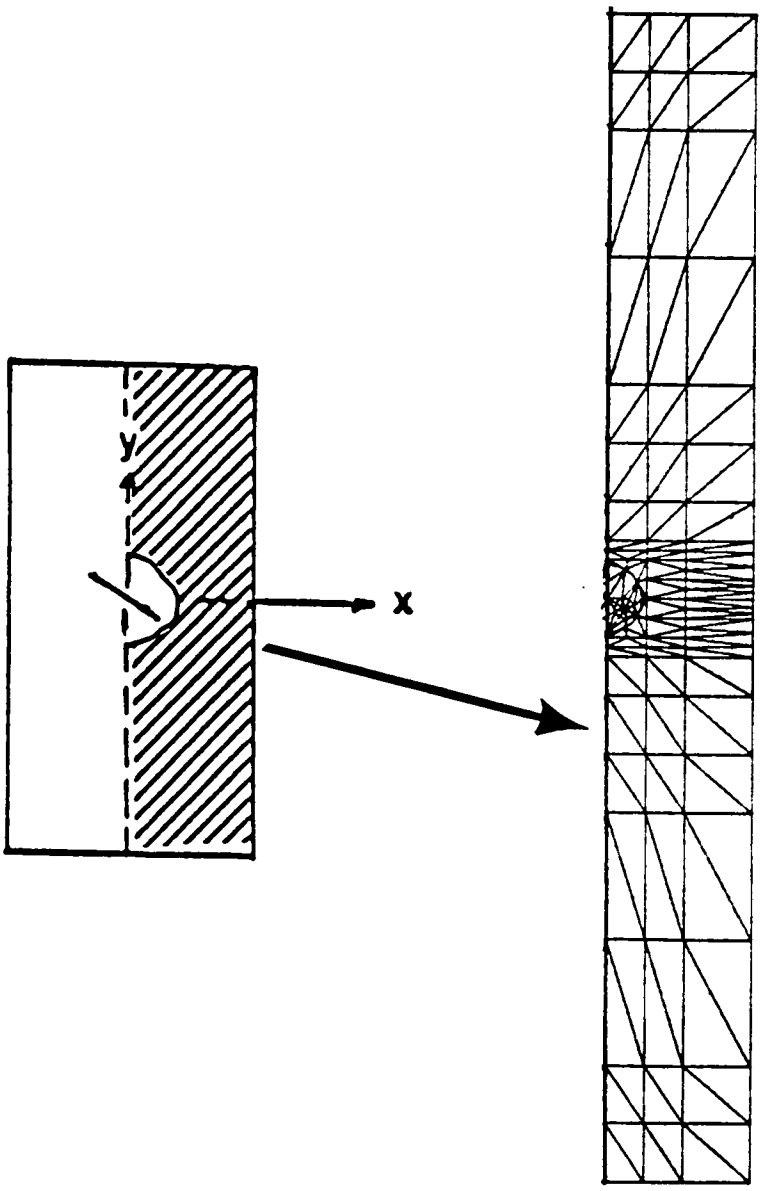

Figure 23. QPE Mesh Using Inversion Symmetry, Crack = -30°

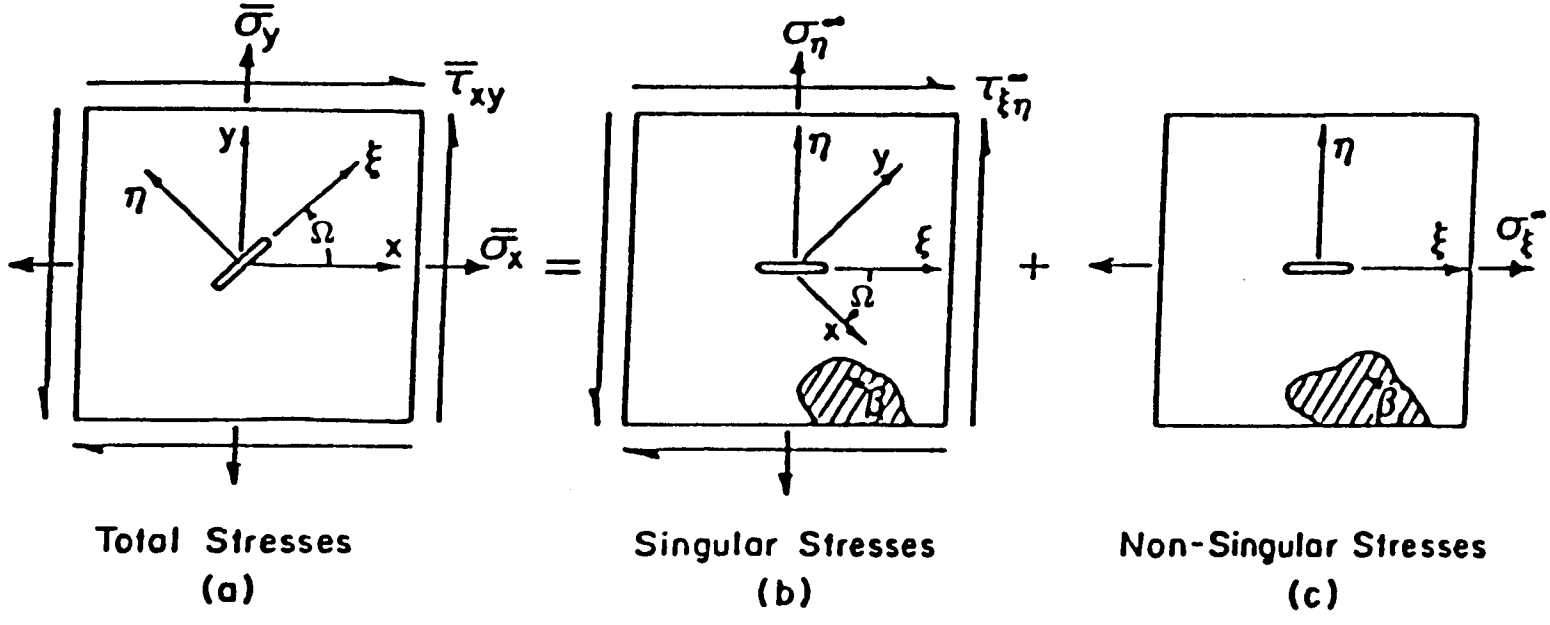

Figure 24. Superposition Method of Far-Field Loading for Angled Cracks

4.0 Graphical Simulation of Crack Growth

4.1 Introduction

Research in graphical simulation of crack growth became feasible during the last decade due to dramatic increases in the capabilities and power of interactive computer graphics. Research efforts in the area of tracking crack growth graphically have been limited to isotropic materials and section 1.3.3 presented a review of the literature. The method commonly adopted is outlined in the following paragraph.

Critical stress intensity factors (or critical strain energy rates) are considered as material properties for linear, isotropic materials, and plots for K_I (stress intensity factors) vs. Δa (increase in crack length) are documented for commonly used materials. The increment in crack length Δa can then be obtained from the plot for the given stress/displacement field at the crack tip. The crack is allowed to increase by this amount and the analysis continues. A large number of conventional or quarter point elements are typically used to model the crack tip singularity making it necessary for complex remeshing algorithms to update the crack geometry as it changes (propagates).

The approach used for isotropic materials cannot be adopted for composite materials as composite materials are known to behave very differently and the following factors need to be considered :

1. Each fiber angle and notch geometry represents a different 'material' making it impractical to characterize critical curves for each material and crack orientation.

2. Crack growth is generally not self-similar. Obtaining G_I, G_{II} and then using the superposition principle, $G = G_I + G_{II}$, cannot be used as a general rule. Empirical formulae and curve fitting methods to distribute G_I and G_{II} to calculate the total strain energy release rate have been used in the literature, but with little success[67 68 69]. These methods employ constants obtained using experimental data and these constants vary depending on the material system and crack geometry considered.

3. Critical strain energy release rates have been obtained experimentally for composite material systems using delamination type tests[67 68 69]. A recent survey [70] (1987) compared the available data for G_{Ic} and G_{IIc} and found significant variation in the values of G_{IIc}. A consistent, accurate method for the determination of G_{Ic} and G_{IIc} for composite materials remains to be developed.

The applicability of fracture mechanics concepts to composite materials and the lack of consistent, experimentally verified theories for fracture of composites limit the method of simulation that can be employed. A description of the parameters involved in tracking crack growth and details of the algorithm used in the current study are presented in this chapter.

As the first step, the original crack configuration and material system under the given loading is analyzed for the crack tip stress and displacement fields using the singular element developed. Frictional effects due to crack sliding and opening are neglected. The following crack growth considerations need to be addressed and evaluated using the results for the crack tip stress and displacement fields :

1. For the given loading and crack geometry, will the crack grow ?
2. If yes, then experimentally validated crack growth theories are needed to answer:
   a. In what direction ? (The direction of crack extension, ϕ_c.)
   b. By how much ? (The increment in the crack length, Δa .)
   c. Is crack growth stable ? (Will the loading result in failure of the specimen or stable crack growth ?)

Once these questions are answered, the mesh around the crack tip is redefined taking into account the new crack geometry. As the crack front advances through the specimen, the nodal locations of the mesh need to be changed to account for the moving crack. This alters the element sizes in the finite element mesh making it necessary to update the force vectors during propagation. The remeshing procedure (described in a later section) accounts for the changing nodal locations and updates the force vector to maintain uniform loading conditions. The method used is explained using a step-by-step approach.

4.2 Method of Crack Propagation

STEP 1 : The initial geometry of the unidirectional composite with a crack under the specified boundary conditions is analyzed for the crack tip stress and displacement fields using the singular element developed. The details of the element (ASE) are given in Chapters 2 and 3. Inversion symmetry (discussed in Chapter 3) is exploited whenever possible for reducing the total number of degrees of freedom in the finite element model.

STEP 2 : The parameters of crack growth are determined using the stress fields obtained and the criterion for crack extension. The Normal Stress Ratio (NSR) theory (discussed in Section 1.3.2) is a promising theory for the prediction of crack extension in composites[44–53] and is ex-

tended in this study to predict the stability of crack propagation. The NSR theory is used to determine the direction of crack propagation, ϕ_c, from the calculated stress field and the material strength parameters. Equation (1.1) is used to calculate the NSR at a radius r_0 and the direction of crack extension, ϕ_c, is predicted to be along the direction corresponding to the maximum value of the normal stress ratio. The method used to obtain the value of the critical radius, r_0 , is presented in Chapter 5.

For the crack to propagate, a critical value of the stresses must be reached as a stress based failure theory (NSR) is used. Physically, at the critical distance r_0, the crack will grow when the stresses in the predicted direction of propagation reach the strength of the material in that direction (NSR equals unity). Both, the finite element analysis and the NSR theory are linear and this allows for the calculation of the far field stress, σ_i, corresponding to a NSR value equal to unity. This stress (σ_i) is equal to the inverse of the NSR value in the direction of predicted crack extension (ϕ_c), times the far field load, σ_o :

$$\sigma_i = \frac{\sigma_o}{NSR} \tag{4.1}$$

STEP 3: The applied loading is increased from σ_o to σ_i . This loading corresponds to a NSR value of unity and the crack is assumed to grow at this load level. The crack size is then incremented by a small amount Δa as specified by the user (the default of Δa equals r_o itself).

The method used for remeshing and updating the nodal coordinates and forces is given in Section 4.5. It is noted that the increase in crack length will be along the predicted direction of crack propagation. If crack growth is not colinear to the original flaw, then there will be a distinct kink in the crack which makes the determination of stress fields a complex task. The ASE developed assumes a straight crack front and does not allow for kinked crack geometries. The effect of kinking on crack tip stress fields has been studied to some extent in isotropic materials and the method of accounting for it in this study is explained in a later section of this chapter.

STEP 4: The finite element calculations are performed for the new crack length with an applied loading of σ_i. The crack tip stress and displacement fields are obtained from the analysis and substituted into equation (1.1) (the normal stress ratio) to obtain the predicted direction of crack propagation (ϕ_c) for this step. The crack is again incremented by a small amount Δa in the predicted direction of crack extension, ϕ_c.

STEP 5: The loading is held constant at σ_i and the analysis performed at the new crack length. This step is used as an indication of the stability of crack growth. If the value of the NSR exceeds unity at the same load then crack growth is unstable as this implies that no more loading is required for the crack to grow. If there is no significant variation in the value of the NSR at the original load, then the loading is incremented by a specified amount, $\Delta\sigma$, and the analysis continued.

STEP 6: In a window on the PACE display (IBM 5080 workstation), an updated plot of the normal stress ratio versus the step number is drawn at the end of each step as shown in Figure 25. This plot is an indication of the stability of crack growth. The value of the NSR is calculated at a distance r_o from the new crack tip and if the value of the normal stress ratio is less than 1, then the propagation is continued. At the end of each propagation step, after the crack length is incremented by an amount, Δa, the loading is held constant and the analysis performed, as described in STEP 5. If the value of the NSR equals unity (or greater) at the same load, then it implies that no more loading is required for the crack to grow. This predicts the onset of unstable crack growth. If the value of the NSR is less than unity, then the load is incremented by a small amount, $\Delta\sigma$, specified by the user. Steps 4, 5 and 6 are repeated until instability is predicted or until the crack grows to the nearest free edge of the region being studied (failure of the specimen).

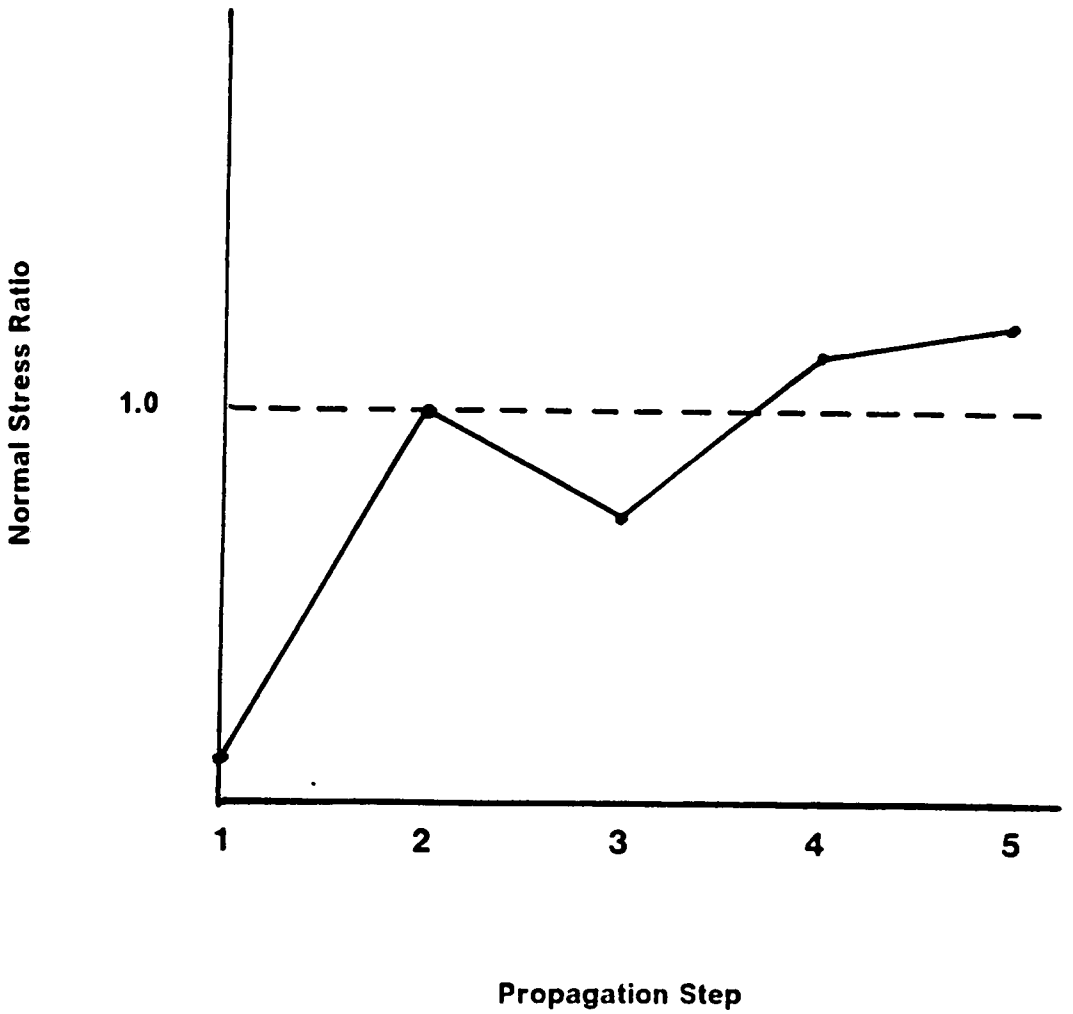

Figure 25. **Plot of Normal Stress Ratio vs Propagation Step**

4.3 Remeshing Algorithm

The new crack of length $a + \Delta a$ can be analyzed using the ASE. This requires updating of the finite element mesh and the nodal forces to account for the increment in crack length. The method used to propagate the finite element mesh and update the nodal forces and/or displacements is described in this section.

4.3.1 Updating Nodal Coordinates

As mentioned in the first section of this chapter, conventional or quarter point elements were typically used in the past for crack simulation studies with a large number of elements surrounding the crack tip. This approach requires complicated remeshing procedures and manipulation of large databases to account for the crack geometry as it propagates, often requiring a large amount of CPU time. No attempt has been made to take advantage of specially formulated singular elements. This study uses an efficient and simple remeshing procedure taking advantage of the fact that only one element surrounds the crack tip. The formulation of the ASE described in Chapter 2 allows for a variable size element with an arbitrary number of nodes making the mesh requirements flexible.

The user specifies the nodes on the left and right edges (nodes L1 to Ln and R1 to Rn in Figure 26) of the region to be modeled in the input data file. This is done by setting a flag for each node in the input data file indicating it to be either an interior node or a boundary node. (Appendix F presents details regarding input requirements along with a sample data file.) When crack propagation occurs, all the interior nodes are moved by an amount equal to the crack length increment along the X-direction; and all the boundary nodes remain fixed. This advances the crack front during propagation. The finite element mesh used specifies the crack always along the X-axis and cracks which are not along the X-axis (cracks which are not perpendicular

to the loading direction) are analyzed using a superposition procedure. This avoids the difficult task of remeshing along different directions as only one mesh is used for all crack angles.

If the new crack is not perpendicular to the loading axis, the superposition method for the loading conditions (described in Chapter 3) is used so that the finite element program only requires the mesh with a crack perpendicular to the loading axis but with the new crack length. If the crack is assumed to be at an angle Ω, then the far field loading σ_y in the X-Y system is transformed to the $\xi - \eta$ system (Figure 27). The finite element program solves the problem in the new coordinate system ($\xi - \eta$) in which the crack is perpendicular to the η – axis subjected to the far field loads : $\sigma_\eta, \tau_{\xi\eta}$. After solving the problem in the $\xi - \eta$ system, the stresses are transformed back to the original X-Y global system to calculate the crack propagation parameters. The remeshing procedure adopted in conjunction with the superposition procedure for cracks at an angle to the loading axis results in an efficient and accurate remeshing algorithm.

It is seen that as the crack propagates, the length of the sides of the elements behind the crack front get larger while the elements in front of crack tip get smaller. This is because, in the remeshing procedure, the boundary nodes remain fixed while the interior nodes are shifted in increments along the X-direction. To avoid large element sizes and element size aspect ratios during remeshing, a novel mesh arrangement is presented. The mesh has one (or more) columns of elements behind the crack front which are initially much smaller than the elements in front of the crack tip (Figure 26). This allows the elements to be of acceptable size as the crack advances.

It is noted that if conventional elements were used instead of the ASE, complex remeshing methods and manipulation of databases would be needed to account for the new crack geometry. Therefore, there is a significant advantage in using only one element surrounding the crack tip. To the authors knowledge, this type of remeshing procedure has not been attempted before.

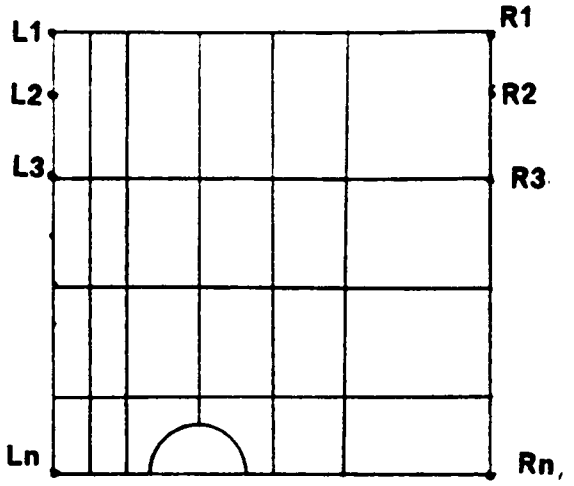

(a) Before Crack Advancement

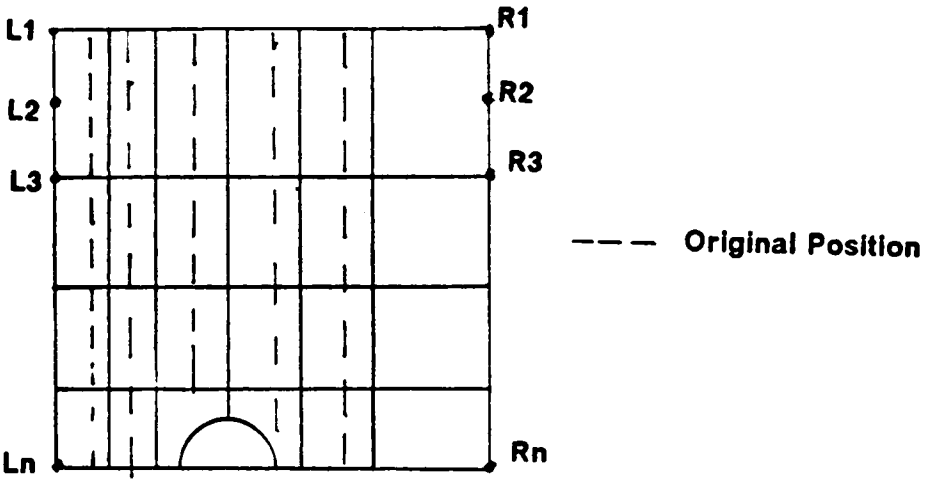

(b) After Crack Advancement

direction of crack advancement ⟶

Figure 26. Updating Nodal Coordinates

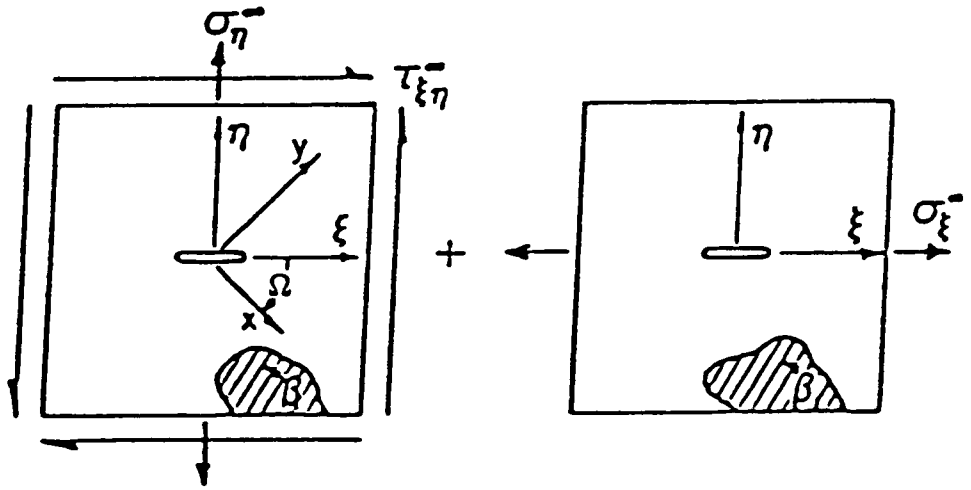

Figure 27. Cracks at an Angle to the Loading Axis

4.3.2 Updating Boundary Nodal Forces

As the nodal coordinates change when the crack propagates, the distribution of nodal forces must to be updated due to the resulting changes in the length of the sides of the corresponding elements. Figure 28 shows a typical element and nodal coordinates before and after the force vector modifications. A subroutine recomputes the distance between the end nodes N1′ and N2′ at the end of each load step and automatically redistributes the force vector along the specified direction so that uniformity in the applied load is maintained.

Method of Load Application

As described in Chapter 3, a superposition method is used for far field stresses to accommodate cracks which are not perpendicular to the loading direction (i.e. angle cracks). This procedure was found to be accurate and simple and eliminated the need for different meshes for cracks at different angles. This superposition method (Figure 27) is used in this study in a unique way to account for the the changing direction of the crack as it propagates. For analyzing a center cracked (crack perpendicular to the loading direction) plate under uniaxial tension, an initial tensile load of $\sigma_o = 1000$ psi and a shear loading of $\tau_{xy} = 1000$ psi is input from the data file. Each elemental (nodal) loading component has a flag to identify it as a shear or a normal component in the data file. The program (PACE) automatically calculates the shear contribution at each load step, depending on the angle of the crack. Figure 29 describes the procedure. For example, an initially horizontal crack (for a plate under uniaxial tension) will have no shear loading and the factor used to calculate the shear contribution will be zero for this case. If the crack then grows at an angle ϕ_c, the superposition method calculates the required shear contribution for that crack angle. This method of updating the loading and crack geometry which has been developed for this study is found to be simple and accurate.

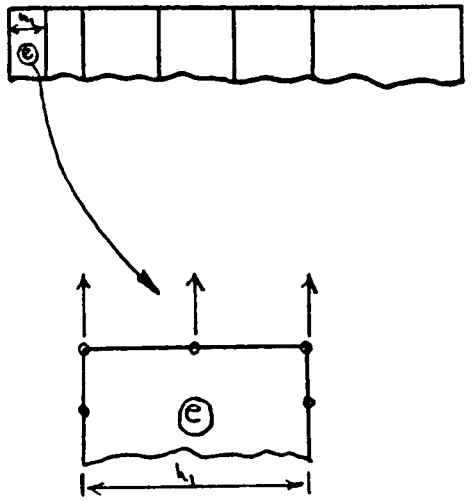

(a) Before Crack Advancement

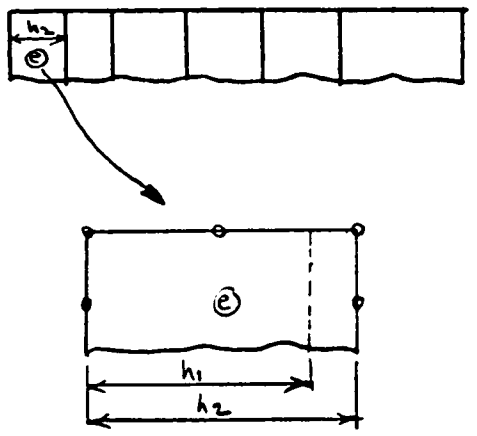

(b) After Crack Advancement

Figure 28. Updating Nodal Forces

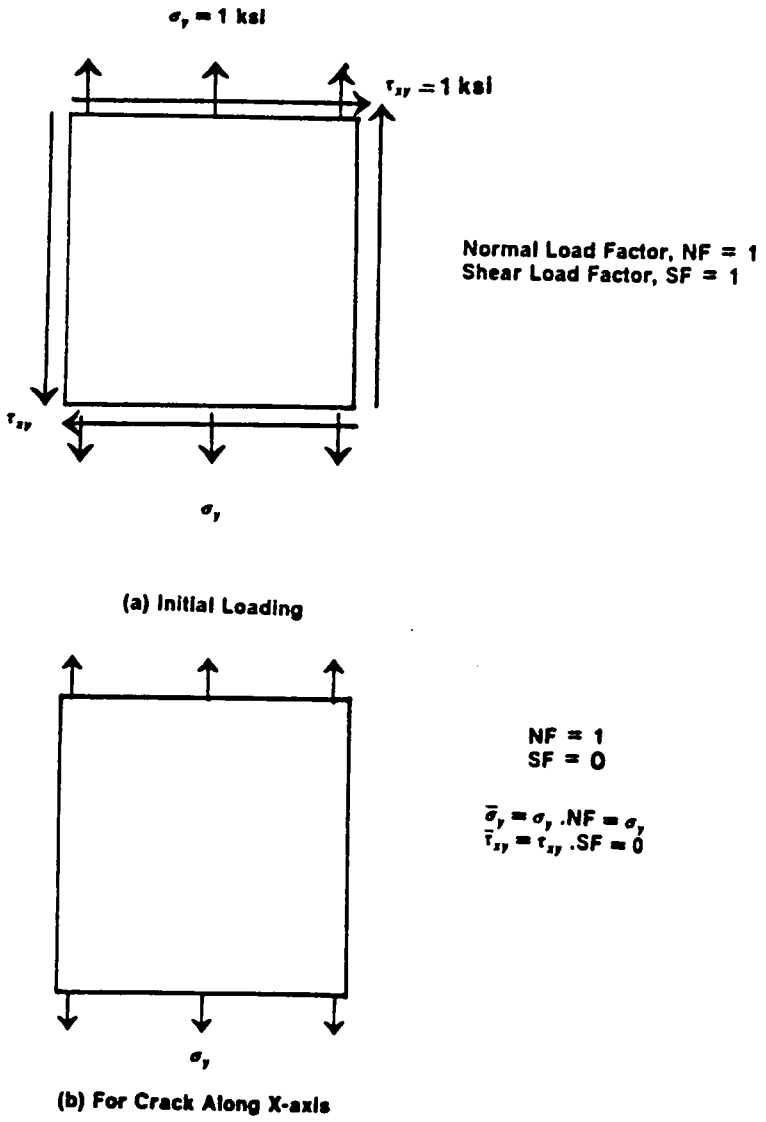

Figure 29. Method of Load Application

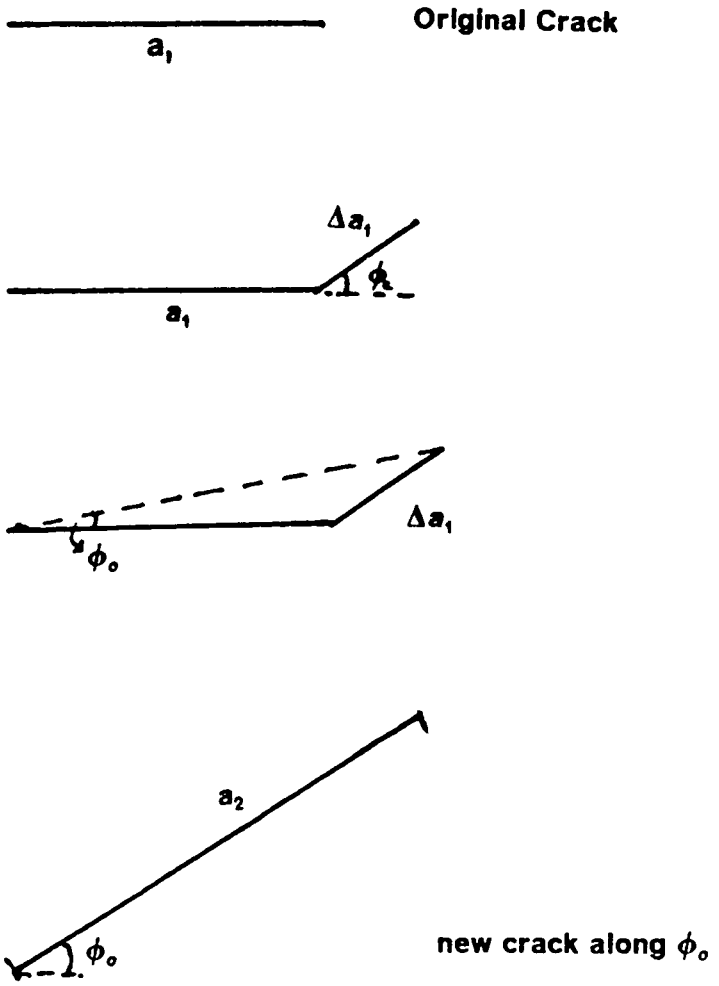

Figure 30. Equivalent Length Method for Kinked Cracks

4.4 Effect of Crack Kinking

If crack growth is not colinear to the original flaw, then as the crack is allowed to propagate, there will be a distinct kink in the crack which makes the determination of the crack tip stress fields a complex task. The singular element developed assumes a straight crack front and does not allow for kinked crack geometries. The effect of kinked cracks (subjected to symmetric and non-symmetric loading) on crack tip stress fields has been studied to some extent in isotropic materials[71] [72] [73] [74]. This is an area of current research and no definite conclusions regarding the analytical approaches to account for kinking effects can be drawn at the present time[72] [73]. Moreover, the classical approach of obtaining strain energy release rates for kinked cracks breaks down when crack growth is not self similar as the energy release rate quantity is defined by taking the segment of the kink in the limit to approach zero. The uniqueness of the energy release rate quantity is doubtful as the kink portion of the crack is set to zero in the limit as two singular points (the crack tip and the re-entrant corner) emerge into one.

The problem is presumably even more complex for anisotropic materials and direct extrapolations and assumptions about kinking behavior based on isotropic material analysis are avoided as composites are known behave very differently. The kink is considered as a weak mathematical singularity and one way to account for this would be to solve the kink as a wedge problem and then superimpose the crack tip solutions and the kink solutions in the element. This can be a major research effort in itself and will not be attempted at this time.

Methods to account for kinked cracks have been proposed and they utilize an 'equivalent length' concept where the kinked crack is replaced by a straight crack of equivalent length obtained by using a projection of the kinked portion [75] [76]. Figure 30 depicts a method that has been adopted for this study. The original crack of length a_1 is shown in Figure 30a. If the predicted direction of crack extension (using the NSR theory) is along an angle ϕ_c, then the incremental crack extension, Δa, is along ϕ_c (shown in Figure 30b). An equivalent crack length of a_1' is then

calculated using the general triangle formula. For the next propagation step, the crack of length a_1' is assumed to be along ϕ_o as shown in Figure 30d.

4.5 Graphics Interface

The singular element developed in Chapter 2 and validated in Chapter 3 was used with the simulation methods described above to monitor crack growth in unidirectional composites. Graphical simulation of crack growth was performed by interfacing computer graphics with the finite element program (written in FORTRAN -77) and the graphics portion was made an integral part of the overall code.

There is a need for powerful, usable application programs to automate processes in the CAD/CAM/CAE environment. PHIGS (Programmers Hierarchical Interactive Graphics System)[77 78 79] is an advanced, fully three dimensional graphics application program interface (API) based on the American National Standards Institute (ANSI) proposed standard. PHIGS is a powerful graphics system that supports the definition, modification and display of hierarchically organized graphics data by letting the user edit, modify and transform graphics entities. The graphics standard allows for: windowing and viewport processing, transformation and clipping, I/O operations with a variety of devices, local storage and a palette of 4096 colors. 'graPHIGS' is the IBM version of PHIGS and is supported at Virginia Tech on the IBM 5080 workstation attached to an IBM 4341 CPU serving as a host computer. With the use of the intelligent workstations (IBM 5080), data exchange with the host is minimized as many graphics operations are done locally.

4.5.1 graPHIGS Highlights

A brief description of the graphics system used is presented in this section. The PHIGS standard contains a full set of functions which serve as efficient and flexible tools to integrate FORTRAN, Pascal or Assembly Language routines with graphics. For a better understanding of the PHIGS system, a list of the essential features are given below :

1. Primitives & Attributes - generation of geometry and specification of attributes:
   - Lines : Connected or broken line strings of different colors and line types
   - Markers : Different types (dot, asterisk, etc.), colors and sizes
   - Polygons : Control over edge type, color ; interior styles (solid, hatched, hollow, etc.) and colors
   - Text : Extensive choice of text types, fonts, heights, colors, etc.
   - Pixel : Allows for direct display of individual elements for fractals and shaded images
2. Structures - data organization constructs that provide for :
   - Parts or complete model definition
   - Modification of structures
3. Input devices - I/O control can be performed from a wide range of devices (given below) and accomplished either synchronously or asynchronously :
   - String : Keyboard
   - Choice : Lighted PF keys
   - Locator : Tablets and Light pens
   - Stroke : Allows freehand and discrete input of coordinate point locations using a Tablet or a Light Pen
   - Pick : Tablet or light pen to identify entities within a hierarchy, usually used for menu pick selections
   - Valuators : Dials for panning, zooming and rotation I/O

4.5.2 Simulation Program, PACE

The program developed for this study is named 'PACE' (Propagation using an Anisotropic Cracked Element) and a complete user's guide and description of input data requirements is given in Appendix F. A flow chart of the program control structure is given along with the user's guide in Appendix F. PACE is a two dimensional finite element program capable of analyzing cracked (and uncracked), anisotropic (and isotropic) structures. It is menu driven at run time and is implemented at Virginia Tech on the IBM 5080 workstation attached to a IBM 4341 CPU serving as the host computer. The program has a library of Q8 (eight noded quadrilaterals) elements and the specially formulated singular anisotropic element (ASE). A complete list of the capabilities of the program is given in Appendix F.

The program is a IBM 5080 version of PACE and the program can be used on any system that provides PHIGS software. Many systems such as the IBM PC RT, MicroVAX, Tektronix, Megatek and the state-of-the-art workstation, IRIS, have versions of PHIGS to which PACE can be transported to with little or no modification. PACE makes use of all the input devices of the 5080. Numerical and text input is allowed via the keyboard, menu choices and pick commands using the tablet and cursor, continuous rotations and zooming input with the valuators (dials) and pre-defined PACE commands using the function keyboard.

For analysis of unidirectional composites with cracks, the stiffness matrix of the singular element is first generated using the singular element and material property parameters. A conventional displacement based finite element program (based on the program developed by Reddy [80]) is used to calculate the stiffness matrix for the remaining part of the structure. As the stiffness matrix of the singular element has displacements as its nodal degrees of freedom, it is superposed onto the global stiffness matrix. PACE is modular in nature with a large number of subroutines; each subroutine performing a specific task. This makes the 'debugging' stage more convenient, and allows for modifications and enhancements to be performed without

much difficulty. The program PACE comprises of 62 subroutines and approximately 6000 lines of source code.

At the end of each load step, the displacement vector generated by the finite element solution is used define a different deformed geometry and each geometry is stored as a graphics 'structure' in PHIGS. Each structure (each deformed mesh) is given a label (number) and can be recalled at a later time to be plotted on the screen without any further processing. Using these 'structures', the total (step by step) deformation pattern of the specimen under investigation can be simulated at the end of the analysis.

Once the crack growth increment is obtained using the method(s) of Chapter 4, the mesh is redefined to account for the new crack length and the analysis continued until instability or fracture of the structure. Appendix F presents a 'cook-book' approach to using PACE, followed by a section on input data requirements and formats.

5.0 Results of Graphical Simulation

5.1 Introduction

The simulation program developed was used for the prediction of crack growth parameters in center cracked unidirectional composite materials. Experimental crack growth data for center cracked AS4/3501-6 graphite epoxy under uniaxial tensile loading is available from Beuth and Herakovich [48] for specimens with fiber angles of $\theta = 0°, 15°, 45°$ & $90°$. Material properties representative of the unidirectional AS4/3501-6 graphite/epoxy material system used in the analysis are given in Table 7 (Appendix B). The dimensions of the specimen are given in Figure 31. The results obtained for the various cases analyzed are presented in this chapter.

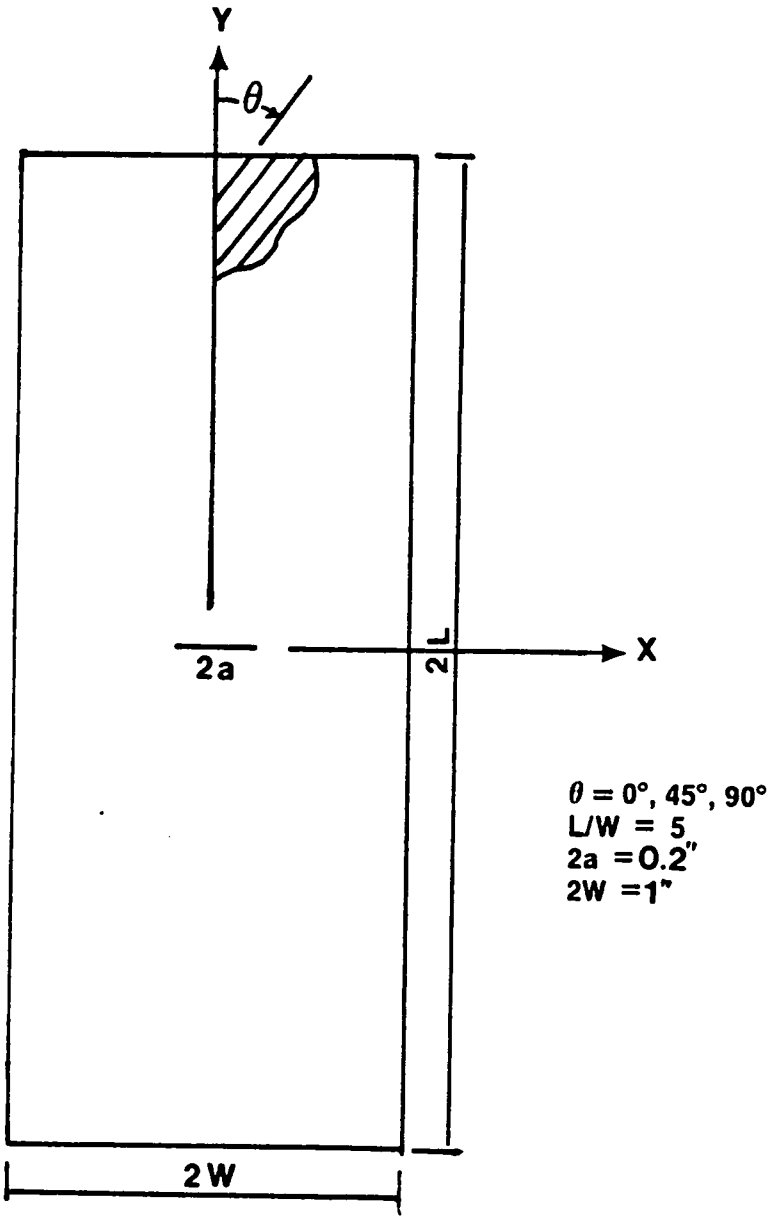

Figure 31. Specimen Dimensions (Ref. [48]).

5.2 Calculation of the Critical Radius

The normal stress ratio (NSR) theory is used as a crack propagation criterion and, as mentioned in Chapter 4, the NSR theory must be applied at a specific radial distance r_o (critical radius) from the crack tip. The value r_o is a normalized value and represents the ratio of the actual distance, r, to the semi-crack length, a ($r_o = \frac{r}{a}$). In order to apply the theory to predict critical stresses, a value for r_o must be found experimentally from a baseline test. Once a value for r_o is found, it is treated as a material constant. The value of r_o and the other material parameters such as E_{11} , E_{22}, X_T, etc. are representative of the material used in the experimental study. The theory can then be applied to predict the direction of crack growth and crack initiation stresses.

It is noted that the assumption of a critical radius for the crack propagation theory defines a 'core region'. This region can be used to define the extent of the singularity effect in the analytical stress field. For composites, r_o can be expected to be a function of the fiber volume fraction, v_f. A different fiber volume fraction v_f will lead to different material and strength properties of the material thereby changing the value of r_o.

The value of r_o used in this study for the graphite epoxy material system is calculated using the baseline test of Beuth and Herakovich [49]. Because all predictions are dependent on the value of r_o calculated from the baseline test, it is important to use a test for which the critical stress is not ambiguous and which can be consistently determined. Thus, specimens experiencing no stable crack extension and consistent fracture stress values are desirable. The 90° coupon was chosen for the baseline test to evaluate r_o because :

1. A crack along the fiber direction resulted in self similar crack growth.
2. No slow crack growth is observed, providing a clear determination of the critical radius, r_o
3. The test is normal stress dominated
4. Tests results are consistent

From the baseline tests [48] the average value of the crack initiation stress was 2.81 ksi. This value was applied as the far-field loading and the finite element method used to calculate the value of the normal stress ratio along the predicted direction of crack extension ($\phi_c = 0°$). Along this direction, the normal stress ratio equalled 1 at a value of $r_o = 0.033$. An infinite domain elasticity solution for a center cracked homogeneous anisotropic plate [58] was used by Beuth and Herakovich [48] to calculate r_o. A value of $r_o = 0.0657$ was obtained in their study. It is noted that the finite element approach accounts for the finite size of the specimen. However, both values of the critical radius are used for the various cases analyzed in this study and the results obtained are compared. To distinguish between the two values of r_o used in this study, the value of 0.033 obtained using the finite element method is denoted as r_o and the value of 0.0657 obtained from Ref. [48] is denoted as $\bar{r}_o$.

5.3 Notched 90° Coupon

A specimen with a crack initially perpendicular to the loading direction and with the fibers at 90° to the Y-axis (Figure 31) was analyzed under an applied uniaxial tensile load. The finite element mesh used in the analysis is shown in Figure 32 and consists of 62 elements and 219 independent nodes. The mesh takes advantage of inversion symmetry (discussed in Chapter 3) and the dependent and independent nodes are shown in the figure. The simulation procedure described in the previous chapter was used to track crack growth with the finite element mesh updated as the crack propagated.

This 90° coupon was the baseline test described in the previous section which was used to determine the value of the critical radius, r_o . A crack initiation stress, value, σ_i of 2.81 ksi was obtained using r_o (value of 0.033), as expected. Using $\bar{r}_o$, a σ_i value of 3.51 ksi was obtained.. Table 2 compares the values of σ_i obtained from the experiments and the various analytical methods for $\theta = 90°, 45°\&0°$. The latter two fiber orientations are discussed in later sections.

The analysis predicted crack extension along the fibers, similar to that obtained in the experiments. It is noted that for the graphite epoxy system studied, the axial strength in the fiber direction (the 1- direction) is very much larger than the transverse strength in the matrix direction (the 2- direction) (Appendix B). Also, the ratio of the moduli, $\frac{E_{11}}{E_{22}}$ is large, with the result that the fibers carry a large portion of the applied load. This fiber dominated behavior results in the crack growth direction to be parallel to the the fibers.

At the end of the first step of propagation during the analysis, the stability criterion used (maintaining the same loading for an incremental extension in crack length) predicted unstable crack growth. This was similar to that observed in the experiments.

5.4 Notched 45° Coupon

A 45° specimen with an initial crack perpendicular to the loading direction (Figure 31) was analyzed. The same finite element mesh used for the 90° coupon is used for this case as changing the fiber angle requires the alteration of only one card in the input data file. A far-field load of 1 ksi (unit load) was applied for the first load step in the propagation analysis. As described in the previous chapter, this step was used to predict the crack initiation load, σ_i, as both, the analysis and the normal stress ratio theory are linear. As expected, the results in Table 2 indicate that that the crack initiation stress depends on the value chosen for the critical radius. Considering r_o as the critical radius, the value of σ_i calculated was 3.65 ksi as compared to 4.12 ksi observed in the experiments. Using $\bar{r}_o$, a crack initiation stress of 4.71 ksi was obtained from the finite element analysis. It is interesting to note that the two values of σ_i obtained from the finite element analysis bracket the experimental value by approximately the same percentage. Both values are a significant improvement over the infinite plate elasticity solution, which predicts a value for σ_i of 5.02 ksi. As the value of the critical radius increases (going away

Table 2. Crack Initiation Stress

CRACK INITIATION STRESSES (ksi)				
Fiber Angle θ	Experiment Ref.[48]	F.E.M. (r_o)	F.E.M. ($\bar{r}_o$)	Elasticity Ref.[48]
90°	2.81	2.81 (0 %)	3.51 (25 %)	2.81 (0 %)
45°	4.12	3.65 (-11 %)	4.71 (14 %)	5.02 (22 %)
0°	38.2	44.16 (16 %)	62.4 (63 %)	20.90 (-45 %)

from the crack tip), the calculated stresses are lower, resulting in a lower value of the NSR, which in turn leads to a higher value of σ_i (as σ_i is proportional to 1/NSR).

As the crack was allowed to propagate by an increment, the load level of σ_i resulted in a value of the NSR to be greater than unity for the new, incremented crack length, thus predicting unstable crack growth. Unstable crack growth was also observed in experiments. As crack growth is unstable, the crack initiation stress of 3.65 ksi is also considered as the failure stress, σ_f. The crack growth direction predicted was parallel to the fibers, as expected.

5.5 *Notched 15° Coupon*

Experiments were conducted on the 15° specimen with several different geometries. Specimen aspect ratios (length/width) of 1,4 and 8 were tested with two different crack orientations[48] . The crack angles analyzed were : (i) crack perpendicular to the loading direction (along the X axis), and (ii) a crack perpendicular to the fiber direction (105° to the loading axis

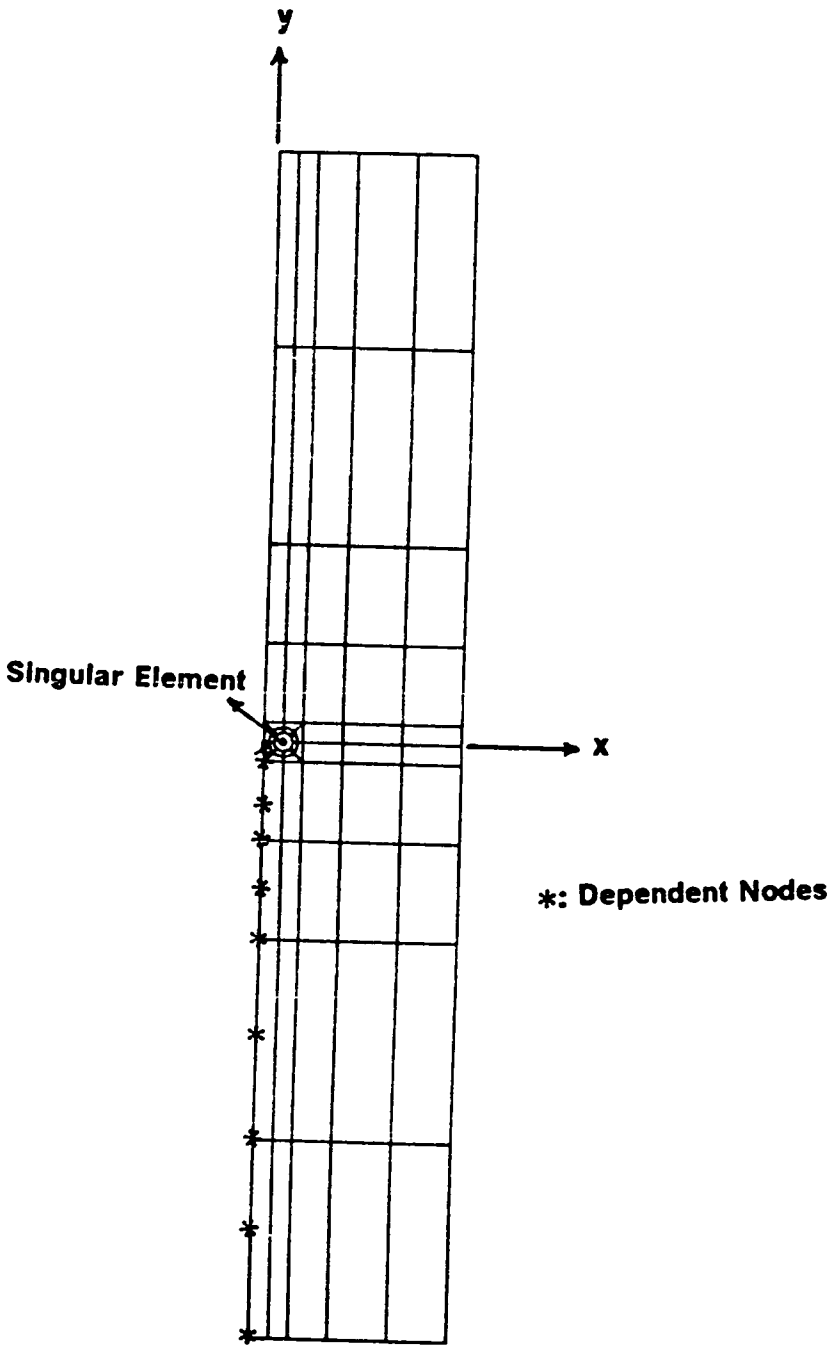

Figure 32. Finite Element Mesh Used

or – 15° to the positive X axis), as shown in (Figure 33). The same geometries were analyzed in this study and the crack growth parameters predicted.

The direction of crack propagation predicted was along the fibers for all the cases analyzed, as observed in the experiments. The initiation stress values obtained by the various methods for this case are shown in Table 3. The values shown in the table are for a specimen aspect ratio of 4. The effect of changing the specimen aspect ratio on the initiation stresses is described in a later section.

From the table it is seen that the finite element prediction for σ_i for the 90° crack is closer to the experimental value than the infinite plate result. However, the opposite is true for the crack perpendicular to the fibers. It was observed in the experiments [48] that the specimens having 90° center notches have higher crack initiation stresses than specimens of the same aspect ratio having 105° notches. A similar behavior was obtained in the finite element study, but not to the same degree.

5.6 *Notched 0° Coupon*

A 0° specimen with an initial crack perpendicular to the loading direction (Figure 31) was analyzed. The same finite element mesh used in the analysis of the 90° coupon was used for this case. Using an initial unit loading for the finite element analysis, the crack initiation stresses predicted were 44.16 ksi (for r_o) and 62.40 ksi (for $\bar{r}_o$). The experimental value was 38.20 ksi (Table 2). It is seen that there is reasonable agreement between the experimental and numerical values for σ_i using a critical radius of 0.033 (obtained using the finite element method). Choosing the critical radius equal to $\bar{r}_o$ resulted in poor agreement. It is interesting that the finite element and not the elasticity results using $\bar{r}_o$ differed from the experimental values by the same percentage with the finite element result being higher and the elasticity results being lower than the experimental value.

Table 3. Crack Initiation Stress for θ = 15 °

CRACK INITIATION STRESSES (ksi)				
Crack Angle	Experiment Ref.[48]	F.E.M. (r_o)	F.E.M. ($\bar{r}_o$)	Elasticity Ref.[48]
90°	8.91	10.2 (14 %)	14.87 (67 %)	7.17 (-20 %)
105°	6.76	9.8 (45 %)	11.3 (67 %)	6.64 (-2 %)

Incremental crack growth resulted in stable crack extension (as observed in the experiments). Also, the 'H' shaped extension observed from the crack tip during the experiments (Figure 34) was reproduced using the simulation algorithm. This was because the value of the maximum normal stress ratio was identical at $\phi = 90°$ and 270° (Figure 34) thus forming the H-shaped crack and then propagating along the fibers until failure. The failure stress could not be predicted for this specimen under stable crack growth. The propagation analysis would require that the crack extend until the top and bottom edges of the specimen at failure. The method to update the finite element mesh used would break down for this extreme case and thus the failure stress cannot be evaluated.

Figures 36a to 36c are photographs showing the deformed mesh during various stages of propagation for this case. The deformation is scaled to accommodate the full specimen on the screen of the IBM 5080 workstation. The crack opening and the mesh advancement which accounts for the growing crack can be clearly seen from the photographs.

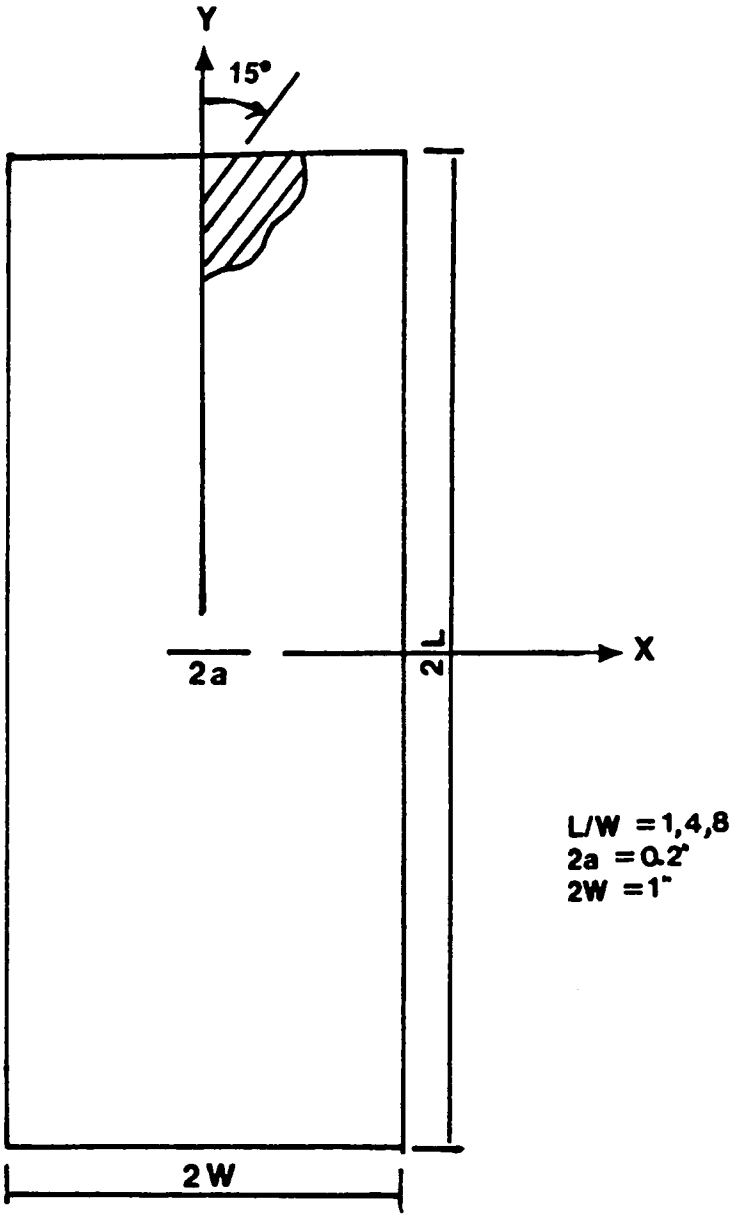

Figure 33. 15 ° specimen (Ref. [48])

5.7 Variation of Crack Initiation Stress

From the experimental results it was noticed that fiber angles of $\theta = 45°, 90°$ resulted in unstable crack growth. On the other hand, a fiber angle of $\theta = 0°$ showed stable crack growth. Crack growth for the 15° case was sporadic and occurred in jumps and could be considered as quasi-stable. This may indicate that there is a 'transition' fiber angle at which the crack growth becomes unstable. To explore the possibility of such an effect, a parametric study was conducted by changing the fiber angle from 15° to 45° in steps of 5°.

Crack growth simulations were performed, but the analyses did not generate any conclusive results regarding a transition stage. However, the values of the crack initiation stresses predicted for the various cases analyzed show a common trend (Figure 36). As the fiber angle is increased, the predicted crack initiation stresses become lower. They range from a high of 44.16 ksi for the 0° case to a low of 2.81 ksi for the 90° case. Experimental data is not readily available for notched specimens of all the fiber angles of the specific graphite epoxy analyzed in this analytical study. However, it is encouraging that the results follow the trend of experimental results for 'so called' unnotched specimens. The ability of the NSR theory to predict initiation stresses for the uniaxial tests can be further tested by conducting experiments for specimens with fiber angles from $\theta = 20°$ to 40° in steps of 5° (maintaining all dimensions the same as used in Ref. [48]). The results obtained could then be compared to the values predicted analytically to further validate the normal stress ratio theory.

Effect of Specimen Aspect Ratio

The effect of specimen aspect ratio was investigated. For fiber angles of $\theta = 0°, 45°$ & 90°, aspect ratios of 2.5, 5 and 10 were analyzed. There is little variation in the value of σ_i for the various aspect ratios as seen in Table 4.

Table 4. Crack Initiation Stress vs Aspect Ratio

EFFECT OF ASPECT RATIO			
Fiber Angle θ	2L/2W = 2.5	2L/2W=5.0	2L/2W=10.0
90°	2.81	2.55	2.57
45°	3.6	3.3	3.44
0°	44.16	43.4	43.5

5.8 Discussion

All the cases analyzed predicted crack growth along the fibers, as expected. There is relatively good correlation between the experimental and predicted values of the initiation stress. This gives confidence in (i) the normal stress ratio (NSR) criterion for predicting the direction of crack propagation, (ii) the NSR criterion for predicting the crack initiation stress.

It is noted that the specimens used in the experimental study had cracks that were actually slots with semi-circular ends [48]. This type of 'crack' mathematically does not produce the inverse square root singularity in the stress fields. In contrast, the singular element developed for this study includes the singular behavior by treating the flaw as a sharp crack. The difference observed between the experimental and predicted values may be attributed to this.

All the predictions of crack extension direction and crack path stability performed in this chapter were based on evaluating the stresses at a particular distance from the crack tip, r_o. It is known that the prediction of crack extension direction is relatively independent of the distance, r_o, using the normal stress ratio theory [48], in contrast the value of r_o is crucial to the accurate determination of the initiation stress. The value of the initiation stress, σ_i predicted using a critical radius $r_o = 0.033$ (obtained using the finite element method) used in this study was

found to be in reasonable agreement with the experimental values. The correlation between the experiments and analytical results supports the basis of choosing the $\theta = 90°$ test as the baseline test. The value of the critical radius , $\bar{r}_o = 0.065$ obtained by neglecting the finite size effects of the specimen (Ref. [48]) predicted higher values for the crack initiation stress, σ_i

The value chosen for the increment of crack length, (Δa), at every load step in the propagation analysis is an assumed value. There is a need for a verified criterion on which crack extension sizes can be calculated. Δa values are available as functions of stress intensity factors for isotropic materials but is impractical to generate such data for composite materials, as mentioned in the introduction to Chapter 4. In this study, the value of Δa was taken to be r_o itself. Choosing a different value for Δa will result in a different crack geometry to be analyzed (using the method to account for kinked cracks, Chapter 4) during the propagation analysis. However, the values of crack initiation stress are independent of Δa as σ_i is calculated at the first step of the analysis.

The propagation portion of this research effort is the first attempt at crack growth simulation in composites and it is realized that there is a need for appropriate, physically backed criteria to characterize stability of crack growth in composites. Crack initiation and growth in composites is a complex process and possibly intractable in general laminates but a macroscopic approach to obtain the increment in crack length Δa and predict stability of crack growth accurately needs to be formulated for the development of useful simulation algorithms.

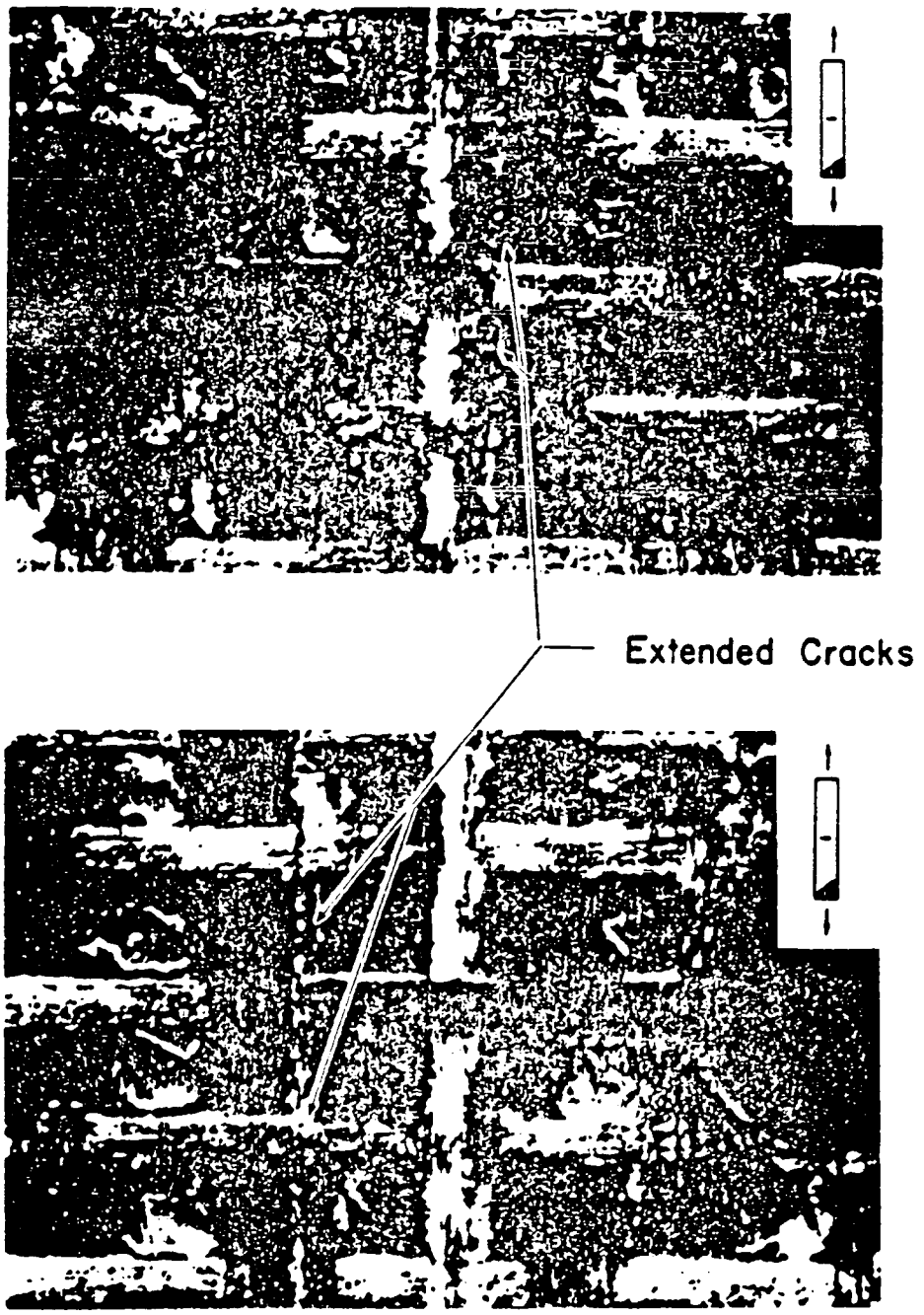

Figure 34. Experimentally Observed Crack Extension in 0° Coupon, Ref.[48]

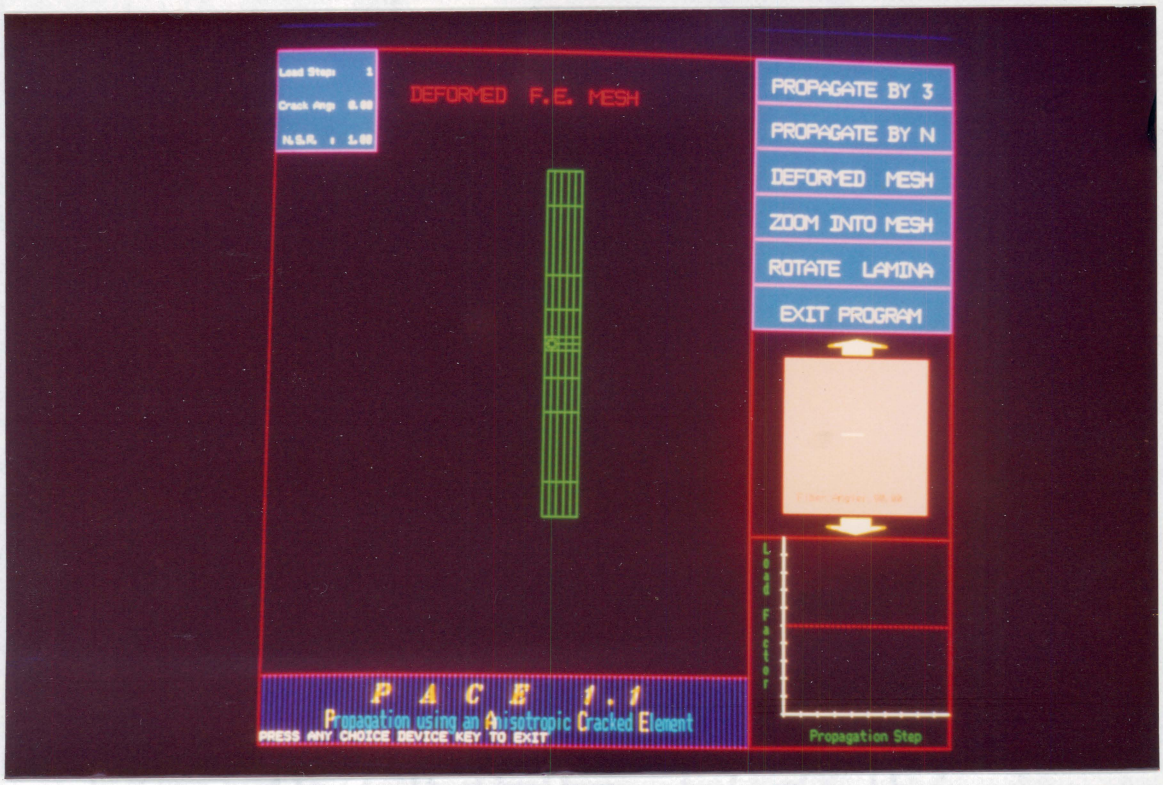

Figure 35. Simulated Crack Extension in 0° Coupon

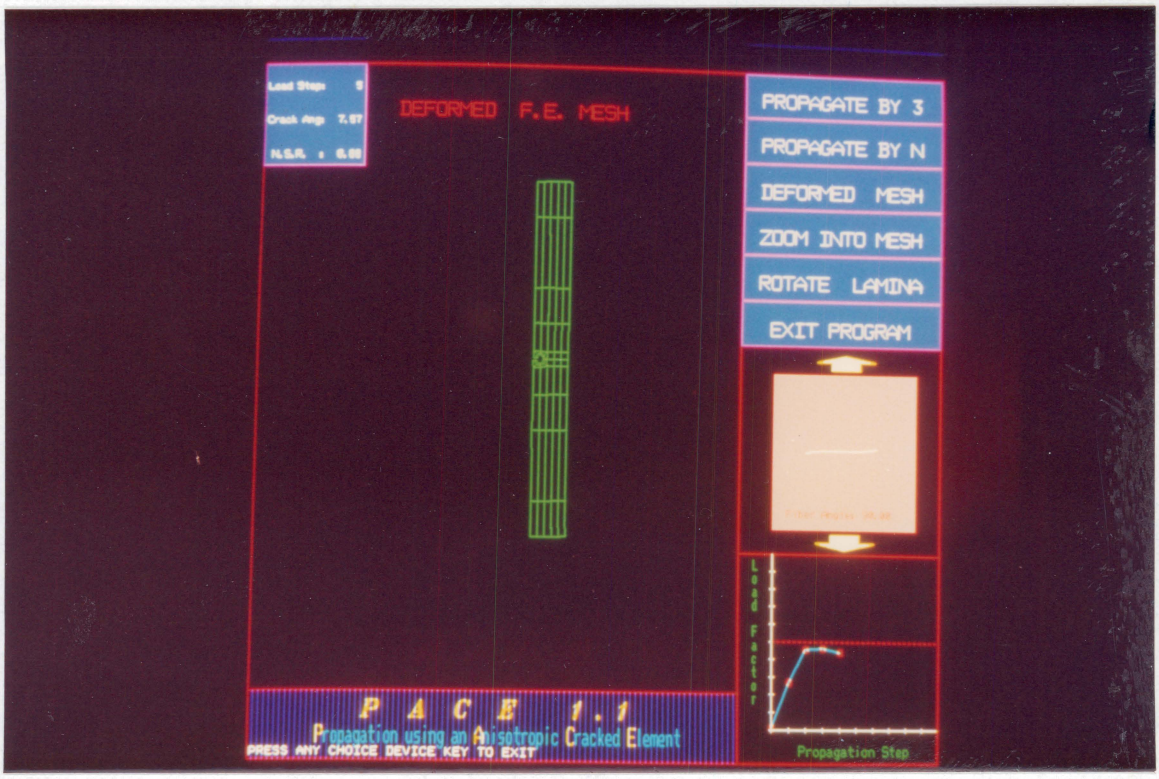
DEFORMED F.E. MESH
PROPAGATE BY 3
PROPAGATE BY N
DEFORMED MESH
ZOOM INTO MESH
ROTATE LAMINA
EXIT PROGRAM
Load Factor
Propagation Step
P A C E 1.1
Propagation using an Anisotropic Cracked Element
PRESS ANY CHOICE DEVICE KEY TO EXIT

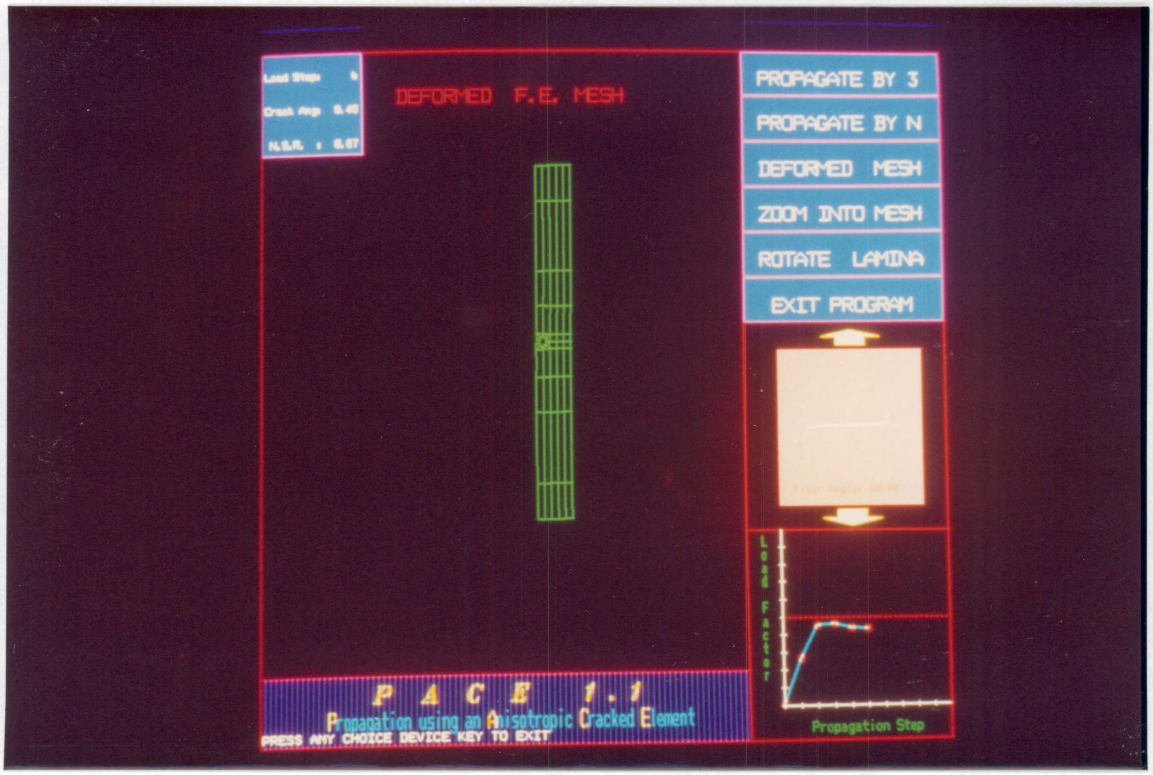
DEFORMED F.E. MESH
PROPAGATE BY 3
PROPAGATE BY N
DEFORMED MESH
ZOOM INTO MESH
ROTATE LAMINA
EXIT PROGRAM
Load Factor
Propagation Step
P A C E 1.1
Propagation using an Anisotropic Cracked Element
PRESS ANY CHOICE DEVICE KEY TO EXIT

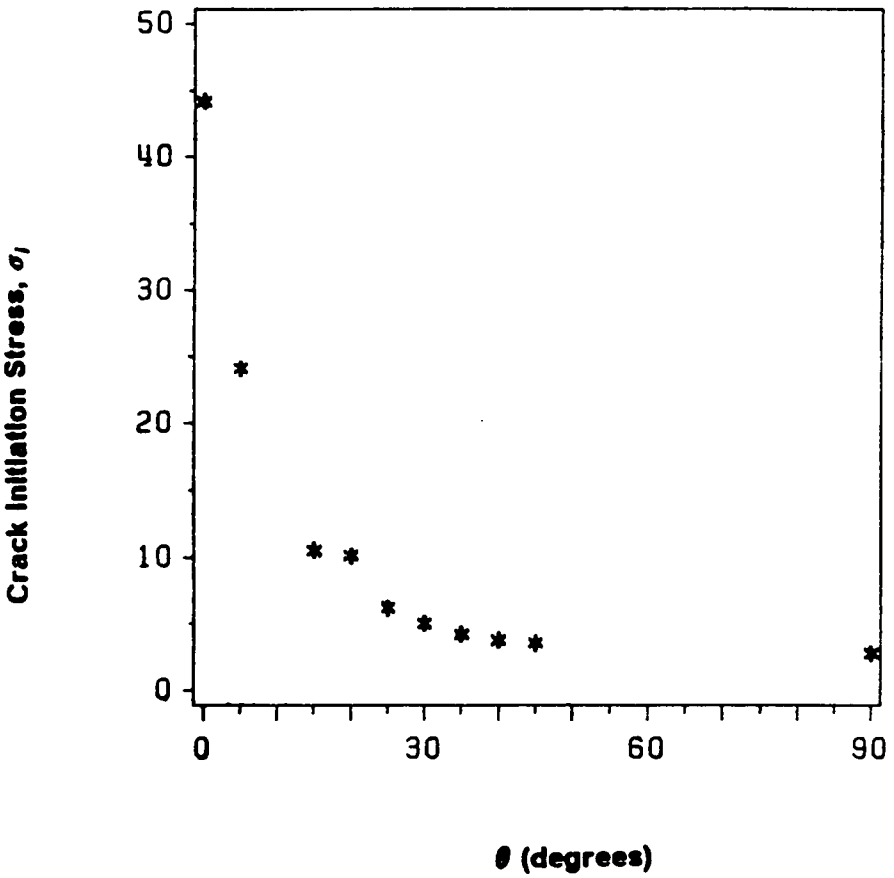

Figure 36. Crack Initiation Stress vs Fiber Angle, θ

6.0 Conclusions

This research effort consisted of two main parts : (i) the formulation and application of an anisotropic singular element (ASE) for analyzing homogeneous anisotropic materials with cracks and, (ii) graphical simulation of crack growth in unidirectional composites. The main conclusions that can be drawn from this study are :

- The anisotropic singular element (ASE) developed in Chapter 2 and validated in Chapter 3 was found to be both accurate and economical for the study of cracked homogeneous anisotropic materials. The element can be applied to analyze cracked anisotropic materials with arbitrary oriented cracks.

- The number of terms in the stress expansion, the size of the element and the number of nodes on the singular element can be varied, depending on the degree of accuracy required and the method of discretization of the adjacent domain. There is a large reduction in the number of elements (and nodes) employed when the ASE is used leading to : (i) easier mesh generation, (ii) a significant reduction in the bandwidth of the global stiffness matrix, and (iii) faster computing times.

- The stress distributions obtained using the ASE compare well with those obtained employing quarter point elements. Stress intensity factor calculations (SIF) are direct and involve no complex post processing. The SIFs obtained using the ASE are in good agreement with those obtained using other methods such as the boundary integral method.

- The superposition method adopted for separating the far field stress components is simple and accurate, avoiding the need of generating new meshes for different crack angles.

- Inversion symmetry used along with the singular element developed reduced the number of degrees of freedom of the problem and was found to give accurate results.

- Application of the normal stress ratio theory within a macroscopic-level sharp crack analysis shows potential for analyzing cracks in unidirectional composites. As noted in previous works, the direction of crack propagation predicted using the normal stress ratio theory is in excellent agreement with the experimentally observed values.

- The crack initiation stress predicted using the normal stress ratio theory were in reasonable agreement with the experimental values. The extension of the NSR theory to predict initiation stresses has provided a significant test of its validity. This also gives confidence in the choice of the baseline test used to evaluate r_o.

- PHIGS is found to be a flexible programming interface for integrating graphics with the finite element program.

This is the first attempt at graphical simulation of crack growth in composites and the simulation methods and remeshing algorithm presented provides a method to track crack growth in unidirectional composites. The major emphasis of the second stage of this study was to integrate interactive computer graphics with singular finite elements to demonstrate and take advantage of the power and flexibility of computer based analysis to aid the design process. Future analytical efforts should include the use of the normal stresses ratio theory for charac-

terizing the parameters of crack growth in a simulation algorithm such as presented in this study. Appendix E presents possible areas of extending the current research effort.

The features unique to this research effort are :

- development and application of the anisotropic singular element (ASE)
- extension of the normal stress ratio (NSR) theory for stability analysis
- use of the latest industry ANSI (and ISO) graphics standard, PHIGS, for crack growth simulation
- the propagation (remeshing) algorithm presented
- Integration of all the above with inversion symmetry and load superposition methods.

7.0 References

[1] Herakovich, C.T. "Influence of Layer Thickness on the strength of Angle-Ply Laminates," *Journal of Composite Materials*, Vol. 16, 1982, pp. 216-227.

[2] Kanninen, M.F., and Popelar, C.H., "Advanced Fracture Mechanics " Oxford University Press Inc., N.Y., 1985.

[3] Swedlow, J.L., Williams, M.L., and Yang, W.H., "Proceedings of the First International Conference on Fracture," 1966, p.259.

[4] Kobayashi, A.S., Maiden, D.E., and Simon, B.J., ASME paper # 69-WA/PVP-12, American Society of Mechanical Engineers, 1969.

[5] Chan, S.K., Tuba, I.S., and Wilson, W.K., "On the Finite Element Method in Linear Elastic Fracture Mechanics," *Engg. Fracture Mechanics*, Vol. 2, No.1, 1970, p.1.

[6] Oglesby, J.J. and Lomacky, O., "An evaluation of Finite Element Methods for the computation of Elastic Stress Intensity Factors," Navy Ship Research and Development Center, NAVSHIPS Project SF35422.210, Task 15055, Report # 3751, December 1971.

[7] Fawkes, A.J., Owens, D.R., Luxmoore, A.R., "An Assessment of Crack Tip Singularity Models for use with Isoparametric Elements," *Engg. Fracture Mechanics*, Vol.11, 1979, pp. 143-159.

[8] Gallagher, R.H., "A Review of Finite Element Techniques in Fracture Mechanics," Proc. of the First International Conf. on Numerical Methods in Fracture Mechanics, 1978, p.1.

[9] Kobayashi, A.S., "Numerical Analysis in Fracture Mechanics," *Proceedings of the International Conference on Applications of Fracture Mechanics to Materials and Structures, June 20-24,1983,* edited by Sih, G.C., Sommer, E., and Dahl, W., M. Nijhoff Publishers, 1984.

[10] Maschke, H.G., and Kuna, M, "A Review of Boundary and Finite Element Methods in Fracture Mechanics," *Theoretical and Applied Fracture Mechanics*, Vol. 4, 1985, pp. 181-190.

[11] Atluri, S.N., and Nakagaki, M., "Computational Methods for plane problems of fracture," *in Computational Methods in the Mechanics of Fracture,* edited by S.N. Atluri, Vol. 2, North Holland, 1986.

[12] Freese, C.E., and Tracey, D.M., "The Natural Isoparametric Triangle versus Collapsed Quadrilateral for Elastic Crack Analysis," *Int. Jour. of Fracture,* Vol.12, 1976, pp.767-771.

[13] Henshell, R.D., and Shaw, K.G., "Crack Tip Finite Elements are Unnecessary" *Int. Jour. for Numerical Methods in Engineering* Vol.9, 1975, pp.495-507.

[14] Barsoum, R.S., "Triangular Quarter-point Elements as Elastic and Perfectly Plastic elements," *Int. Jour. for Numerical Methods in Engineering,* Vol. 11, 1977, pp.85-98.

[15] Saouma, V.E, and Schwemmer, D., "Numerical Evaluation of the Quarter Point Crack Tip Element," *Int. Jour. for Numerical Methods in Engineering,* Vol.20, 1984, pp. 1629-1641.

[16] Manu, C., "Quarter Point Elements for Curved Crack Fronts," *Computers and Structures* Vol. 17, 1983, pp.227-231.

[17] Gregory, M.A., Choksi, G.N., Herakovich, C.T., "Orthotropic Fracture using a Singular Isoparametric Element," Pressure Vessel Components Design and Analysis, PVP Vol.98-2, edited by : Gwaltney, R.C., ASME, N.Y., 1985.

[18] Choksi, G.N., Herakovich, C.T., "Fracture of Composites," Proceedings of the IV International Conference for Numerical Methods in Fracture, edited by : Owens, Luxmoore and Rajapakse, San Antonio, March 1987.

[19] Pu, S.C., Hussain, M.A., and Lorensen, W.E., "The Collapsed Cubic Element as a Singular Element for Crack Problems," *Int. Jour. for Num. Meth. in Engg.,* Vol.12, 1978, pp 1727-1742.

[20] Nayfeh, A.H., and Nassar, E.A.N., "Mathematical Simulation of Singularities for Isoparametric Elements of Arbitrary Orders," *Int. Jour. for Num. Meth. in Engg.,* Vol.17, 1981, pp 465-476.

[21] Blackburn, W.S., "Calculations of Stress Intensity Factors at Crack Tips using Special Finite Elements". *in The Mathematics of Finite Elements and Application,* Ed. J.R. Whiteman, Academic Press, 1973, pp.327-336.

[22] Stern, M., "Families of Consistent Conforming Elements with Singular Fields " *Int. Jour. for Num. Meth. in Engg.,* Vol.14, 1979, pp 409-421.

[23] Akin, J.E., "The Generation of Elements with Singularities " *Int. Jour. for Num. Meth. in Engg.,* Vol.10, 1976, pp 1249-60.

[24] Wilson, W.K., "Finite Element Methods for Elastic Bodies Containing Cracks," *Mechanics of Fracture,* Vol. 1, edited by Sih, G.C., Noordhoff International Publishing, Leyden, 1973, pp. 484-500.

[25] Williams, M.L., "Stress Singularities Resulting from Various Boundary Conditions in Angular Corners of Plates in Extension," *J. of Applied Mechanics,* Vol. 19, 1952, pp. 526-528.

[26] Gross,B., Roberts,E.,Jr., and Srawley, J.E., "Stress Intensity Factors Using the Boundary Collocation Method " *Int. Jour. of Fracture Mechanics* Vol. 6, 1970, p. 87.

[27] Byskov, I., "The calculation of stress intensity factors using the finite element method with cracked elements," *Int. Jour. of Fracture Mechanics* Vol. 6, 1970, pp.159-167.

[28] Benzley,S.E., "Representation of singularities with isoparametric finite elements," *Int. Jour. Num. Meth. Engg.,* Vol. 8, 1974, pp.537-545.

[29] Foschi, R.O., and Barrett J.D., "Stress Intensity Factors in Anisotropic Plates using Singular Isoparametric Elements " *Int. Jour. Num. Meth. Engg.*, Vol. 10, 1976, pp.1281-87.

[30] Heppler, G., and Hansen, J.S., "Mixed mode fracture analysis of rectilinear anisotropic plates by high order finite elements " *Int. Jour. Num. Meth. Engg.*, Vol. 17, 1981, pp. 455-464.

[31] Pian, T.H.H., Tong, P., and Luk, C.H., "Elastic crack analysis by a finite element hybrid method" *Proc. 3rd Conf. on Matrix Methods in Structural Analysis*, Wright Patterson AFB, AFFDL-TR-71-160, pp. 661-682 (Dec. 1973)

[32] Tong, P., and Atluri, S.N., "On hybrid crack element techniques for fracture analysis," *Proc. Int. Conf. on Frac. Mechanics in Engg. & Tech.*, Ed. G.C.Sih (Noordhoff, The Hague, 1977).

[33] Tong, P., Pian,T.H.H., and Orringer, O., "Fracture mechanics analysis with hybrid 'crack' elements," in *Case Studies in Fracture Mechanics*, AMMRC MS 77-5 (Army Materials and Mechanics Research Center, 1977) pp.2.4.1-2.4.16.

[34] Wang, S.S., "Elasticity Solutions for a Class of Composite Laminate Problems with Stress Singularities," *Mechanics of Composite Materials: Recent Advances*, Hashin, Z., and Herakovich, C.T. (editors), Pergamon Press, 1983.

[35] Wu, E.M., "Strength and Fracture of Composites," *Composite Materials*, Vol 5.,edited by L.J. Broutman, Academic Press, New York, 1984, pp. 191-247.

[36] Sih, G.C., "A Special Theory of Crack Propagation, " *Method of Analysis and Solutions of Crack Problems*, Noordhoff Int., 1972.

[37] Sih, G.C., Chen, E.P., Huang, S.L. and McQuillen, E.J., "Material Characterization on the Fracture of Filamant-Reinforced Composites," *Journal of Composite Materials*, Vol. 9, 1975, pp. 167-186.

[38] Zweben, C., "Fracture Mechanics and Composite Materials : A Critical Analysis " *Analysis of the Test Methods for High Modulus Fibers and Composites* ASTM STP 521, 1973, pp. 64-67.

[39] Wu, E.M. , "Some Unique Crack Propogation Phenomenon in Unidirectional Composites and their Mathematical Characterization, " *Structure,Solid Mechanics and Engineering Design*, Proceedings of the Southampton 1969 Civil Engineering Materials Conference, Part 2, edited by M. Te'eni, Wiley-Interscience,1969.

[40] Wu, E.M. , "Failure Criteria and Fracture Mode Analysis of Composite Laminates," Advisory Group for Aerospace Research & Development Conference Proceedings, AGARD-CP-163, NATO, 1974.

[41] Lo, K.H., Wu, E.M., and Konishi, D.Y., "Failure Strength of Notched Composite Laminates," *Journal of Composite Materials*, Vol. 17, 1983, pp. 384-398.

[42] Sih, G.C. and Chen, E.P., "Mechanics of Fracture," Vol.6 , Martinus Nijhoff Publishers, 1981.

[43] Whitney, J.M. and Nuismer, R.J., "Stress Fracture Criteria for Laminated Composites containing Stress Concentration," *Journal of Composite Materials*, Vol. 8, 1974, pp.253-265.

[44] Buczek, M.B. and Herakovich, C.T., "Finite Element Models for Predicting Crack Growth Characteristics in Composite Materials," VPI-E-82-29, College of Engineering, Virginia Polytechnic Institute & State University, Blacksburg, Virginia, 1982.

[45] Buczek, M.B. and Herakovich, C.T., "Direction of Crack Growth in Fibrous Composites," Mechanics of Composite Materials 1983, AMD-Vol.58, edited by Dvorak, G.J., American Society of Mechanical Engineers, 1983.

[46] Gregory, M.A. and Herakovich, C.T., "Prediction of Crack Extension Direction in Unidirectional Composites," CCMS-84-11, VPI-E-84-27, College of Engineering, Virginia Polytechnic Institute & State University, Blacksburg, Virginia, 1984.

[47] Beuth, Jr., J.L., Gurdal, Z., and Herakovich, C.T., "Composite Fracture using the Normal Stress Ratio Theory " *Proceedings, AMSE WInter Annual Meeting* , 1986. (to be published)

[48] Beuth, Jr., J.L. and Herakovich, C.T., "An Analytical and Experimental Study of Crack Extension in Center-Notched Composites " CCMS-87-09, VPI-E-87-10, College of Engineering, Virginia Polytechnic Institute & State University, Blacksburg, 1987.

[49] Buczek, M.B. and Herakovich, C.T., "A Normal Stress Criterion for Crack Extension Direction in Orthotropic Composite Materials " *J. of Composite Materials*, Vol.19, No.6, Nov. 1985, pp.544-553

[50] Gregory, M.A, Beuth, Jr.,J.L.,Barbe, A., and Herakovich, C.T., "Application of the Normal Stress Ratio Theory for Predicting the Direction of Crack Growth in Unidirectional Composites " *Fracture of Fibrous Composites* , (C.T.Herakovich, Ed.) ASME, AMD Vol.G00294, NY, 1985.

[51] Beuth, Jr., J.L. and Herakovich, C.T., "On Fracture of Fibrous Composites " *Composites '86: Recent Advances in Japan and the United States*, K.Kawata, S. Umekawa & A. Kobayashi, Ed., Proc. Japan-US CCM-III, Tokyo, 1986.

[52] Gurdal,. Z., and Herakovich, C.T., "Effect of Initial Flaw Shape on Crack Extension in Orthotropic Composite Materials " *Theo. and App. Fracture Mech.*, Vol. 8, 1987, pp.59-75.

[53] Barbe, A., and Herakovich, C.T., "A Critical Assessment of Crack Growth Criteria in Unidirectional Composites " CCMS-85-09, VPI-E-85-20, College of Engineering, Virginia Polytechnic Institute & State University, Blacksburg, 1985.

[54] Souma, V.E., "Mixed Mode Crack Propagation in Homogeneous Anisotropic Solids, " *Engg. Fracture Mechanics*, Vol. 27,No. 2 ,1987, pp. 171-184.

[55] Yehia, N.A. "Automatic Tracking of Crack Growth via Finite Elements," *Dissertation*, Rensselaer Polytechnic Institute, New York, 1984.

[56] Sih, G.C., and Chen, E.P., "Fracture Analysis of Unidirectional Composites," *J. of Composite Materials*, Vol. 7, 1973, pp. 230-244.

[57] Poe, C.C., and Sova, J.A., "Fracture Toughness of Boron/Aluminum Laminates with various Proportions of 0 and 45 Plies," NASA TP-1707, Nov. 1980.

[58] Hedgepeth, J.M., and Van Dyke, P., "Local Stress Concentrations in Imperfect Filamentary Composite Materials," *J. of Composite Materials*, Vol.1, pp.294-309.

[59] Souma "Interactive Finite Element Analysis of Reinforced Concrete : A Fracture Mechanics Approach " *Ph.D. Dissertation*, Dept. of Civil Engg., Cornell University, 1981.

[60] Ingraffea, A.R., and Souma, V.E., "Numerical Modelling of Discrete Crack Propagation in Reinforced and Plain Concrete Structures " *Application of Fracture Mechanics to Concrete Structures* A. Carpinteri, A. DiTommaso, A.R. Ingraffea and G.C. Sih, editors, Martinus Nijhoff Publishers, 1983.

[61] Lekhnitskii, S.G., "Theory of Elasticity of an Anisotropic Elastic Body," English translation by Brandstatton, Holden-Day Inc., San Francisco, 1963.

[62] Heng, Z.D., McCammond, D., Tabarrok, B.T., "Stress Determination in Edge-Cracked Anisotropic Plates by an extension of Boundary-Collocation Method," *Comp. Meth. in App. Mech. & Engg.*, Vol. 54, 1986, pg.187-195.

[63] Jones, R., and Callinan, R.J., "On the use of Special Crack Tip Elements in Cracked Elastic Sheets," *Int. Jour. of Fracture*, Vol. 13, 1977, pp. 51-64.

[64] Snyder, M. D., and Cruse, T.A., "Crack Tip Stress Intensity Factors in Finite Anisotropic Plates " *Air Force Materials Laboratory* , AFML-TR-73-209, Aug. 1973.

[65] Chou, C.S., Anderson, J.M., Bartdof, W.J., Aberson, J.A., "Finite Element Computer Program to Analyze Cracked Orthotropic Sheets" *NASA CR-2698* , July 1976.

[66] Noor, A.K., and Mathers, M.D., "Finite Element Analysis of Anisotropic Plates " *Int. Jour. Num. Meth. Engg.*, Vol.11, 1977, pp.289-307.

[67] Wu, E.M., and Reuter Jr., R.C., "Crack Extension in Fiberglass Reinforced Plastics " T & AM Report No. 275 (University of Illinois, USA), 1965.

[68] Kim, R.Y., "On the Off-axis and Angle-Ply Strength of Composites " *ASTM STP 734* (American Society for Testing and Materials, 1981) pp 91-108.

[69] Donaldson, S.L., "Fracture Toughness Testing of Graphite/Epoxy and Graphite/Peek Composites " *Composites*, 1985, pp.103-112.

[70] Tay, T.E., Williams, J.F, and Jones, R., "Characterization of Pure and Mixed Mode Fracture in Composite Laminates " *Theo. and App. Fracture Mechanics*, Vol. 7, 1987, pp.115-123.

[71] Bilby, B.A. and Cardew, G.E., "The Crack with a Kinked Tip, " *Int. Jour. of Fracture*, Vol. 11, 1975, pp.708-711.

[72] Cotterell, B., and Rice, J.R., "Slightly Curved or Kinked Cracks, " *Int. Jour. of Fracture*, Vol. 16, No. 2, 1980, pp.155-169.

[73] Karihaloo, B.L., Keer, L.M., and Nemat-Nasser, S., "Crack Kinking Under Nonsymmetric Loading, " *Engg. Fracture Mechanics*, Vol.13, 1980, pp.879-888.

[74] Melin, S., "Fracture from a Straight Crack Subjected to Mixed Mode Loading ", *Int. Jour. of Fracture*, Vol. 32, 1987, pp.257-263.

[75] Smith, C.W., "Optical Methods in Fracture Mechanics ", *Fatigue and Fracture Assessment by Analysis and Testing*, PVP-Vol. 103, edited by Bhandari, S.K., Zamrick, S.Y., and An-Yang, M.K., ASME, 1986.

[76] Herrmann, K.P., and Grebner, H., "Curved Thermal Crack Growth in Non homogeneous Materials with Different Shaped External Boundaries : I. Theoretical Results, " *Theo. and App. Fracture Mechanics*, Vol. 2, 1984, pp.133-146.

[77] "Introducing graPHIGS, " IBM document No. SC33-8100, IBM Corp., Kingston, NY, 1986.

[78] "Understanding graPHIGS, " IBM document No. SC33-8102-0, IBM Corp., Kingston, NY, 1986.

[79] "Writing Applications with graPHIGS " IBM document No. SC33-8103-1, IBM Corp., Kingston, NY, 1986.

[80] Reddy, J.N., "An Introduction to the Finite Element Method ", McGraw Hill Book Company, New York, NY 10020.

[81] Delale, F., "Stress Singularities in Bonded Anisotropic Materials," *Int. Jour. of Solids and Structures,* Vol. 20, 1984, pg.31-40.

[82] Ting, T.C.T., and Hoang, D.H., "Singularities at the Tip of a Crack Normal to the Interface of an Anisotropic Layered Composite," *Int. Jour. of Solids and Structures,* Vol. 20, 1984, pp. 439-454.

Appendix A. Terms of the Compliance Matrix

This appendix presents the individual members of the compliance matrix used in equation (2.2). The strain - stress equation is :

$$\{\varepsilon\} = [A]\{\sigma\}$$

The elements a_{ij} of the symmetric matrix, A are :

$$a_{11} = S_{11}\cos^4\theta + (2S_{12} + S_{66})\sin^2\theta\cos^2\theta + S_{22}\sin^4\theta$$

$$a_{12} = S_{12}(\sin^4\theta + \cos^4\theta) + (S_{11} + S_{22} - S_{66})\sin^2\theta\cos^2\theta$$

$$a_{22} = S_{11}\sin^4\theta + (2S_{12} + S_{66})\sin^2\theta\cos^2\theta + S_{22}\cos^4\theta$$

$$a_{16} = (2S_{11} - 2S_{12} - S_{66})\sin\theta\cos^3\theta - (2S_{22} - 2S_{12} - S_{66})\sin^3\theta\cos\theta$$

$$a_{26} = (2S_{11} - 2S_{12} - S_{66})\cos\theta\sin^3\theta - (2S_{22} - 2S_{12} - S_{66})\cos^3\theta\sin\theta$$

$$a_{66} = 2(2S_{11} - 2S_{22} - 4S_{12} - S_{66})\sin^2\theta\cos^2\theta + S_{66}(\sin^4\theta + \cos^4\theta)$$

where

$$S_{11} = \frac{1}{E_1} \quad , \quad S_{12} = -\frac{\nu_{12}}{E_1} = -\frac{\nu_{21}}{E_2} \quad , \quad S_{22} = \frac{1}{E_2} \quad , \quad S_{66} = \frac{1}{G_{12}}$$

and θ and the directions 1,2 are defined in Figure 37.

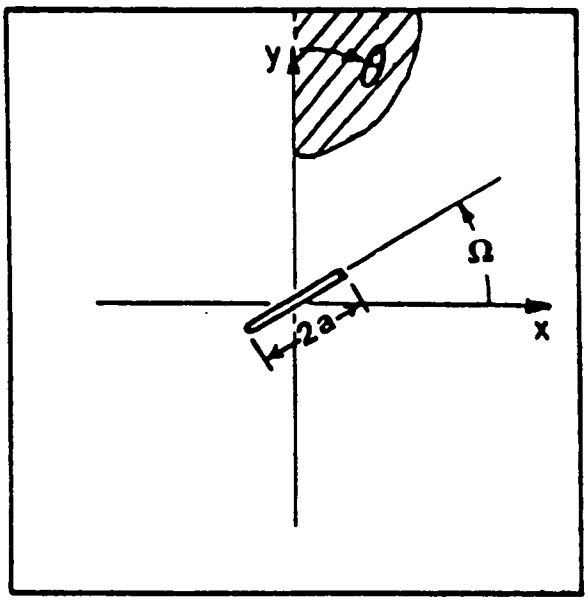

Figure 37. Lamina Geometry

Appendix B. Material Properties

Table 5. Properties of Gr/Ep used for comparison of stress components with Quarter Point Elements

ELASTIC PROPERTIES
$E_1 =$ 149.0 *GPa* (21.6 *msi*)
$E_2 =$ 13.5 *GPa* (1.96 *msi*)
$G_{12} =$ 5.72 *GPa* (0.830 *msi*)
$\nu_{12} = 0.280$

Table 6. Properties of Gr/Ep used for comparison of finite width correction factors, Y

ELASTIC PROPERTIES (from Refs. [30,64,65])
$E_1 =$ 144.795 *GPa* (21.0 *msi*)
$E_2 =$ 11.722 *GPa* (1.70 *msi*)
$G_{12} =$ 9.653 *GPa* (1.40 *msi*)
$\nu_{12} = 0.210$

Table 7. Properties used for graphite epoxy in crack propagation studies

ELASTIC PROPERTIES (from Ref. [48])
$E_1 =$ 126.178 *GPa* (18.3 *msi*)
$E_2 =$ 9.998 *GPa* (1.45 *msi*)
$G_{12} =$ 5.613 *GPa* (0.814 *msi*)
$\nu_{12} = 0.305$
STRENGTH PROPERTIES
$X_T =$ 1.448 *GPa* (210.0 *ksi*)
$Y_T =$ 53.4 *MPa* (7.75 *ksi*)
$S =$ 99.3 *MPa* (14.4 *ksi*)

Appendix C. Stress Intensity Factors

Stress intensity factors can be derived directly for the various cases using the stress expansions of Chapter 2. Section 3.2 detailed the derivation of the Mode I stress intensity factor (SIF) for equal real parts of the roots of the characteristic equation (eqn. (2.8)). This was defined as Case (i). Case (ii) is when unequal real parts of equation (2.8) are obtained. This Appendix presents the derivation for :

1. K_{II} for Case (i)
2. K_I for Case (ii)
3. K_{II} for Case (ii)

As the stress intensity factor is the 'strength' of the singular (the first) term in the stress expansions, the following values are common to all the cases described below :

$$\omega = -\frac{1}{2}, \quad \zeta = \frac{3}{2}, \quad \psi = \frac{1}{2}, \quad r_1^{\omega} = r_2^{\omega} = \frac{1}{\sqrt{r}}, \quad \theta_1 = \theta_2 = 0 \tag{C.1}$$

1. K_{II} for Case (i)

By definition, the mode II stress intensity factor K_{II} is :

$$K_{II} = \lim_{r \to 0} \sqrt{2\pi r}\, \tau_{xy}|_{\phi=0} \tag{C.2}$$

Substituting for the first term of the stress expansion, for $\tau_{xy}|_{\phi=0}$, (eqn. 2.23) yields :

$$\tau_{xy}|_{\phi=0} = -2\zeta\psi \frac{1}{\sqrt{r}} \left[b_{1j} \left(-\frac{\alpha\delta}{\beta} + \gamma\right) + b_{2j}(\beta - \delta)\right] \tag{C.3}$$

Substituting (C.3) into (C.2) :

$$K_{II} = -\sqrt{2\pi}\, \frac{3}{2} \left[b_{1j} \left(-\frac{\alpha\delta}{\beta} + \gamma\right) + b_{2j}(\beta - \delta)\right] \tag{C.4}$$

where β and δ are the imaginary parts and α and γ are the real parts of the roots of the characteristic equation (eqn. 2.8). The terms b_{1j} and b_{2j} are the values of the constants in the stress function obtained by substituting the displacements $\underline{\delta}$ from the finite element solution into equation (2.33).

2. K_I for Case (ii)

By definition, the mode I stress intensity factor K_I is :

$$K_I = \lim_{r \to 0} \sqrt{2\pi r}\, \sigma_y|_{\phi=0} \tag{C.5}$$

Substituting for the first term of the stress expansion, for $\sigma_y|_{\phi=0}$, (eqn. 2.25) yields :

$$\sigma_y|_{\phi=0} = \frac{1}{\sqrt{r}} \left[a_{1j} + \frac{3}{2} b_{1j}\right] \tag{C.6}$$

Substituting (C.6) into (C.5) :

$$K_I = \sqrt{2\pi}\,[a_{1j} + \frac{3}{2} b_{1j}] \qquad (C.7)$$

where the terms a_{1j} and b_{1j} are the values of the constants in the stress function obtained by substituting the displacements $\underline{\delta}$ from the finite element solution into equation (2.35).

3. K_{II} for Case (ii)

By definition, the mode II stress intensity factor K_{II} is :

$$K_{II} = \lim_{r \to 0} \sqrt{2\pi r}\, \tau_{xy}|_{\phi=0} \qquad (C.8)$$

Substituting for the first term of the stress expansion, for $\tau_{xy}|_{\phi=0}$, (eqn. 2.25) yields :

$$\tau_{xy}|_{\phi=0} = -\frac{1}{\sqrt{r}} \left[a_{1j}(\alpha - \beta + \frac{\beta^2 - \beta\delta}{\alpha - \gamma}) + \frac{3}{2} b_{1j}(\gamma - \delta + \frac{\beta\delta - \delta^2}{\alpha - \gamma})\right] \qquad (C.9)$$

Substituting (C.9) into (C.8) :

$$K_{II} = -\sqrt{2\pi}\,\left[a_{1j}(\alpha - \beta + \frac{\beta^2 - \beta\delta}{\alpha - \gamma}) + \frac{3}{2} b_{1j}(\gamma - \delta + \frac{\beta\delta - \delta^2}{\alpha - \gamma})\right] \qquad (C.10)$$

where β and δ are the imaginary parts and α and γ are the real parts of the roots of the characteristic equation (eqn. 2.8). The terms a_{1j} and b_{1j} are the values of the constants in the stress function obtained by substituting the displacements $\underline{\delta}$ from the finite element solution into equation (2.35).

Appendix D. Simulation Based on Classical Methods

D.1 Introduction

Chapter 4 presented a method based on the normal stress ratio theory to predict crack growth direction and crack initiation stresses. Classical fracture mechanics based approaches were also used in this study to predict stability of crack propagation. They are described in this appendix. The methods used are :

- Method 1: Based on Strain Energy Release Rates (G_c approach)
- Method 2: Based on Stress Intensity Factors (Fracture Toughness, K_c approach)

These methods were incorporated into the program (PACE) and as the analysis was performed, crack propagation parameters obtained from all three (the NSR theory and Methods 1,2 above) were updated. The methods were used only to predict onset on unstable crack propagation and the NSR theory was used to predict the direction of crack propagation.

D.2 Method 1 : Based on Strain Energy Release Rates

As described in the method of Chapter 4, a step-by-step procedure is adopted. Steps are not repeated if they are similar to that of Chapter 4 (using the NSR theory).

STEP 1 : Same as Step 1 of the method in Chapter 4 where the initial cracked plate geometry subjected to the given boundary conditions is analyzed for the crack tip displacement and stress fields using the singular element developed.

STEP 2 : The direction of crack propagation is predicted using the NSR theory as described previously. For the graphite-epoxy material system analyzed (Chapter 5) in this study, the experiments of Beuth and Herakovich [48] indicate that after the first increment of crack growth in a non-self similar manner, the crack grows for the remainder of its trajectory along the fiber direction until failure. This implies that after the first increment, the crack growth is self-similar. This type of behavior simplifies the analysis a great deal. The only assumption is that an arbitrary small Δa be specified at the end of Step 1 in the predicted direction of propagation.

Calculation of G

For the propagation analysis, the stress intensity factors, K_I and K_{II} are calculated directly using the results of the singular element, as described in Chapter 3. Using the relation given below [70],

$$G_I = K_I^2 \left[\frac{1}{2} E_{11} E_{22}\right]^{1/2} \left[\left(\frac{E_{11}}{E_{22}}\right)^{1/2} - \nu_{12} + \frac{E_{11}}{2G_{12}}\right]^{1/2} \qquad (D.1)$$

When the total strain energy release rate equals G_{IC} , unstable crack growth occurs. This method is only applicable for cases when the crack is along the fibers as crack growth is then

self similar. The calculation of G_c for the material analyzed is given in a later section of this appendix.

D.3 Method 2 : Based on Fracture Toughness

This method is very similar to the method described above with the only difference that fracture toughness instead of the critical strain release rate is used as a criterion for instability.

For an initial central horizontal crack, calculation of the critical stress intensity factor K_{Ic} for the first propagation step is performed using a method similar to that of the NSR theory. As K_{Ic} is related directly to stress, a second order tensor transformation is used to obtain the critical intensity factor along any direction :

$$K_{IC} = K_{IC}^{0} \cos^2\beta + K_{IC}^{90} \sin^2\beta \tag{4.4}$$

where K_{IC}^{0} and K_{IC}^{90} are derived as shown in Figure 4.

As the propagation continues, the crack grows along the fiber direction (from the test results of the graphite epoxy system analyzed) and a K_c can be defined, similar to that used for defining G_c. This value of K_c is then used as a criterion for predicting the onset of instability.

D.4 Calculation of Fracture Toughness & Strain Energy Release Rate

Calculation of the critical strain energy release rate G_c and fracture toughness (critical stress intensity factor) K_c can be performed using the values obtained from the baseline test (described in Chapter 5). For the graphite-epoxy material system analyzed, the required quantities are obtained from the test results of Beuth & Herakovich [48]. For the 90° center cracked coupon under tensile loading,

$$K_{IC} = \sigma_c \sqrt{\pi a} \tag{D.2}$$

where σ_c is the experimentally obtained failure stress. The critical strain energy release rate can then be calculated[70] :

$$G_{IC} = K_{IC}^2 \left[\frac{1}{2} E_{11} E_{22}\right]^{1/2} \left[\left(\frac{E_{11}}{E_{22}}\right)^{1/2} - \nu_{12} + \frac{E_{11}}{2G_{12}}\right]^{1/2} \tag{D.3}$$

Two values for fracture toughness are tabulated below. K_{Ic}^0 is the fracture toughness for a specimen with a central horizontal crack, with the fibers at $\theta = 0°$. K_{Ic}^{90} is the fracture toughness for a specimen with a central horizontal crack, with the fibers at $\theta = 90°$. These two values are required for the criterion based on fracture toughness described in Chapter 4 (Method 3).

Crack growth simulations were performed on the material system analyzed (Chapter 5) for different fiber angles and crack path stability predicted. The predictions of stability of crack growth using the two methods described in this appendix were not found to be consistent with the experimental results. No definite conclusions regarding the prediction of onset of unstable crack growth based on the these methods are drawn at the present time.

Table 8. Properties for Gr/Ep

Quantity	Value
K_{IC}^{0}	32.957 ksi $\sqrt{in}$
K_{IC}^{90}	1.575 ksi $\sqrt{in}$
G_c	1.3E-6

Appendix E. Recommendations

E.1 Element Formulations

Solutions using a complex variable approach and stress function expansions are available in the literature [34] [81] [82] for the case of a general two wedge problem shown in Figure 38. Both layers are assumed to be homogeneous and anisotropic and the formulation assumes generalized plane strain conditions.

Wang [34], Delale [81], and Ting [82] have studied different forms of the two wedge formulation for cases shown in Figure 39. Changing the angles α & ϕ results in different geometries. The same approach used for developing the ASE can be used to generate special elements for the cases shown in Figure 39. The asymptotic expressions for the stress and displacement fields presented in the references can be used for the formulation. The stiffness matrix generated can then be introduced into any displacement based finite element program. Figure 39a shows two bonded layers with a stress free-edge which can be used to study edge effects or boundary layer effects in laminates. This case is obtained by setting $\alpha = \phi = 90°$. The case of a ply drop-off ($\alpha = 90°$, $\phi = 180°$) is shown in Figure 39b. A wedge bonded to a half-plane is shown in Figure 39c. ϕ is set to 180° and the angle of the wedge, α can be varied for this case. A

special element for a crack along the interface ($\alpha = \phi = 180°$) can be generated (Figure 39d). Stress expansions for a crack perpendicular to the interface of two anisotropic materials has been obtained by Ting [82] (Figure 39e) and a singular element can be generated using the least squares method.

E.2 Crack Growth Predictions

Interactive computer graphics combined with the flexibility and power of the finite element method provides the analyst with a powerful and attractive technique. Graphical simulation of crack growth can be a useful tool to aid in the characterization process of materials with flaws. Expensive experiments needed to analyze materials with cracks can be reduced by conducting a parallel analytical-experimental study, making use of simulation programs. To achieve this and to obtain meaningful results from the analysis, experimentally proven theories which can account for crack path stability in composite materials need to be developed, as mentioned in Chapter 6. Also, future efforts should include a model to predict crack initiation stresses. These theories can then be incorporated into PACE.

The program PACE is written using an international graphics standard (PHIGS) and FORTRAN 77 and can be modified or extended easily. It provides the foundation for graphics and finite element procedures upon which other special purpose programs can be built up. The program is general and can be integrated with general purpose finite element codes to simulate deformation patterns of beams in buckling or bending, vibrations of plates, etc. No modifications to the graphics portion is necessary to perform this. Interfacing the graphics portion with specialized finite element (or boundary element) schemes is straightforward as the graphics part requires only the nodal coordinates and element connectivity.

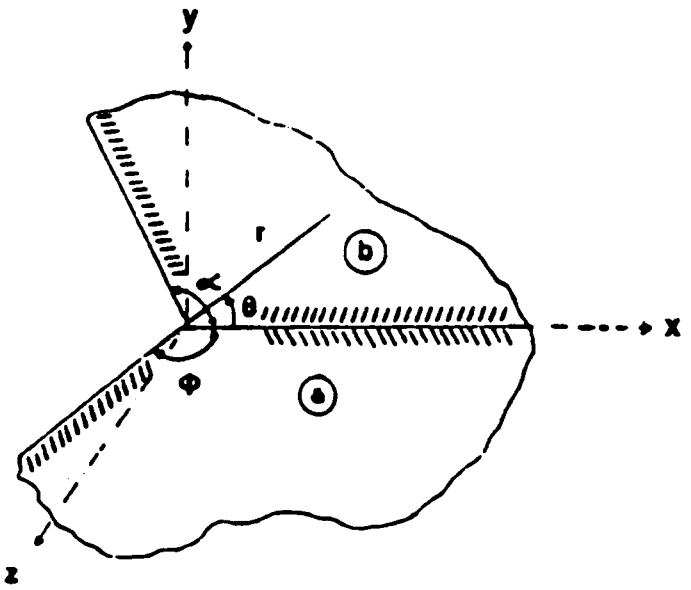

Figure 38. General Two Wedge Problem

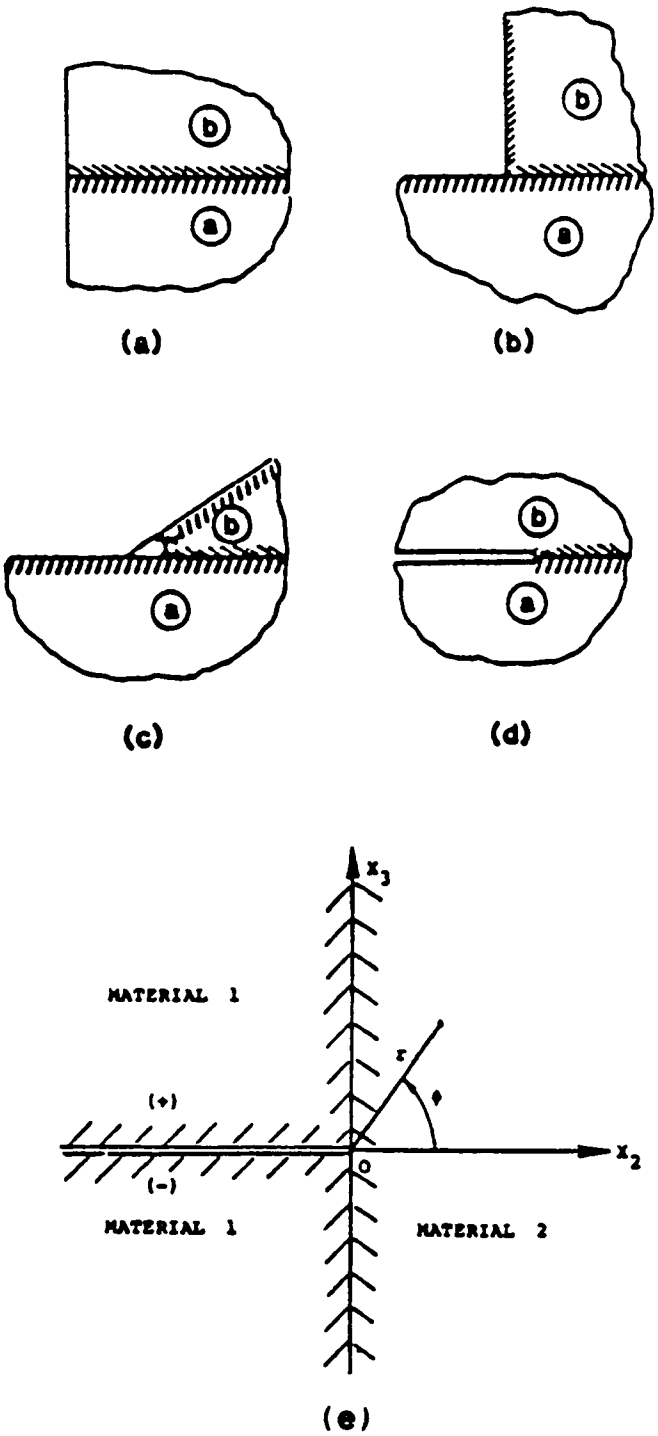

Figure 39. Interface Geometries as Special Cases of the Two Wedge Problem

Appendix F. Programmers Guide to PACE 1.1

F.1 Introduction

PACE (Propagation using an Anisotropic Cracked Element) is a two dimensional finite element program capable of analyzing cracked (and uncracked) anisotropic (and isotropic) structures. Chapter 4 presented a description of the program and its capabilities. This appendix presents a complete 'programmers manual' and 'user's guide' to PACE 1.1. PACE is menu driven at run time and is implemented at Virginia Tech on the IBM 5080 workstation attached to a IBM 4341 CPU serving as the host computer.

F.2 Capabilities of PACE

The program can be implemented on any system that has PHIGS software. The IBM PC RT, MicroVAX, Tektronix, Megatek are some of the popular systems that have implemented

versions of the PHIGS standard. The following is a list of the highlights and capabilities of PACE:

- 2-D displacement based code
- displacement and traction boundary conditions
- library of 2 different elements
- simulation of crack growth
- instability prediction during crack growth
- inversion symmetry
- output at nodes/gauss points
- output of displacements, stresses, strains, and strain energies
- calculation of stress intensity factors
- continuous zooming and rotations of undeformed and deformed meshes
- display of undeformed and deformed meshes at any load step
- simulation of the total deformation pattern of the structure
- choice of user defined load steps
- warm restart option (to continue analysis at a later time by saving all current parameters)
- plots of various parameters in a window on the screen
- generation of 'universal' files to interface output data with IBM/CAEDS to plot stress and displacement contours, shaded images, etc.

A description of the implementation and overall structure of the program is given next, followed by the method on how to use the program. The user input data formats and requirements are given as the last section to this Appendix.

F.3 Program Structure

The program is modular in structure with approximately 6000 lines of source code. The program is divided into 62 subroutines, each subroutine performing a specific task. This makes debugging and modifications easier. The ASE developed (Chapter 2) is incorporated into a

conventional displacement based program and integrated with graphics. Figure 40 gives the flow chart of the program. This flow chart should be consulted before any modifications to the program are attempted as it gives an overall view of the sequence of events in the program.

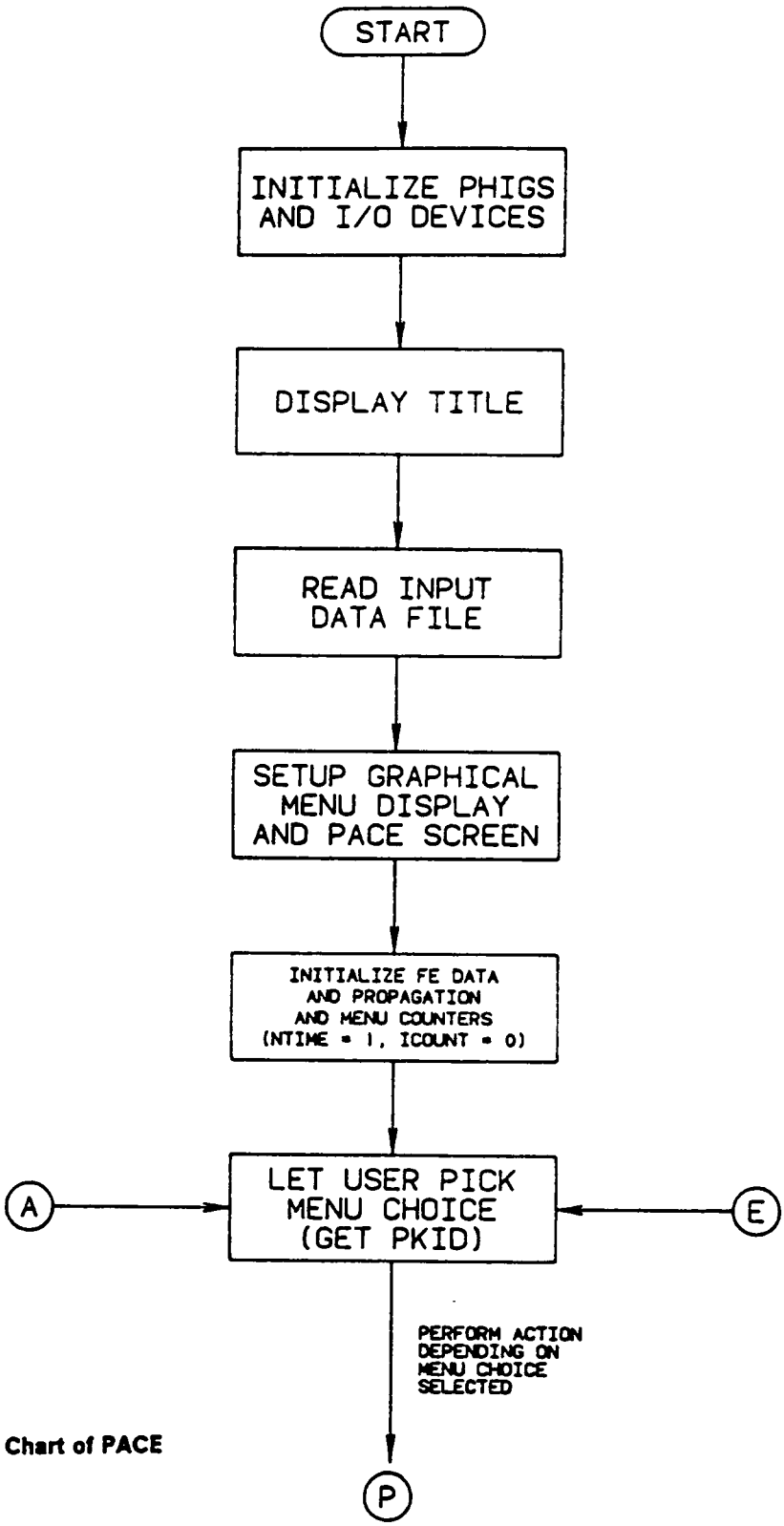

Figure 40. Flow Chart of PACE

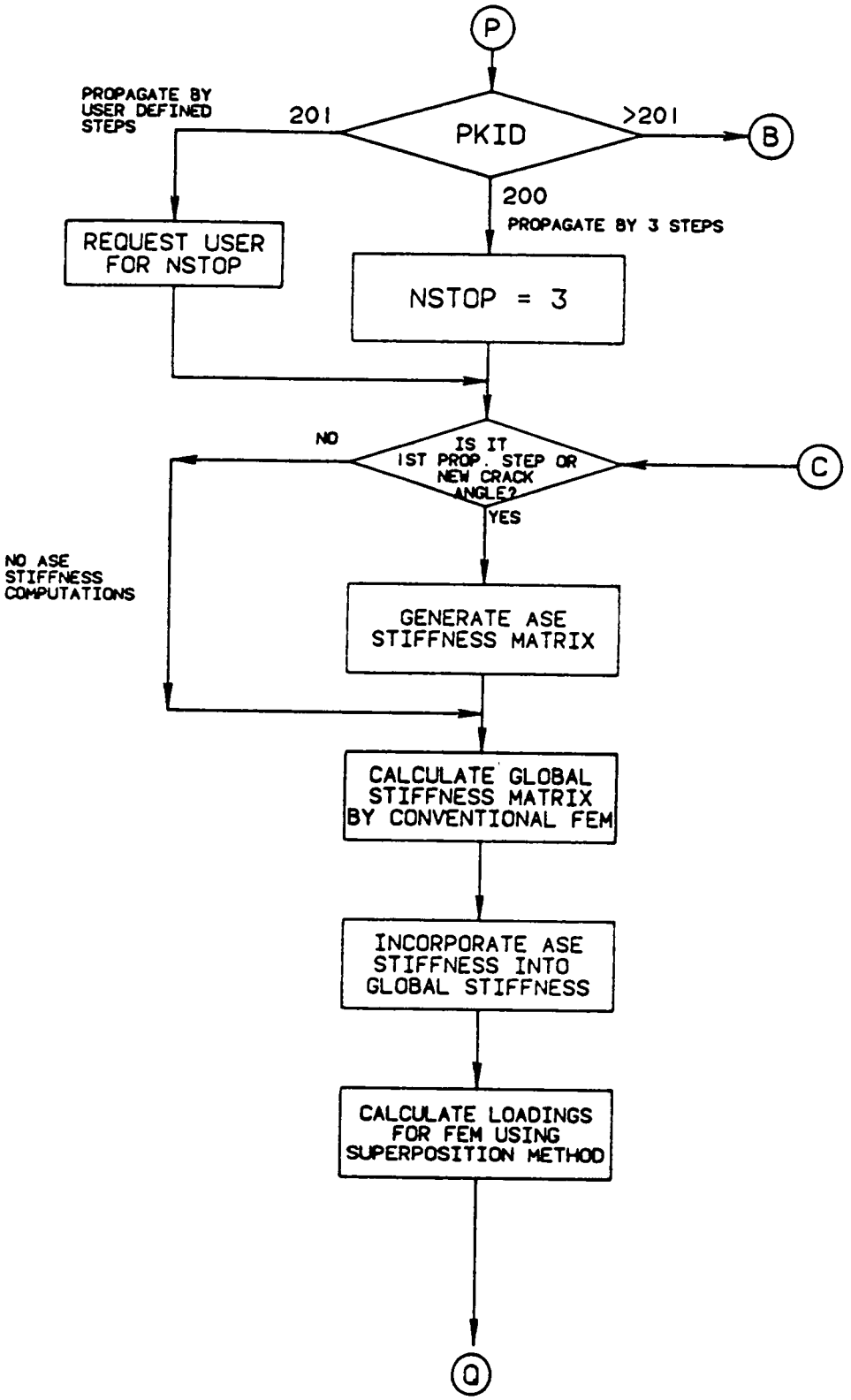
P
PROPAGATE BY USER DEFINED STEPS
201
PKID
>201
B
200
PROPAGATE BY 3 STEPS
REQUEST USER FOR NSTOP
NSTOP = 3
NO
IS IT 1ST PROP. STEP OR NEW CRACK ANGLE?
C
YES
NO ASE STIFFNESS COMPUTATIONS
GENERATE ASE STIFFNESS MATRIX
CALCULATE GLOBAL STIFFNESS MATRIX BY CONVENTIONAL FEM
INCORPORATE ASE STIFFNESS INTO GLOBAL STIFFNESS
CALCULATE LOADINGS FOR FEM USING SUPERPOSITION METHOD
Q

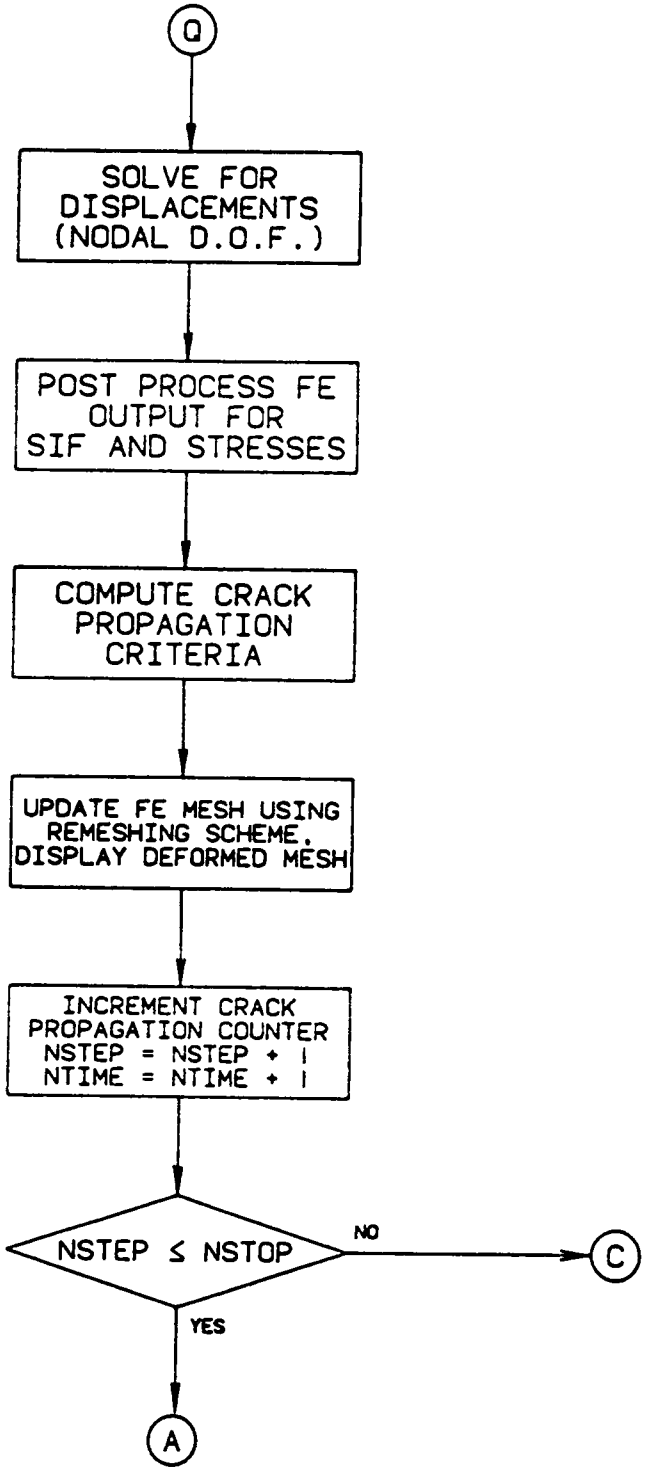
Q
SOLVE FOR DISPLACEMENTS (NODAL D.O.F.)
POST PROCESS FE OUTPUT FOR SIF AND STRESSES
COMPUTE CRACK PROPAGATION CRITERIA
UPDATE FE MESH USING REMESHING SCHEME. DISPLAY DEFORMED MESH
INCREMENT CRACK PROPAGATION COUNTER
NSTEP = NSTEP + 1
NTIME = NTIME + 1
NSTEP ≤ NSTOP
NO
C
YES
A

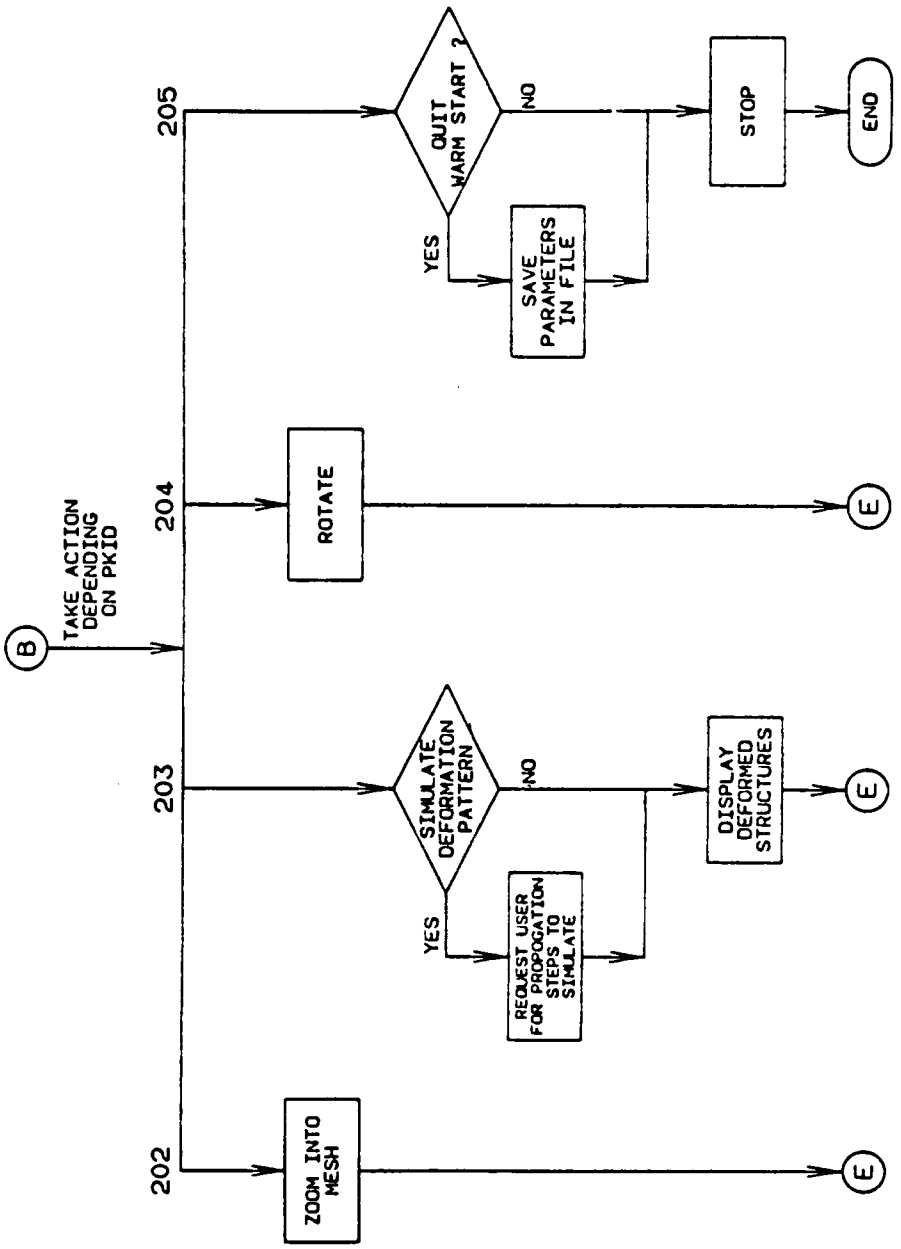
B
TAKE ACTION DEPENDING ON PKID
202
ZOOM INTO MESH
E
203
SIMULATE DEFORMATION PATTERN
YES
REQUEST USER FOR PROPOGATION STEPS TO SIMULATE
NO
DISPLAY DEFORMED STRUCTURES
E
204
ROTATE
E
205
QUIT WARM START ?
YES
SAVE PARAMETERS IN FILE
NO
STOP
END

F.4 Using PACE

The user first logs onto the IBM 5080 workstation which allows the user to toggle back and forth between the graphics and text screens on the 5080. To start PACE, the user types in 'PACE' in the text screen and toggles to the graphics screen to access the program. All further text input and presentation of results are done in the graphics mode entirely to avoid switching between the text and graphics modes. After the title is displayed on the screen (Figure 41) the user is presented with the PACE screen display format showing the menu choices, finite element mesh, plotting window, lamina window and the diagnostics window (Figure 42).
The menu choices are :

1. **PROPAGATE BY 3 STEPS**

2. **PROPAGATE BY USER DEFINED LOAD STEPS**

3. **DEFORMED MESH DISPLAY**

4. **ROTATION OF LAMINA ABOUT X,Y OR Z AXIS**

5. **ZOOM INTO REGIONS OF THE MESH**

6. **EXIT THE PROGRAM**

The user makes a selection by moving the cursor to the particular choice and the choice is input by depressing a button on the cursor pad. Each of the menu actions is described.

Choice 1 : The user can choose to propagate the crack automatically by three load steps at a time before control is returned to him/her. The propagation method and finite element method adopted is described in Chapters 2-4. At the end of each load step, a plot of the deformed mesh

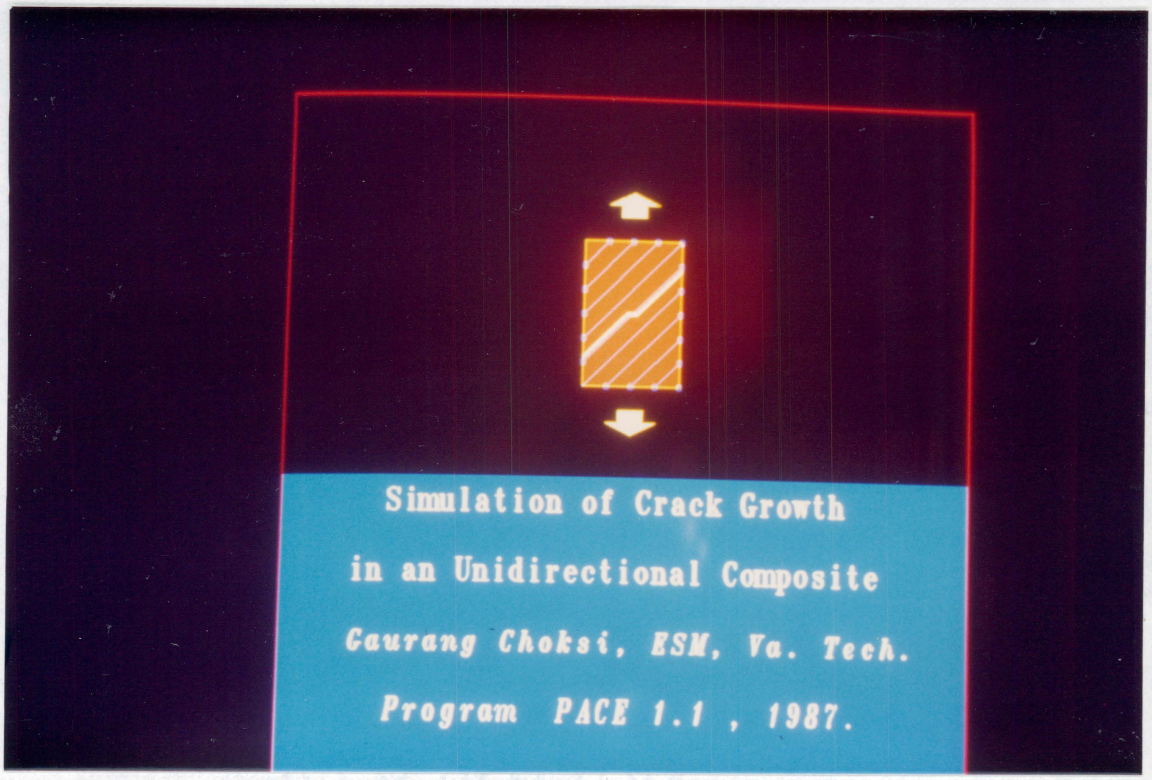

Figure 41. Screen Layout Showing Title of PACE

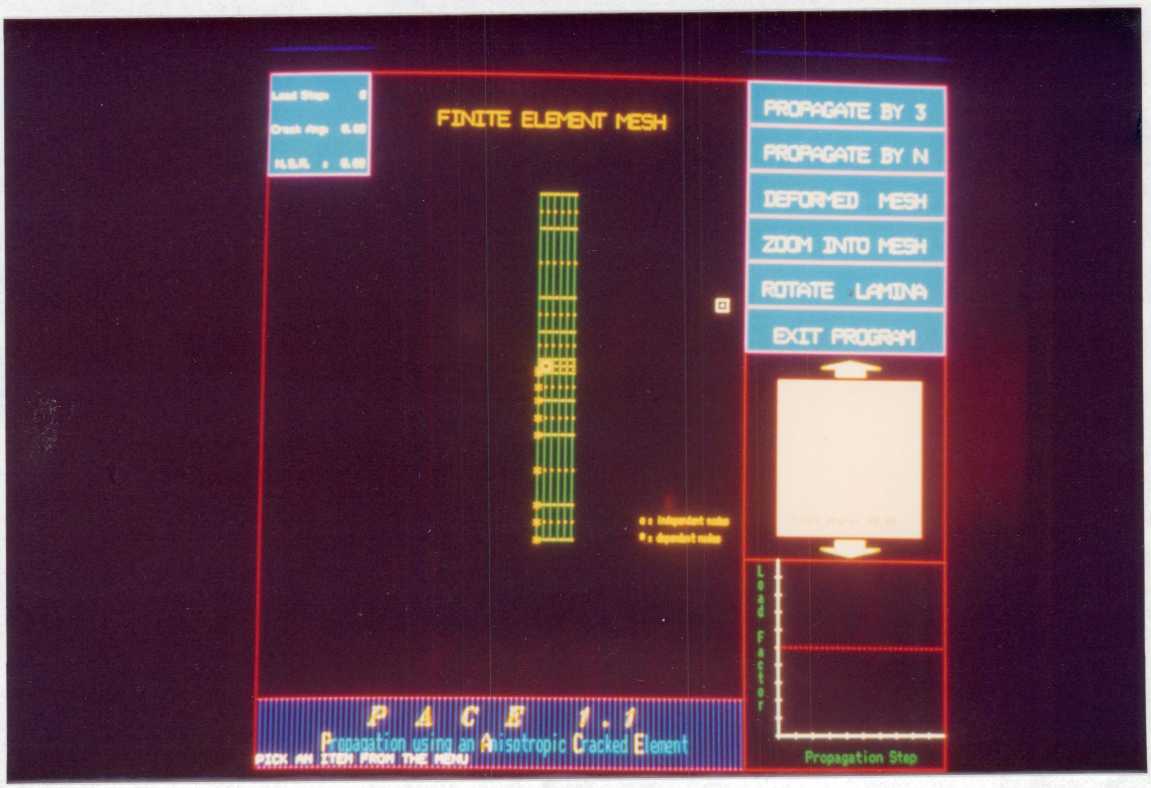

Figure 42. Screen Layout of PACE

is updated on the screen in the main display area. The diagnostics window and the plot of the normal stress ratio (NSR) w.r.t the propagation step number are also updated. The diagnostics window keeps track of the current crack length, current crack angle from the horizontal (X-axis), and the far field loading applied. The plot of the NSR vs the propagation step is an indication of the stability of crack growth using the NSR theory. Onset of instability using the strain energy release rate method and the fracture toughness approach is indicated by flashing the message on the screen as there in no need of plotting the parameters involved. At the same time, all the important parameters, such as the displacements, stresses, strains, values of the NSR, K_I, G_I etc. are written in output files for further review by the user.

Choice 2 : The user also has the option of a finer control over the propagation process. This choice allows the user to input the number of propagation steps to be performed for that menu choice. The user is requested for the number of propagation steps needed and the program calculates the crack growth parameters and plots the deformed meshes as the loading progresses. This freedom allows the user to increment the load one step at a time when the specimen is about to fail or when onset of instability is predicted.

Choice 3 : Plots of deformed meshes as the loading increases are updated on the screen. This menu choice allows the user to review the displacement at a particular propagation step or to simulate the deformation pattern from propagation step P1 to any propagation step P2 (P2 > P1). It is noted that the finite element solution should have already been completed for the propagation step(s) requested so that the displacement vectors are available. Once this choice is made, the user is prompted by the following message : 'Do you want to simulate the deformation pattern ? (Y/N) '. If the response is 'Y', then the user is requested for the initial and final propagation step numbers and the deformed pattern is drawn on the screen one step at a time and the user can pause between the load steps by depressing any key on the function keypad (choice device). If the response is 'N' to the simulation question, then the user is asked to input the propagation step number for which the deformed geometry is required to be drawn.

Choice 4 : Continuous rotations about the X,Y and Z axes is possible using the three valuators (dials). Dials # 1,2,3 are for rotations about the X,Y and Z axes respectively. This is provided mainly as a feature for future versions where it is expected that three-dimensional finite element meshes will be used to analyze different phenomenon.

Choice 5 : Valuator #4 is used for continuous zooming within the fine element mesh to look at regions of high mesh density. All the user has to do is rotate the dial to the degree of zoom required.

Choice 6 : This menu selection exits the program and returns control to the operating system environment (VM/CMS). The total CPU time, total number of menu picks, total number of propagation picks and steps are all calculated, updated and written onto the main output file for further review by the user. The program at this time, also allows the user to restart the analysis at a later time (warm start) by saving all the current mesh parameters and crack growth data in a sequential file. This file is accessed if a warm start is requested.

F.5 PACE Input Data File

A description of each input statement required by PACE is given in this section. The statements described are given in the order to be followed in the input file.

NOTE : The input is FORMAT FREE and no statement can be skipped.

Job Title Statements (2 cards)

Variable Name	Description
ITIT1	Title1
ITIT2	Title2

Two titles should be used to describe and document the case being run. They will be printed by PACE at the top of all the output files.

Fiber Angle and Propagation Step Number (1 card)

Variable Name	Description
THETA	Fiber angle, θ (measured cw from the positive Y-axis)
ISTEP	Propagation Step Number (ISTEP = 0 for starting propagation)

Material & Crack Properties (1 card)

Variable Name	Description
PROP(1)	Modulus along fiber direction, E_{11}
PROP(2)	Modulus perpendicular to fiber, E_{22}
PROP(3)	Poisson's ratio, ν_{12}
PROP(4)	Shear modulus, G_{12}
PROP(5)	Thickness of plate (Lamina), t
PROP(6)	Fiber angle, θ (measured cw from the positive Y-axis)
PROP(7)	Input echo print control (1 : echo input, 0 : no echo)

Strength Properties (1 card)

Variable Name	Description
XT	Strength along fiber (tensile), X_t
XC	Strength along fiber (compressive), X_c
YT	Strength perpendicular to fiber (tensile), Y_t
YC	Strength perpendicular to fiber (compressive), Y_c
SHEAR	Shear Strength, S

Singular Element (ASE) Data (1 card)

Variable Name	Description
NUMNOD	No. of nodes on singular element
NUMTRM	No. of terms to be taken in stress expansion
RADS	Radius of Singular Element, r_e
IELT	Geometry of ASE (1 : semi-circular 2: circular)

Loading Data (1 card)

Variable Name	Description
SIGBXY(1)	Far-field σ_{xx}
SIGBXY(2)	Far-field σ_{yy}
SIGBXY(3)	Far-field τ_{xy}
FRCTH1	Mode I fracture toughness, K_{IC}
FRCTH2	Mode II fracture toughness, K_{IIC}
GCRIC1	Mode I critical strain energy release rate, G_{IC}
GCRIC2	Mode II critical strain energy release rate, G_{IIC}

Specimen Geometry Data (1 card)

Variable Name	Description
ALAMW	Width of plate (lamina)
ALAML	Length of plate (lamina)
AINITL(1)	Initial loading factor, $\bar{\sigma}_x$
AINITL(2)	Initial loading factor, $\bar{\sigma}_y$
AINITL(3)	Initial loading factor, $\bar{\tau}_{xy}$

Crack Propagation Data (ISTEP + 1 cards)

Variable Name	Description
CRKANG(I)	Crack angle at load step I
CRKLEN(I)	Crack length at load step I
PROPFC(I)	Propagation Factor at load step I

ASE Nodal Coordinate Data (NUMNOD cards)

Variable Name	Description
RADI(N)	Radius of node N (measured from crack tip)
APHI(N)	Angular position of node N (in degrees)

These are the coordinate locations of each node of the singular element specified on separate cards. The node numbering scheme is shown in Figure 43.

Finite Element Mesh Parameters (1 card)

Variable Name	Description
NEM	Total no. of elements in mesh
NNM	Total no. of nodes in mesh
NSDF	No. of displacement b.c.'s
IFORBC	No. of force b.c's
ISNFLG	Flag for singular element (0 : No singular element) (1 : Singular element present)

Scale Factors (1 card)

Variable Name	Description
SCALX	Scale factor to be used for the X direction
SCALY	Scale factor to be used for the Y direction

Connectivity Data (NEM cards)

Variable Name	Description
ELEMN	Element number
NOD(N,1)	Node #1 of Element N
NOD(N,2)	Node #2 of Element N
NOD(N,3)	Node #3 of Element N
NOD(N,4)	Node #4 of Element N
NOD(N,5)	Node #5 of Element N
NOD(N,6)	Node #6 of Element N
NOD(N,7)	Node #7 of Element N
NOD(N,8)	Node #8 of Element N
IELFLG(N)	Type of Element (0 : has no dependent nodes) (1 : has dependent nodes)

The connectivity of each element is specified on these cards. The node numbering scheme is shown in Figure 44. The flag for element type indicates inversion symmetry problems. For structures with no inversion symmetry, no element will have dependent nodes.

Nodal Coordinate Data (NNM cards)

Variable Name	Description
NODN	Node number
X(N)	X-coordinate of node N
Y(N)	Y-coordinate of node N
INDFLG(N)	Flag for node type (0 : independent -1 : dependent)
NDBDRY(N)	Flag for boundary node (0 : interior node 1: boundary node)

The flags for node type refer to inversion symmetry problems. If inversion symmetry is not exploited, all nodes will be independent. The boundary (or interior) node flag is required for the remeshing procedure as the crack propagates.

Element Force Data (IFORBC cards)

Variable Name	Description
ELEMN	Element number
IDFN	Direction (d.o.f.) of specified force (Examples :) (3 : force along X dirn. at node 2 of element (6 : force along Y dirn. at node 3 of element)
FORCE	Value of specified force

Propagation Data (1 card)

Variable Name	Description
NUMPTS	No. of points at which to evaluate propagation data
RADIUS	Radius r_o at which to evaluate propagation data

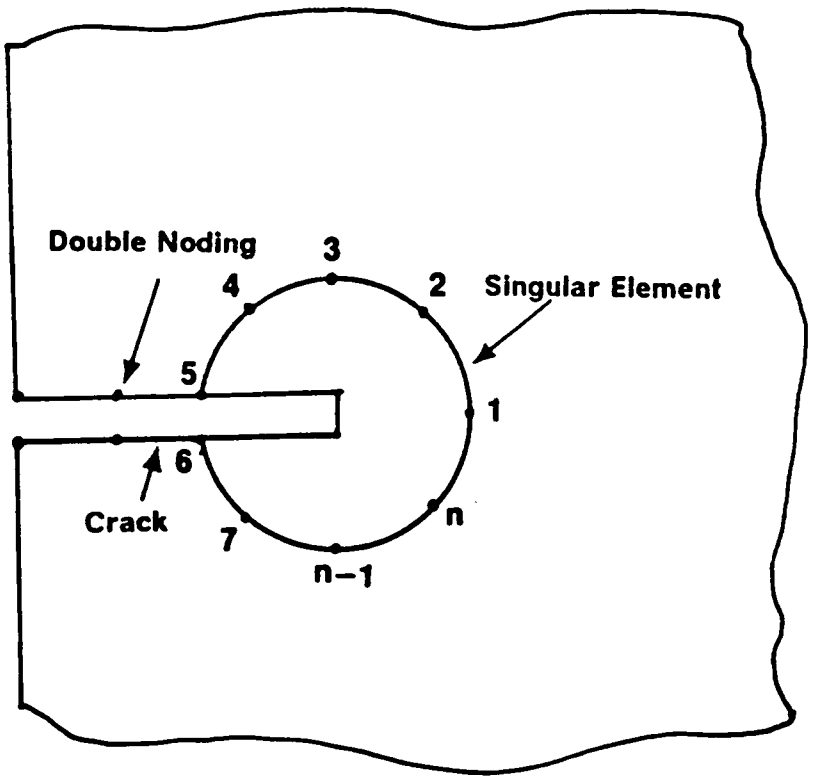

Figure 43. Node Numbering Scheme for the Singular Element (ASE)

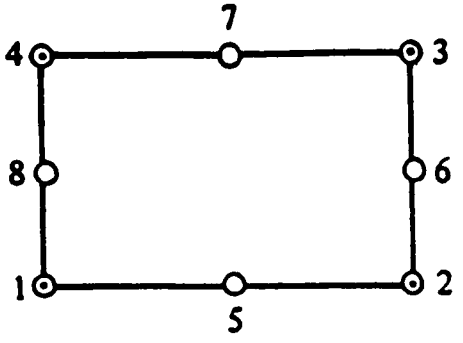

Figure 44. Node Numbering Scheme for the Q8 Element

F.6 Example Data File

An example problem is given next. The mesh shown in Figure 45 is used. Figure 45 shows the singular element geometry and the total mesh of the structure. Inversion symmetry is exploited and the flags for the dependent nodes and elements are also given in the sample data file. A far field loading of 1 ksi (1000 psi) is applied along the Y direction. The mesh consists of 16 elements, 69 independent nodes and the singular element with 17 nodes along its boundary. Note that a 'double node' numbering scheme is adopted along the crack faces to account for the physical presence of the crack. A sample data file listing is given below :

FILE PACEX DATA

```
Example file for PACE, Inversion symmetry used, 17 Noded ASE, Mar. 1988.
Fiber=90.0, Plate= 3.0" x 6.0", Crack=1.0", Radius=0.5
90.0,0
21.6E+06,1.96E+06,0.28,0.83E+06,1.0,1
282.0E+03,-282.0E+03,10.0E+03,-10.0E+03,14.2E+03
17,1,0.5,2
0.0,1000.0,0.0,32.957E+3,1.57E+3,1.3E-6,0.5E-6
3.0,6.0,1.0,2.0,1.0
0.0,0.1,1.0
0.5,0.0
0.5,22.5
0.5,45.0
0.5,67.5
0.5,90.0
0.5,112.5
0.5,135.0
0.5,157.5
0.5,180.0
0.5,180.0
0.5,202.5
0.5,225.0
0.5,247.5
0.5,270.0
0.5,292.5
0.5,315.0
0.5,337.5
16,69,0,60,1
1.0,1.0
  1   1  27  41   3  18  30  19   2   0
  2   3  41  39   5  19  40  20   4   0
  3   5  39  37   7  20  38  21   6   0
  4   7  37  35   9  21  34  22   8   0
  5  10  36  37  12  23  34  24  11  -1
  6  12  37  45  14  24  44  25  13  -1
  7  14  45  47  16  25  46  26  15   0
  8  16  47  27   1  26  32  18  17   0
  9  27  47  49  29  32  48  33  28   0
 10  27  29  43  41  28  31  42  30   0
 11  57  37  39  59  50  38  51  58   0
 12  59  39  41  61  51  40  52  60   0
```

13	61	41	43	63	52	42	53	62	0
14	37	57	65	45	50	64	54	33	-1
15	45	65	67	47	54	66	55	46	0
16	47	67	69	49	55	68	56	48	0

1	0.150000D+01	0.000000D+00	0	0
2	0.146194D+01	0.191342D+00	0	0
3	0.135355D+01	0.353553D+00	0	0
4	0.119134D+01	0.461940D+00	0	0
5	0.100000D+01	0.500000D+00	0	0
6	0.808658D+00	0.461940D+00	0	0
7	0.646447D+00	0.353554D+00	0	0
8	0.538060D+00	0.191342D+00	0	0
9	0.500000D+00	0.000000D+00	0	0
10	0.500000D+00	0.000000D+00	0	0
11	0.538060D+00	-0.191341D+00	0	0
12	0.646446D+00	-0.353553D+00	0	0
13	0.808658D+00	-0.461940D+00	0	0
14	0.100000D+01	-0.500000D+00	0	0
15	0.119134D+01	-0.461940D+00	0	0
16	0.135355D+01	-0.353554D+00	0	0
17	0.146194D+01	-0.191342D+00	0	0
18	0.175000D+01	0.000000D+00	0	0
19	0.153033D+01	0.530330D+00	0	0
20	0.100000D+01	0.750000D+00	0	0
21	0.469670D+00	0.530330D+00	0	0
22	0.250000D+00	0.000000D+00	0	0
23	0.250000D+00	0.000000D+00	0	0
24	0.469669D+00	-0.530330D+00	0	0
25	0.999999D+00	-0.750000D+00	0	0
26	0.153033D+01	-0.530331D+00	0	0
27	0.200000D+01	0.000000D+00	0	0
28	0.250000D+01	0.000000D+00	0	0
29	0.300000D+01	0.000000D+00	0	1
30	0.200000D+01	0.500000D+00	0	0
31	0.300000D+01	0.500000D+00	0	1
32	0.200000D+01	-0.500000D+00	0	0
33	0.300000D+01	-0.500000D+00	0	1
34	0.000000D+00	0.500000D+00	-1	1
35	0.000000D+00	0.000000D+00	-1	1
36	0.000000D+00	0.000000D+00	-1	1
37	0.000000D+00	0.100000D+01	-1	1
38	0.500000D+00	0.100000D+01	0	0
39	0.100000D+01	0.100000D+01	0	0
40	0.150000D+01	0.100000D+01	0	0
41	0.200000D+01	0.100000D+01	0	0
42	0.250000D+01	0.100000D+01	0	0
43	0.300000D+01	0.100000D+01	0	1
44	0.500000D+00	-0.100000D+01	0	0
45	0.100000D+01	-0.100000D+01	0	0
46	0.150000D+01	-0.100000D+01	0	0
47	0.200000D+01	-0.100000D+01	0	0
48	0.250000D+01	-0.100000D+01	0	0
49	0.300000D+01	-0.100000D+01	0	1
50	0.000000D+00	0.200000D+01	-1	1
51	0.100000D+01	0.200000D+01	0	0
52	0.200000D+01	0.200000D+01	0	0
53	0.300000D+01	0.200000D+01	0	1
54	0.100000D+01	-0.200000D+01	0	0
55	0.200000D+01	-0.200000D+01	0	0
56	0.300000D+01	-0.200000D+01	0	1
57	0.000000D+00	0.300000D+01	-1	1
58	0.500000D+00	0.300000D+01	0	0
59	0.100000D+01	0.300000D+01	0	0
60	0.150000D+01	0.300000D+01	0	0
61	0.200000D+01	0.300000D+01	0	0
62	0.250000D+01	0.300000D+01	0	0
63	0.300000D+01	0.300000D+01	0	1
64	0.500000D+00	-0.300000D+01	0	0
65	0.100000D+01	-0.300000D+01	0	0
66	0.150000D+01	-0.300000D+01	0	0
67	0.200000D+01	-0.300000D+01	0	0
68	0.250000D+01	-0.300000D+01	0	0

```
  69  0.300000D+01 -0.300000D+01   0   1
11,2,166.667
11,16,666.667
11,8,166.667
12,2,166.667
12,16,666.667
12,8,166.667
13,2,166.667
13,16,666.667
13,8,166.667
14,4,-166.667
14,12,-666.667
14,6,-166.667
15,4,-166.667
15,12,-666.667
15,6,-166.667
16,4,-166.667
16,12,-666.667
16,6,-166.667
11,1,166.667
11,15,666.667
11,7,166.667
12,1,166.667
12,15,666.667
12,7,166.667
13,1,166.667
13,15,666.667
13,7,166.667
14,3,-166.667
14,11,-666.667
14,5,-166.667
15,3,-166.667
15,11,-666.667
15,5,-166.667
16,3,-166.667
16,11,-666.667
16,5,-166.667
11,2,-333.333
11,10,-1333.33
11,4,-333.333
4,4,-166.667
4,12,-666.667
4,6,-166.667
5,4,-166.667
5,12,-666.667
5,6,-166.667
14,2,-333.333
14,10,-1333.33
14,4,-333.333
13,8,333.333
13,14,1333.33
13,6,333.333
10,6,166.667
10,12,666.667
10,4,166.667
9,8,166.667
9,14,666.667
9,6,166.667
16,8,333.333
16,14,1333.33
16,6,333.333
72,0.008
```

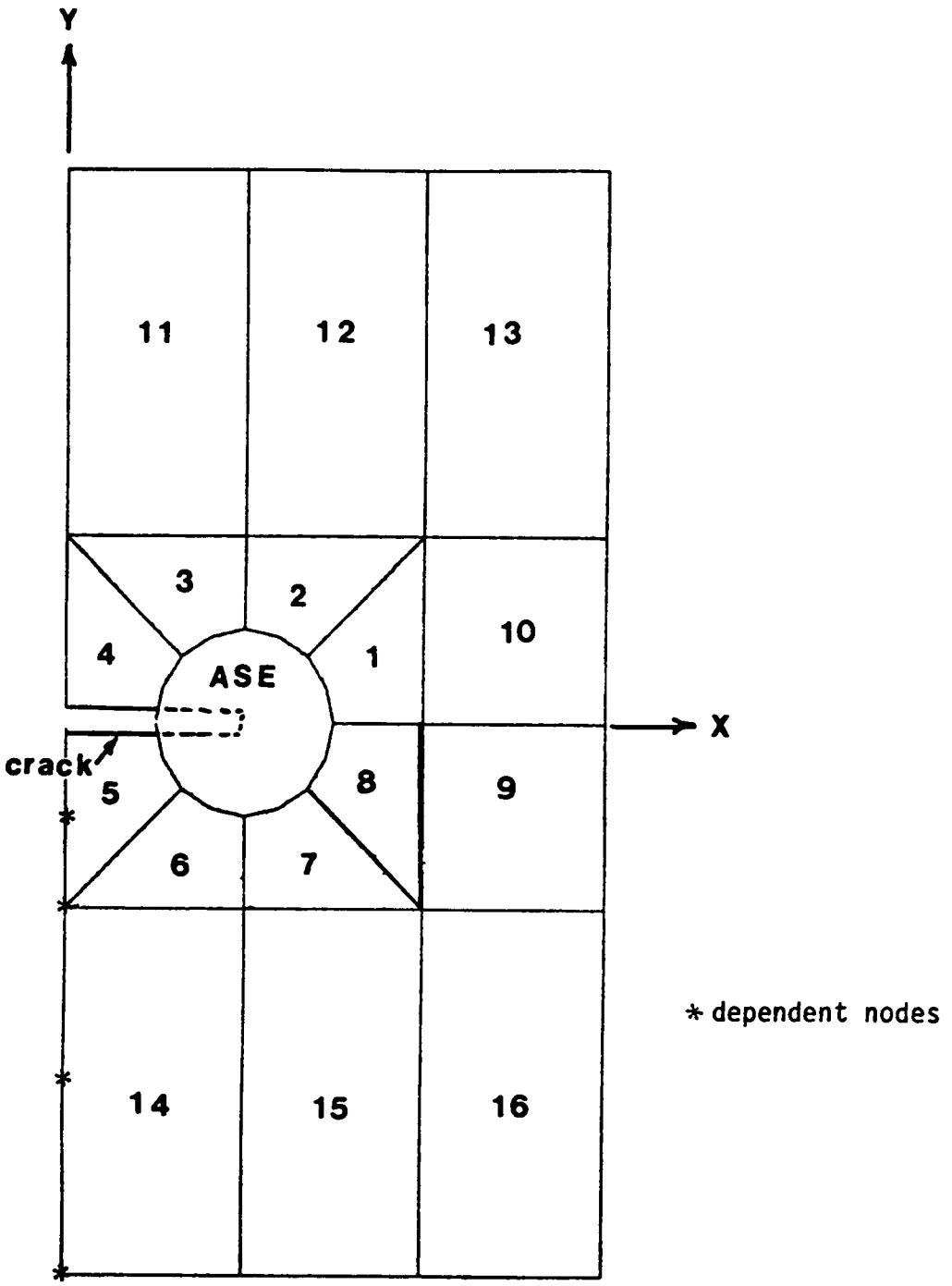

Figure 45. Finite Element Mesh for Example Problem

The vita has been removed from the scanned document